RHODES UNIVERSITY
*Where leaders learn*

# Analysis of saprolite-hosted Rutile-Graphite deposit:

# A case study of Malingunde saprolite-hosted Rutile-Graphite project in Central Malawi


**By**

**ANSEL ALIKO ZABULA**

**(18Z1230)**

**Supervised by**

**Prof. RE ''Jock'' Harmer**


A dissertation submitted in partial fulfilment of the requirements for the degree of

Master of Science (Exploration Geology)


Rhodes University

Grahamstown

South Africa


15th September, 2024

**Declaration**

By submitting this thesis electronically, I, **Ansel Zabula**, declare that the entirety of the work contained therein is my own, original work, that I am the sole author thereof (save to the extent explicitly stated otherwise), that reproduction and publication thereof by Rhodes University will not infringe any third party rights and that I have not previously in its entirety or part submitted it for obtaining any qualification.

**Abstract**

The Malingunde graphite project, owned by Sovereign Metals Ltd (SML), has revealed significant potential for rutile and high-grade graphite in saprolite. This study addresses the complexity of mineral assemblages in the Malingunde area, emphasizing the coexistence of graphite and rutile. SML's exploration activities, including extensive drilling and soil sampling, have uncovered variations in associated minerals, such as muscovite, kyanite, garnets, and ilmenite. Rutile, initially discovered incidentally, has prompted further investigation, impacting the financial model of the project.

This research aims to analyse the Malingunde deposit, focusing on understanding its mineralogy, formation, and potential for elements like vanadium. Geological surveys reveal the distribution of graphite in the Precambrian to lower Palaeozoic age basement complex, hosted in saprolite resulting from tropical weathering of graphitic gneisses.

Exploration techniques, including remote sensing, and geophysics, are crucial in targeting graphite and rutile deposits. Ground electromagnetic surveys, airborne electromagnetic data, and GIS applications aid in identifying and quantifying mineralised areas. Geochemical analysis and metallurgical tests further contribute to understanding the ore body and processing methods.

Results indicate an inverse relationship between graphite and rutile concentrations, influencing the economic viability of different regions within the project area. Correlation matrices and regression analyses reveal distinct geological conditions influencing the association of vanadium and graphite in Lifidzi and Malingunde.

The study concludes with exploration potential outside the Malingunde project, highlighting regional prospects and potential byproducts like vanadium pentoxide. The ongoing metallurgical tests and pilot plant design signify the project's evolution toward production. Additionally, neighbouring licenses show potential, emphasizing the need for comprehensive research to define and quantify resources in the region.

This research provides valuable insights for the mining industry, informing strategies for exploration, resource assessment, and potential byproduct utilization in similar geological settings.

**Acknowledgements**

Firstly, I thank Prof. J. Harmer and Mrs. A. Goddard of the Exploration Geology program, Geology Department, Rhodes University, for their leadership, guidance, and unconditional assistance during this program. They have always gone out of their way to ensure students are always well-supported. Without their commitment to this program, the students would not be privileged to have such a wealth of knowledge and experience within the mineral exploration industry.

I am also thankful for Sovereign Metals Management's support throughout the programme, including allowing me to take time off for my studies and their consent to use the company's data for my research; this played a significant role in my successfully completing my dissertation.

A special thank you to my wife, my daughters, Anaiah and Ariella, my sister Esnor and my mum, Patricia Kachingwe for the support and encouragement throughout the journey; you kept me going and believed that there was light at the end of the tunnel.

Lastly, this story wouldn't have been complete without Julian Baring Scholarship Fund, which supported me with my tuition for the programme, I will forever be grateful for the support.

To my fellow students who enrolled in the course with me, I enjoyed every second we shared in the seminars, field trips and study sessions, I know it was an emotional journey, but there is always light at the end of the tunnel; go shine and go beyond the sky.

## Table of Contents

## Table of Figures

## Table of tables



## List of appendices

**Abbreviations**

CAGR - Compound annual growth rate

EM - Electromagnetic

EPL – Exclusive Prospecting Licence

FERP – Ferruginous pedolith

HFSE - High field strength element

MOTT – Mottled zone

MRE - Mineral resource estimate

MT - Metric tonnes

PGEs - Platinum group elements

PSAP – Palid saprolite

SAPR – Saprolite rock

SEM - Scanning electron microbe

SML – Sovereign Metals Limited

SSV - Sandstone-hosted vanadium

TGC – Total graphitic carbon

UV - Ultraviolet

VRFB - Vanadium redox flow battery

VTEM - Versatile time domain electromagnetics

VTM - Vanadiferous titanomagnetite

XRF - X-ray fluorescence

XRD - X-Ray diffraction

# Chapter 1: Introduction

This dissertation will focus mainly on an analysis of the Malingunde graphite project in Malawi:- a saprolite-hosted deposit dominated by flake graphite and rutile.

## 1.1 Project description and location

The Malingunde saprolite-hosted graphite project is owned by Sovereign Metals Ltd (SML), an Australian company exploring graphite and rutile in Malawi. The company has an exclusive prospecting license (EPL) that covers 3993 km$^2$ with a potential for flake graphite and a high potential for rutile (SML, 2019). The Malingunde project is located about 20km southwest of Lilongwe. Figure 1 below shows the location of project area.

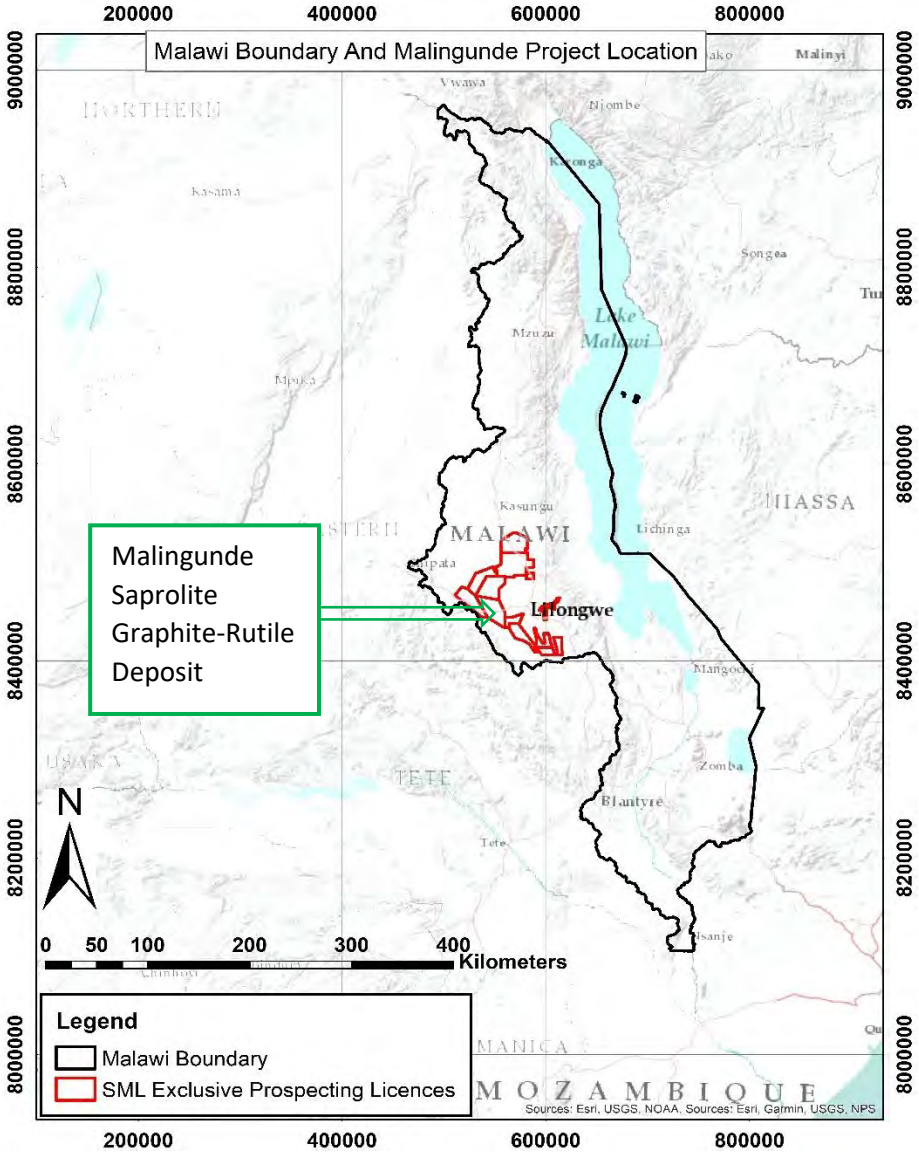


*Figure 1: Map of Malawi showing Malingunde Saprolite hosted Graphite project. (Generated by Ansel Zabula)*

So far, SML has carried out a sampling exercise (including drilling) of the ground around the Lilongwe area, which is within its exploration licenses among others, including Duwi, Malingunde and Lifidzi, as shown in Figure 2 below.

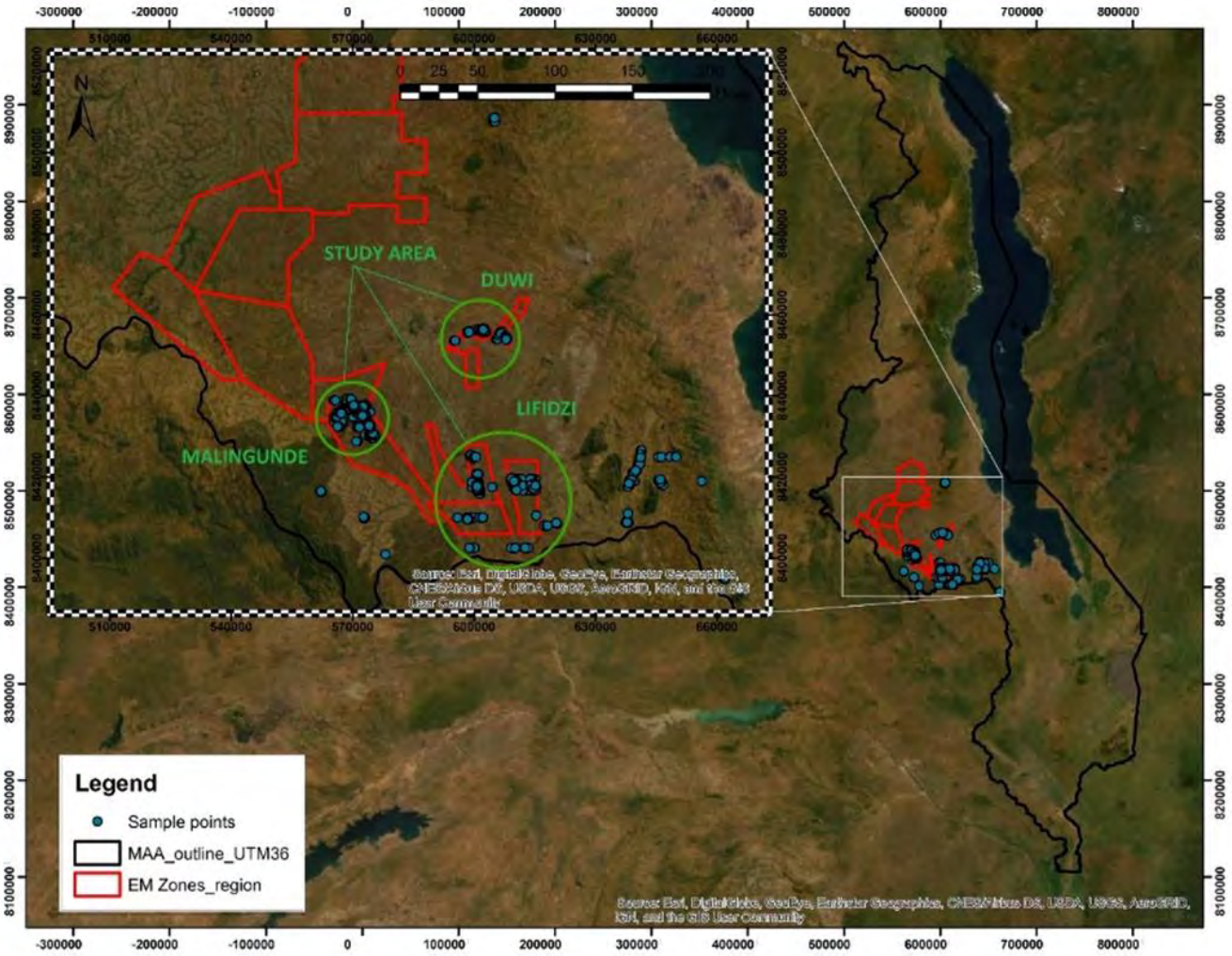


*Figure 2: Map showing Localities for sampling Exercise by Sovereign Metals Ltd. (generated by Ansel Zabula)*

Figure 2- shows the distribution of sampling completed within the Lilongwe region. This exercise identified several targets, which will be the main focus of the discussion in this dissertation.

The Malingunde saprolite hosted project was the main target that led to the extension and discovery of the other targets. It is a base for this study mainly because of the focus and depth of research conducted in the area.

## 1.2 Problem statement

Studies conducted by SML uncovered a large region enriched in graphite and rutile, particularly in the Malingunde and surrounding areas. These studies included drilling programs (auger, diamond, air core, etc) and extensive soil sampling.

In some samples, a wide variation of associated minerals, such as muscovite, kyanite, garnets, ilmenite, and more, were observed. Beyond the northwest of the 3km strike mentioned above, an increase of muscovite was observed, and an abundance of kyanite was observed west of the strike.

As a graphite project, most samples were initially analysed for carbon content until later in the project, when some samples showed a potential for rutile after further analysis.

The mineral assemblage may impact the financial model of a potential mine. For example, if rutile proves to be present in the area, feasible to mine and recover, the value of the project would be upgraded. Therefore, understanding the mineral assemblage would be necessary for this kind of deposit. There would also be a need to find the appropriate processing of these minerals. Further to that, there is also a need to identify the most effective way of targeting different areas for graphite and/or rutile exploration in the region.

Therefore, it is necessary to analyse the Malingunde deposit because of different variations in the minerals found in the area and compare it with the other targets identified in central Malawi.

### 1.2.1 Aim of study

- To analyse the Malingunde graphite and rutile deposit hosted in saprolite.

### 1.2.2 Objective of study

- To assess the formation of the Malingunde graphite and rutile deposit
- To identify the mineralogy and associated minerals of the Malingunde graphite and rutile project
- To explore the potential for other elements or minerals e.g. vanadium

- To investigate the implications of the type of deposit in relation to the Malingunde graphite and rutile deposit
- To identify exploration techniques of saprolite-hosted graphite and rutile deposit
- To explore the relationship between the graphite and/or rutile deposit and remote sensing
- To conduct a market analysis for graphite, rutile and vanadium.

## 1.3 My contribution to the Malingunde graphite-rutile project and this research

During the studies at the Malingunde project, I was involved and contributed to the following activities between 2016 and 2019:

- Planned and managed the Malingunde project (including Lifidzi and at a regional level).
- Supervised drilling rig during several drilling programmes (including air core, diamond drilling and augering) for Malingunde, Duwi, Lifidzi, and regional exploration.
- Logged over 60% of the samples retrieved from various exploration programmes. Including sub-sampling.
- Analysed the exploration results, created maps for the thesis using ArcGIS, and created all sections using Geosoft. During my actual tenure at Sovereign Metals Limited, MapInfo was used to perform this task. Therefore, I had to create and analyse the data from scratch using the software and the skills I acquired during the Master's degree programme.
- Carried out the market analysis in the thesis.

# Chapter 2: Geology and Geological setting

The geology of Malawi is characterised by the Malawi Basement Complex, consisting of Precambrian to lower Paleozoic crystalline rocks that have undergone prolonged structural and metamorphic transformations with Karoo supergroup being deposited between the Permian and late Jurassic age (Carter and Bennet, 1973). Throughout the late Paleozoic (Karoo System) and late Mesozoic (Chilwa Province), many rocks underwent chemical weathering and erosion due to sedimentation driven by rifting and igneous processes. The region's current shape was fully formed during the Cenozoic through peneplanation and fluvial incisions under subtropical climatic conditions. The planation was active from the Cretaceous to the Quaternary, after which it was replaced by erosion and deposition due to significant fluvial incision during the Quaternary. So, in most cases, mineral concentration is highly controlled by geomorphology, erosion, and weathering (Bloomfield et al., 1966).

The Precambrian basement complex, comprising granulites, gneisses, and schists, underlies most of Lilongwe and parts of the Dedza and Mchinji areas. These gneisses are typically rich in graphite and contain both pyrite and pyrrhotite sulphides (Thatcher and Walter, 1968).

Metasedimentary rocks of the Mafinga and Mchinji Groups, which rest upon basement cordierite gneiss with an angular unconformity, are also present and recognised as distinct lithological units (Thatcher, 1974).

In the Malingunde area, graphite mineralisation occurs within a broader Proterozoic paragneiss package, where multiple bands of graphite gneisses are present (Walter, 1972). These rocks in the Malingunde area have been metamorphosed to lower almandine-amphibolite facies, while the granite-kyanite-mica-gneisses have reached upper almandine-amphibolite metamorphic grades. This highlights the unique metamorphic conditions and compositional variations within the broader almandine-amphibolite facies, underscoring the geological diversity and complexity of the Malingunde region (Thatcher and Walter, 1968).

Significant graphite mineralisation in Malingunde is hosted in saprolite, a product of millions of years of active tropical weathering of the gneisses. Extensive fieldwork, including soil sampling, surface feature analysis, and geophysical and geochemical studies, led to the discovery of a substantial graphite deposit with mineralisation concentrated along a strike of approximately 3 km and a width of about 1 km. Additionally, rutile was found to be abundant and is also hosted in the saprolite within the Malingunde area (SML, 2018).

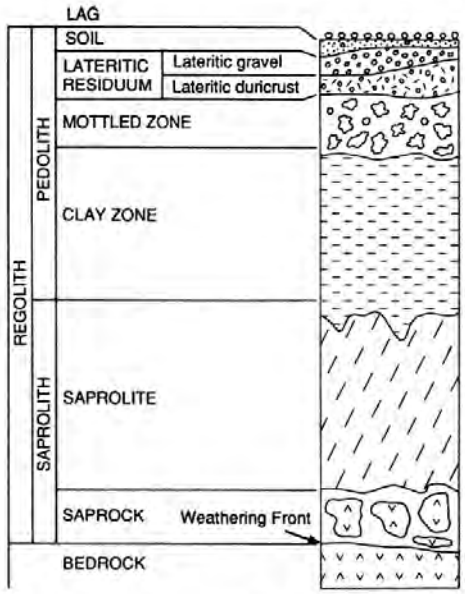


*Figure 3: Regolith terminology used deeply weathered laterite profile Modified after Anand and Butt (1988)*

Studies by SML have outlined a typical weathering profile of the region, which includes, from the surface downward, layers of soil, ferruginous pedolith (FERP), mottled zone (MOTT), pallid saprolite (PSAP), saprolite rock (SAPR), and fresh rock (SML, 2019). Figure 3 above illustrates the typical weathering profiles.

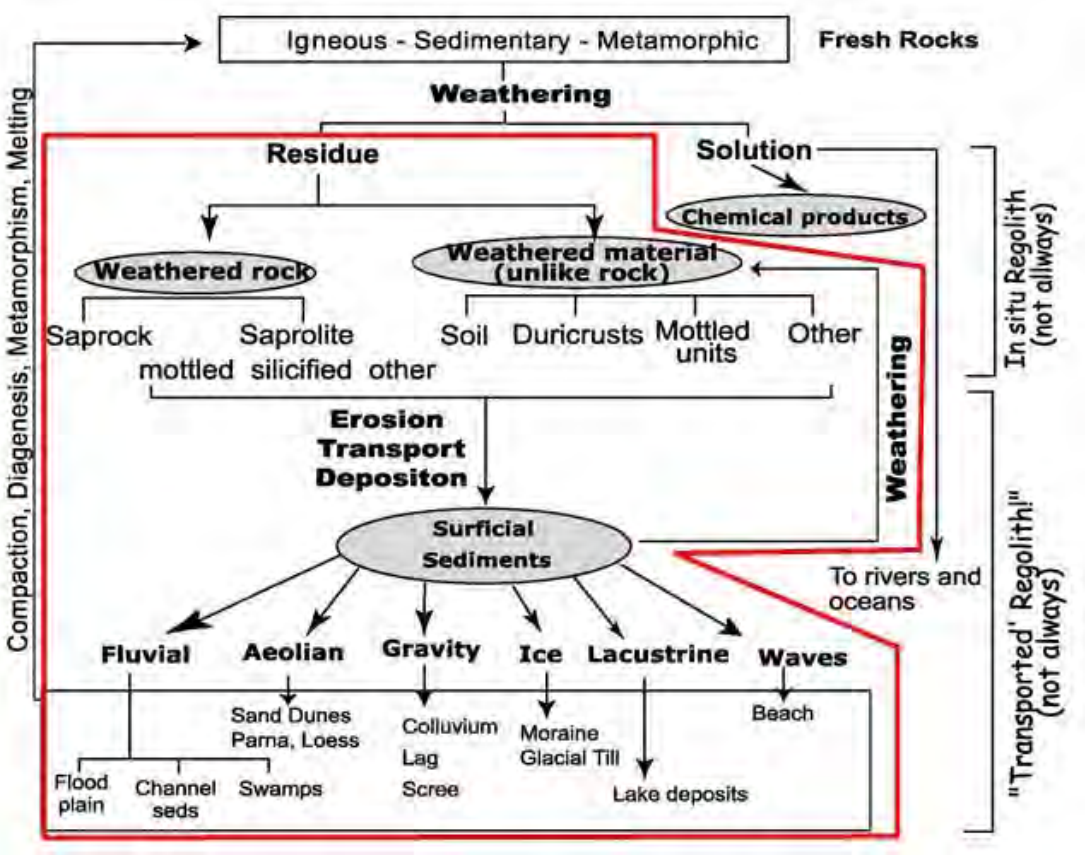


*Figure 4: Genesis of weathering profiles (CRC Leme 2007) – Mineral Council Australia*

Figure 4 above further breaks down the processes and types of deposits associated with weathering and transportation. Therefore, the graphite and rutile targets for the Malingunde project can fall under residue as they are dominated by weathered rock with a higher possibility of erosion, transportation, and deposition of other minerals like heavy minerals.

This chapter further discusses the characteristics, origin, and known deposits of graphite, rutile, and vanadium in Malawi.

## 2.1 Graphite

### 2.1.1 Characteristics, origin and global occurrences

Graphite is one of the naturally occurring crystalline forms of carbon, its main characteristics being its flaky habit, extreme softness, high conductivity of heat and electricity, and refractory properties, It is used for lining foundry moulds and crucibles, and in paint production. In addition, graphite has widespread applications as a lubricant and in the electrical industry (Carter and Bennet, 1973).

Natural graphite is mainly found in three types, vein, amorphous and flake depending on its crystallinity, grain size, and morphology. These three natural graphite variants differ in their purity, uses, geological setting and prices (Simandl et al., 2015; Olson, 2011). These deposits are usually associated with other minerals such as kyanite, pyrite and depending mainly on the geological setting and environment. As much as graphite can be found as a natural mineral, synthetic graphite also exists which is a manufactured from carbon material such as coal tar pitch or made by high temperature treatment from non carbon material such as petroleum coke (Tamashausky, 2006).
Graphite occurs in metamorphic, igneous and sedimentary rocks that has undergone through regional or contact metamorphism, as well as in fluid-precipitated veins. However, the graphite that occurs in metamorphic and igneous rock has no economic importance but the ones formed in carbonaceous sedimentary rocks are classified as significant deposits. Extraction of graphite from metamorphic and igneous rocks presents technical challenges and tends to be economically less feasible when compared to carbonaceous sedimentary rocks. The procedures for processing graphite hosted in metamorphic and igneous rocks are often complex and expensive. However, deposits of flake graphite and amorphous graphite are typically mined using open-pit methods, which are less demanding in terms of labour and involve simpler processing, especially in weathering environments where graphite remains stable. The grades of graphite deposits and the ease of mining are improved by weathering, which leads to the deterioration of other minerals present. In some cases,

sedimentary deposits that undergone significant weathering, allowing for free dig mining using shovels and other hand tools (Robinson et al., 2017).

Graphite deposits commonly occur alongside various minerals, with sulphides, particularly pyrite and pyrrhotite, being the predominant impurities in the Malingunde area (Thatcher and Walter, 1968). Alongside these sulphides, associated minerals include feldspar, quartz, biotite, pyroxene, and garnets. However, the economic viability of a deposit might be constrained by the prevalence of impurities like silica, sulphides, or biotite. Surface weathering of graphite deposits may result in the replacement of sulphide minerals with sulphates or replacement of silicate minerals such as feldspar by kaolinite (Scogings, 2015). Weathered rocks were also noted in the Malingunde area, and south Lilongwe plain (Thatcher and Walter, 1968), where the Malingunde saprolite hosted graphite-rutile project is located.

Mapping, trenching, geophysics, drilling, assaying of graphitic content, and mineralogical testing are some of the techniques used in graphite exploration. In addition, GIS and remote sensing are also emerging techniques used in the exploration or targeting (Scogings, 2000).

As of 2021, deposits in China, Brazil, Mozambique, Russia, Madagascar, and Ukraine are the main sources of crystalline flake graphite, the high-grade crystalline flake graphite resources from China being the largest in the world (U.S. Geological Survey, 2023). Most of these graphite ore deposits occurrence ranges from Neoarchean to Late Proterozoic mica gneiss and schist belts, which may be related to a series of orogenic events in the Gondwana supercontinent formation (Wilde et al., 1999) possibly formed by distinct processes.

### 2.1.2 Classification of graphite deposits

Table 1 below is a summary of the features of graphite deposits, applications, and commodities, by commodity category. The table also demonstrates that texture plays a crucial role in graphite. It is evident that the prices are different throughout the classifications, the deposit type also demonstrates a difference, and the properties differ. It is also apparent that the main uses for the different textures are different, as summarised in Table 1 to mention a few notable critical differences. The Malingunde project has both textures, however, it is dominated by flake graphite, which gives it more value because of its favourable combinations of the associated deposit tonnages, prices, mine operation processes, grade and main uses as described in Table 1

*Table 1 : Kinds of graphite commodities, their industrial applications, market pricing, and explanations of the related geologic environments and deposit types. (Robinson et al., 2017)*

| Characteristics | Commodity type | | | |
|---|---|---|---|---|
| | Amorphous | Flake | Lump or Chip | Synthetic |
| **Deposit type** | Amorphous | **Disseminated flake** | vein | N/A |
| **Crystallinity** | Microcrystalline | **Crystalline** | Crystalline | Microcrystalline to crystalline |
| **Properties (Crystallinity, form)** | Microscopic crystals with grain sizes < 4µm | **Well-developed crystal platelets. Grain sizes range from 40µm and 4 cm (but often less than 1 m), and thicknesses of 1 to 150µm** | Meshed up coarse crystals. Particle sizes ranging from powders to 10cm pieces | 2µm powders to 2cm pieces particle sizes |
| **Origin** | Regional metamorphism of carbonaceous deposits, often coal, or contact metamorphism, which is frequently caused by diabasic or granitic intrusions | **Carbonaceous sediments regionally metamorphosed at or above amphibolite facies conditions.** | Formed as epigenetic veins and lodes in high-grade metamorphic rocks (such as granulites) by metamorphic fluids. | Heat treatment (graphitization) or chemical deposition form, hydrocarbon materials above 2,000 °C produce synthetic graphite. |
| **Orebody** | Layers, seams and lenses in carbonaceous rock, with varying thicknesses, length and may be folded and faulted. | **Strata-bound; up to 33 metres thick; thousands of metres long; tabular or lens shape. Graphite content varies both inside and across lenses, and folds are uneven where the hinges reside.** | Vein and fracture-filling within or crosscutting metamorphic structures and rock contacts. Individual veins are usually less than 0.3m thick but range from 0.05 to 3m. up to 100m long but in less than 10m intervals. | N/A |
| **Ore grade (Percent carbon)** | 50 to 90 | **5 to 30, normally higher** | 40 to 90 | N/A |
| **Deposit tonnage (Million metric tons)** | 0.1 to 500 | **0.1 to 100** | Tiny deposits. | N/A |
| **Mine operations** | Open pit surface mine | **Open pit surface mines. Graphite grades and weathering destruction of gangue minerals enhance ease the of mining.** | Small mines with demanding labour and underground, can be 30 to 400m deep. Ore is hand sorted, washed and screened. | N/A |
| **Product grade (Percentage graphite)** | 60 to 90 | **75 to 97** | 90 to 99.9 | 99.95 |
| **Main uses** | Batteries, steel industry products, paint & coatings, and refractories | **Applications include expandable graphite, refractories, brake linings, lubricants, and batteries** | Carbon brushes, brake linings and lubricants | Graphite electrodes, batteries, carbon brushes, and nuclear moderator rods (porosity unsuitable for refractory applications) |
| **Major producers and resources (in order of production level)** | China, Brazil, Mozambique, India, and Canada (U.S. Geological Survey, 2022) | **China, Brazil, Mozambique, India, and Canada (U.S. Geological Survey, 2022)** | China, Brazil, Mozambique, India, and Canada (U.S. Geological Survey, 2022) | China, Japan, the United States, India, and German (U.S. Geological Survey, 2022) |
| **Prices** | This lower-purity type of graphite was priced between $300 and $500 per ton and is primarily used in less critical applications such as foundries, pencils, and lubricants (Roskill, 2023). | **Prices ranged from $800 to $1,200 per ton. The higher end of this range typically corresponded to larger flake sizes, which are highly valued for applications like lithium-ion batteries. (Roskill, 2023).** | This grade is known for its high purity and large crystal structure. It was priced between $1,800 and $2,500 per ton. It is often utilized in specialized applications that require large, high-purity flakes (Roskill, 2023). | Battery-grade synthetic graphite is priced between $7,000 and $20,000 per ton, reflecting the high demand and stringent purity requirements for use in electric vehicle batteries.<br><br>Industrial-grade synthetic graphite is priced between $3,000 and $7,000 per ton. Due to its lower purity requirements, this type is used in applications like refractories and steelmaking (Roskill, 2023). |

### 2.1.3 Known graphite deposits in Malawi

Several areas in Malawi are known to have graphite concentrations. A notable occurrence is the flaky graphite-enriched deposit of Katengeza in the Salima district, which is believed to contain 2.7 million tons of graphite at a grade of 5.8wt.% carbon (Carter and Bennett, 1973). At Katengeza, the graphite is associated with sequences of kyanite-bearing paragneisses, hornblende–biotite gneisses and quartzo–feldspathic granulites (Habgood, 1962a). However, the lithology of the graphite mineralisation over the larger area has not yet been established because the area has not been explored extensively.

Sulphide (pyrite and pyrrhotite) mineralisation was also identified in the Katengeza area, although not significant enough to qualify for an ore grade for base metal or sulphur (Habgood, 1962b).

However, the age, metamorphic conditions and geological settings of these deposits are similar to the Malingunde area and suggest it is associated with the Pan-African orogenic belt and boosts the confidence of the potential for similar deposits.

## 2.2 Rutile

Rutile develops in diverse geological settings (Choukroun et al., 2005). Rutile occurrences are widespread in metamorphic rocks, igneous rocks, mantle xenoliths, lunar rocks and meteorites; whereas authigenic growth of rutile is also observed in sedimentary rocks. Although titanium dioxide ($TiO_2$) has various polymorphs, the most commonly found natural forms are primarily rutile, anatase, and brookite (Pereira, 2019). Brookite exhibits orthorhombic crystal symmetry, setting it apart from the tetragonal structures of rutile and anatase (Tian et al., 2019). Rutile-bearing quartz veins also serve as potential sites for crystallization in specific cases (Cengiz, 2018).

While rutile is notably associated with metallic ore deposits, the scientific focus has been predominantly on metamorphic rutile as opposed to hydrothermal rutile (Pereira, 2019). In the geological context of Malawi, rutile is prevalent in igneous and gneiss formations (Carter and Bennett, 1973) and for Malingunde is hosted in gneiss formation (Thatcher and Walter, 1968).

Rutile is a valuable heavy mineral in clastic sediments due to its stability and importance as a titanium source (Tonje et al., 2014). Rutile's high mechanical and chemical stability is crucial in weathering, transportation, and diagenesis (Morton and Hallsworth, 1999), making rutile an essential tool for source-rock classification as its trace element and isotopic composition provide insights into source

rocks characteristics; its resistance to abrasion and weathering may indicate the extent of sedimentary processes; and can also help to correlate certain sendimentary features with other source rocks. Silva et al. (2016) assert that sediment composition depends on the source rock and the intensity of chemical weathering. Morton and Hallsworth (1999) also suggest that transport, deposition, and diagenesis can alter sediments during the sedimentation cycle.

Quartz, feldspars, and mica are major components in alluvial sediments, with minor quantities of zircon, rutile, tourmaline, garnet, epidote, and chrome spinel constituting the heavy mineral complement. Predominantly, rutile, zircon, brookite, tourmaline, andalusite, and kyanite constitute the heavy mineral assemblage (Meinhold et al., 2008).

### 2.2.1 Characteristics and Origin

Larger rutile crystal are commonly found within specific geological settings, such as certain granite pegmatites and veins containing apatite and quartz (Deer et al., 1992). These occurrences are closely linked to syn-metamorphic quartz veins observed within the eclogite facies (Gao et al., 2007). Hydrothermal alteration (chloritisation) of Ti-rich biotite (Carruzzo et al., 2006), is another way where secondary rutile is formed. Other than that, it may also develop by the oxidation of ilmenite (Sakoma and Martin, 2002) or the exsolution of titanium from phases like garnet and clinopyroxene that contain titanium (Zhang et al., 2003). Apart from the secondary rutile, there is also primary igneous rutile which usually consists of high concentrations of field strength elements (HFSE: Zr, Nb, Ta); primary igneous rutile grains are generally small, usually 0.04mm to 0.28mm in size. Heavy mineral sands and fine-grained clastic sediments, also known as placer deposits, are the largest sources of sedimentary rutile. These placer deposits can contain zircon, rutile and ilmenite at economic grade concentrations (Dill, 2007). In sedimentary rocks, rutile, anatase, and brookite are formed by diagenesis from Ti-rich pore solutions that result from the alteration of ilmenite, titanite, and biotite. (Valentine and Commeau, 1990).

### 2.2.2 Known Rutile Deposits in Malawi

Chimwadzulu (gem-quality corundum), Thambani (opaque corundum and zircon) and Kapiridimba (kyanite and rutile) in Malawi, are considered placer deposits as there is evidence of accumulation of single crystals and mineral aggregates within the weathering loam and also scattered on the surface (Dill, 2007). Regarding titanium (Ti) placer deposits in East-Africa, Malawi is one of the few countries with significant and noticeable amounts. These deposits include Tengani ilmenite-rutile deposit (Ministry of Energy and Mining, 1997), Mpyupyu Hill heavy mineral sands (Ministry of Mines and

Natural Resources and Environment, 2004), and the western shoreline of Lake Malawi in Salima and Mangochi (Coakley and Mobbs, 2001). Despite being genetically similar, placer deposits can exhibit significant variations in terms of grade from one location to another. For instance, the heavy mineral composition in Salima along Lake Malawi differs from that observed in Lake Chilwa (Dill, 2007).

## 2.3 Vanadium

### 2.3.1 Characteristics and origin

Vanadium, a first-row transition metal with an atomic number of 23, was one of the first discovered in its group. Initially found in vanadinite ($Pb_5(VO_4)3Cl$), its early discovery further underscored its significance. The isolation of pure vanadium involve hydrogen reduction of vanadium dichloride ($VCl_2$) and vanadium nitrate (VN), followed by refining processes involving smelting, leaching, and roasting with calcium metal, resulting in 99.7% pure vanadium from vanadium pentoxide ($V_2O_5$). Commercially, vanadium is sourced from carnotite, vanadinite, roscoelite, and vanadium-bearing magnetite (Sutradhar,2020).

$V_2O_5$ is the most stable vanadium oxide, with other oxides including VO, $VO_2$, and $V_2O_3$). The versatility of $V_2O_5$ in technological applications is due to its diverse morphologies, structures and various synthetic methods (Cestarolli, and Guerra, 2021). Despite its geochemical significance, vanadium has not been extensively investigated compared to other transitional metal elements.

Vanadium is distributed in igneous and sedimentary rocks, with the primary source most likely being local country rocks, especially shales and mafic rocks from the early Paleoproterozoic basement (Kelley et al., 2017). It is often found in oil shale, peat, crude oil, bitumen, and sediments from volcanic regions. It is sensitive to redox conditions and commonly incorporated into clay minerals during diagenesis (Awan et al., 2021).

Vanadium occurs in various minerals and deposit types, including vanadate, shale-hosted, sandstone-hosted vanadium (SSV), and vanadiferous titanomagnetite (VTM) deposits (Kelley et al., 2017).

The main vanadium-bearing ore minerals in VTM deposits are magnetite ($Fe_3O_4$) and ilmenite ($FeTiO_3$), while some occurrences also contain hematite ($Fe_2O_3$), perovskite ($CaTiO_3$), and rutile ($TiO_2$). In addition, vanadiferous titanomagnetite deposits found in mafic-ultramafic layered intrusions, like the Bushveld Complex and Zimbabwe's Great Dike, are currently the primary source of vanadium (Simandl & Paradis, 2022) in Africa (Boni et al., 2023).

SSV deposits often contain barite, carbonates, and quartz, while shale-hosted deposits feature vanadium-rich black shales associated with organic matter. (Dahlkamp, 2010). Vanadates are a type of inorganic compound that encompass polyatomic oxyvanadium (or oxovanadium) ions with a negative charge, containing vanadium in its highest oxidation state of +5. These deposits develop in oxidized zones of base-metal deposits, with descloizite, mottramite, and vanadinite being the most vanadium-rich minerals (Kelley et al., 2017).

In addition to global distribution of vanadium, these various types of deposits and vanadium resources (resources vary from one county to the other and the type of deposit) have been identified in several African countries, which include South Africa, Zimbabwe, Burundi, Mozambique, Madagascar, Kenya, Tanzania, Ethiopia, Uganda, Angola, Burkina Faso, Guinea, Morocco, Mauritania, Namibia and Botswana. Africa's vanadium resources include primary deposits and by-products from other mining activities. The economic viability of these resources depends on global demand, market prices, and the political stability of host countries (Boni et. al., 2023).

### 2.3.2 Known vanadium deposits in Malawi

The literature does not cover the occurrence of vanadium in Malawi much despite records that $V_2O_5$ was one of the compounds (among niobium, tantalum, and zirconium ore) exported from Malawi in 2020 (OEC, 2020).

However, an adjacent country, Mozambique, has seen the discovery of vanadium oxide in graphite projects, for example, Mustang Resources Ltd's Caula Vanadium-Graphite project (Market Screener, 2018), which revealed that $V_2O_5$ can be mined and processed as a byproduct. Therefore, the Malingunde project can potentially mine $V_2O_5$ as a byproduct.

# Chapter 3: Exploration History

SML commenced its exploration activities on the Malingunde project in 2017, primarily focusing on graphite. However, rutile was unexpectedly discovered within the project during the exploration process. This revelation occurred when it was decided to analyse the initial samples for other elements, based on the discovery of rutile traces in the Duwi graphite deposit (SML, 2016), which is located approximately 40km east of the Malingunde deposit, still within SML's exploration license in the central region of Malawi.

The proximity between the Duwi and Malingunde deposits instilled confidence that rutile could also be present in the Malingunde area. Subsequent targeted sampling within the Malingunde deposit confirmed this expectation, leading to an extensive exploration program to delineate the available resources.

It is important to note that this chapter primarily focuses on graphite exploration, as the samples that identified the other elements were collected using the techniques used when targeting graphite. Additionally, while $TiO_2$ results were encouraging, it's worth mentioning that the assay results also presented positive $V_2O_5$ (vanadium) grades, although vanadium was not later targeted in SML's exploration programmes.

## 3.1 Remote sensing

Malingunde is one of the areas predominantly covered by soil, with a few hills and outcrops dispersed. This makes exploring challenging compared to Duwi and Lifidzi prospects, where outcrops are predominant, and the soil cover is lesser and shallower.

Historically, graphite-rich rocks were found in Malingunde and surrounding areas, this was also evident in several boreholes that were drilled for water supplies in the areas and during the investigation of water supply using geophysical methods, including resistivity equipment at the time where graphitic rocks were observed to determine the boundaries of graphite-gneiss presence. The resistant nature of the unweathered graphite-gneisses displayed resistivities of up to $2 \times 10^3$ ohm-cm, which can often be attributed to areas where the graphite flakes come into contact with the gneiss. In contrast, unweathered gneisses with minimal or no graphite showed specific resistivities of $750 \times 10^3$ ohm-cm, frequently surpassing this value (Thatcher and Walter, 1968). Further, remote sensing came in handy, whereby observations of the different colours of soils provided a starting point for the targeting.

The aster imagery in Figure 5 below shows the correlation between remote sensing and graphite mineralisation at Malingunde, using Bands 468. The greyish-to-black response generally correlated to graphitic bands. Greenish and light brown-tinged areas corresponded to grasses or dambo, and reddish brown spots corresponded to heavily forested areas, trees and cemeteries. This was also helpful in identifying the potential targets.

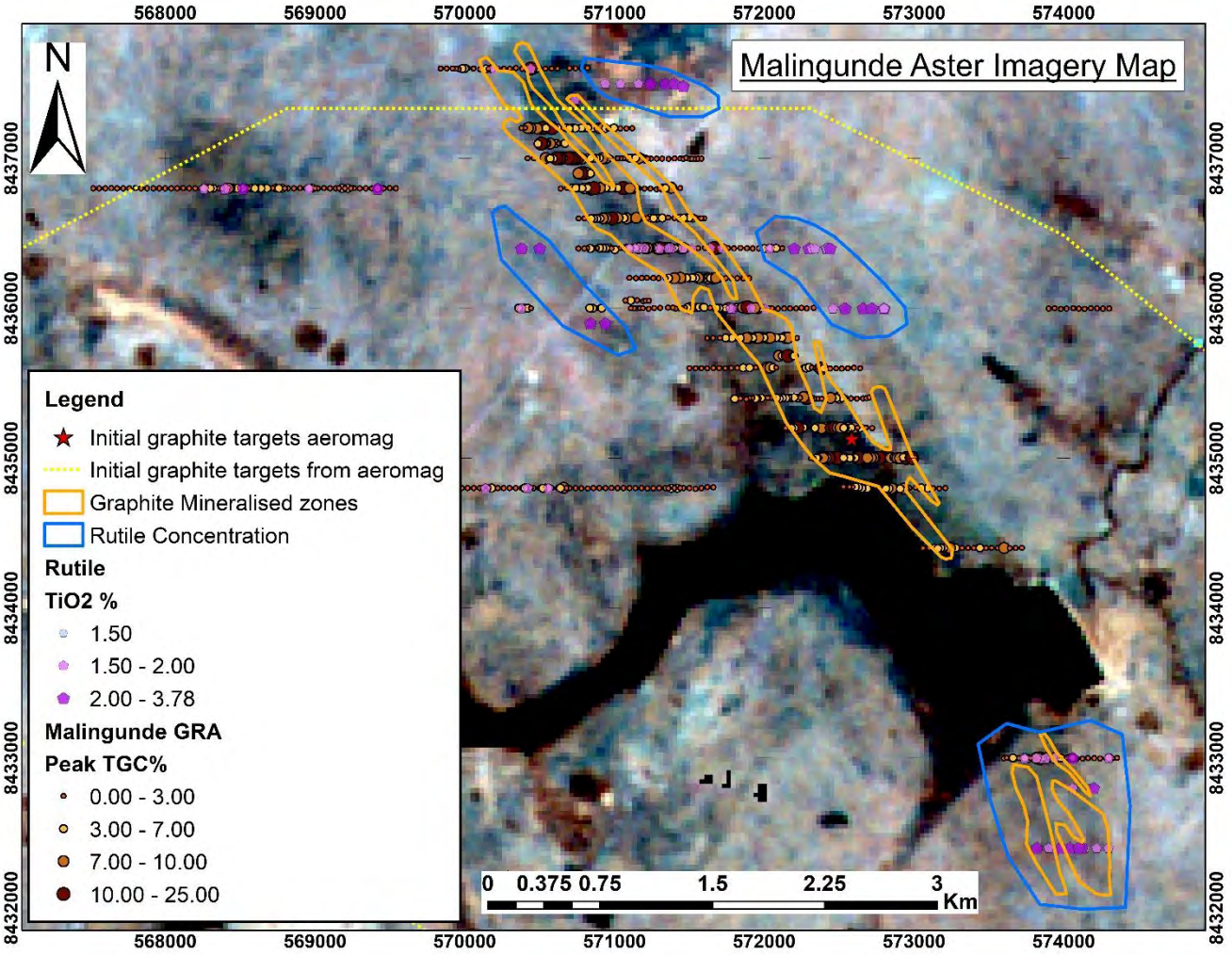


*Figure 5: Malingunde Aster Imagery Map (Generated by Ansel Zabula)*

Prospecting commenced with a ground follow-up using a hand auger as an exploration tool and general soil sampling to at least narrow down the existence of the target area. The hand auger was the quickest and most cost-effective method to cover more ground, delineate the extent of graphite concentration and identify potential targets.

The evidence of graphite's existence around the Malingunde area was also supported by a number of sumps, pits and wells dug by the local community. In addition to that, some small streams also showed some graphite mineralisation, and the local community also used the graphite to decorate their houses, as shown in Figure 6, all this brought confidence to the early stages of exploration.

The initial samples were sent for assay to be tested for graphite (total graphitic carbon - TGC), which revealed various mineralised zones, some exceeding 20% TGC (SML,2017) and then this led to consequent stages of the exploration exercise with the confidence that was gathered

*Figure 6: A house in Malingunde area decorated by graphite (Photo by: Ansel Zabula)*

## 3.2 Exploration geophysics and GIS application

Geophysics and GIS also played a significant role in graphite exploration in the Malingunde deposit. I used ArcGIS to make maps, and analyse data (i.e. assay, geophysical and geochemical data) to understand the relationship between the data by overlaying and displaying the different types of data mentioned above to identify any correlations. Geophysical datasets from magnetic (as shown in Figure 7 below), VTEM, and electromagnetic aerial surveys were linked to the assay results also to establish the relationship between the graphite deposit and GIS and/or remote sensing.

This was a useful tool for identifying and quantifying additional mineralised areas or extensions to mineralisation in the already identified areas. It also helped with the targeting process, especially for potential areas to schedule infills and air-core or diamond drilling.

### 3.2.1 Airborne electromagnetic

Airborne geophysical data that was acquired before SML took over the Malingunde exclusive prospecting licence was used together with information on the area to identify initial targets for explorations, similar to the Albany graphite project in which the EM anomaly was distinguished by its weak magnetic low response (Legault et al., 2015); SML used a similar approach to establish the targets. Therefore, as shown in Figure 7 below, the targets represented by the red stars were the initial targets.

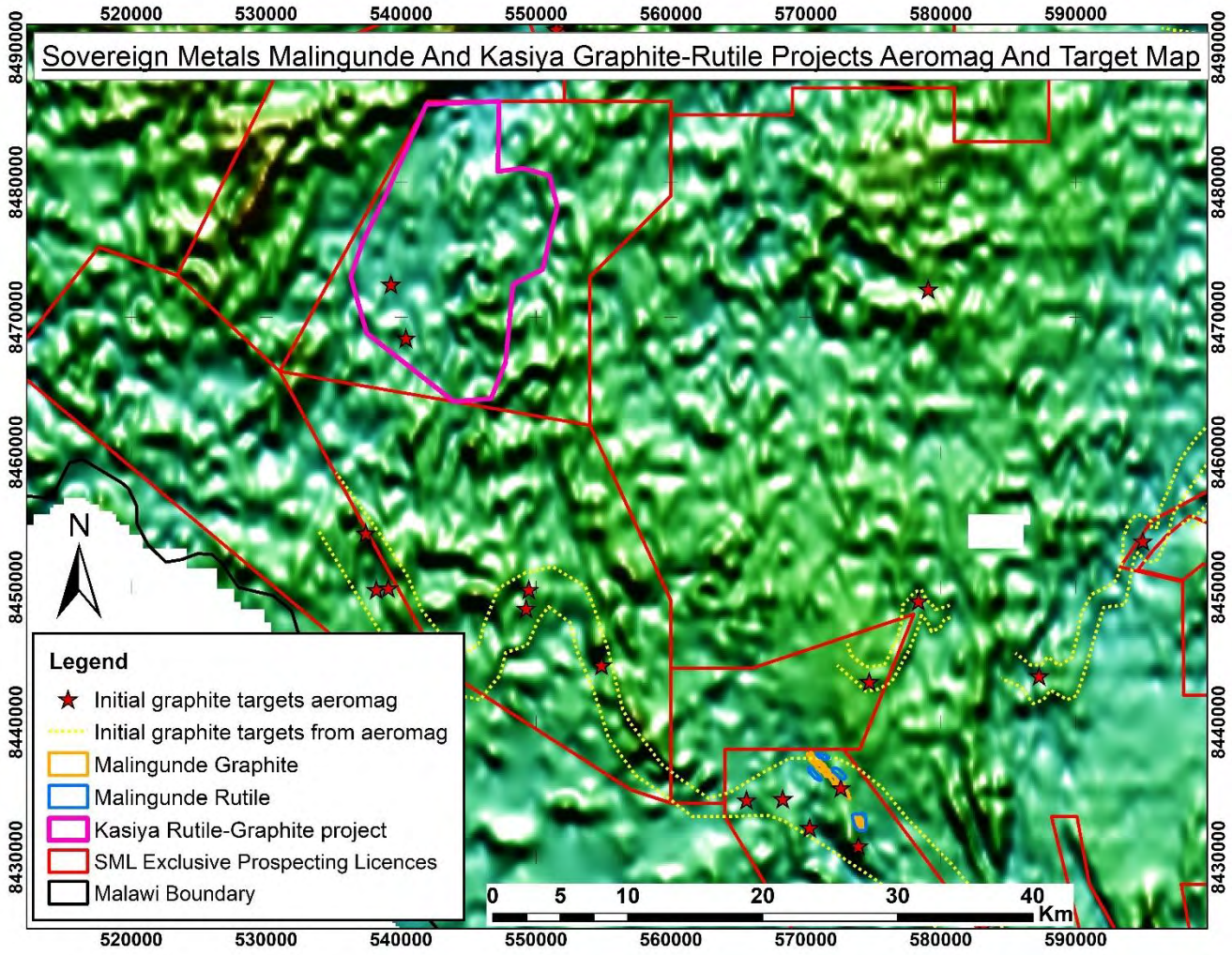


*Figure 7: Sovereign Metals Malingunde and Kasiya graphite-rutile projects and aeromag and target map (generated by Ansel Zabula, aeromag by Malawi Government)*

This was highly used in identifying the target for the graphite exploration, as shown in Figure 7 above.

Later, it was evident when the site work commenced that the graphite concentration in Malingunde was also characterised by the weak magnetic low response, which further helped with targeting.

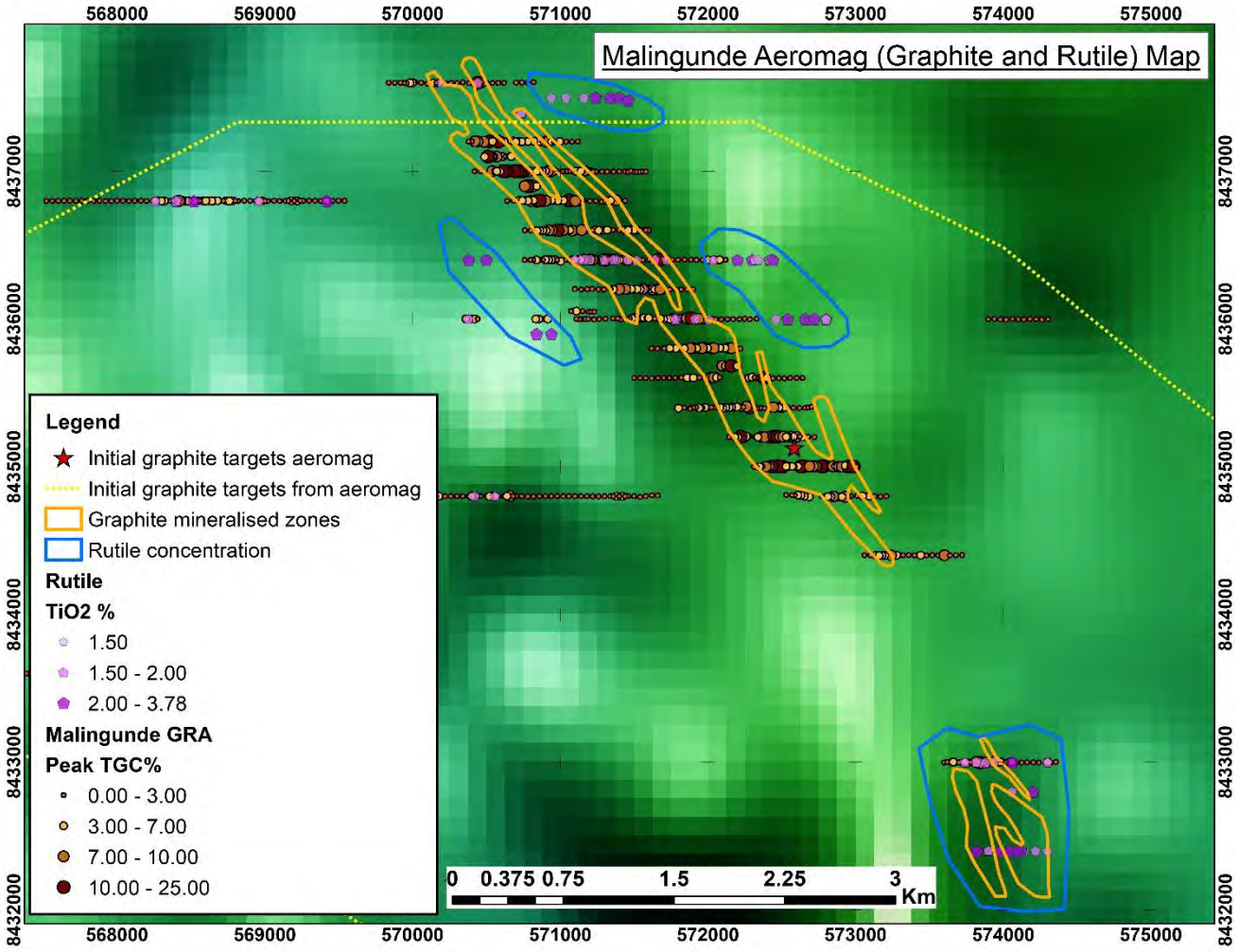


*Figure 8: Malingunde aeromag (graphite and rutile) map - (generated by Ansel Zabula)*

Figure 8 above shows both graphite and rutile concentrations in Malingunde. The initial target, represented by a green star, correlated very well with the graphite concentration and high grades. The lowest EM anomaly (lighter colour) response strongly correlates to a high rutile grade. Figure 8 above also shows that generally, in areas where $TiO_2$ had high grades, there was low or no graphite concentration at all. However, in some places, they occur together, as demonstrated with low to medium grades as shown in Figure 8 above. Ground electromagnetic surveys also validated the aeromagnetic data.

### 3.2.2 Ground electromagnetic surveys

Ground electromagnetic surveys were conducted using MaxMin equipment, which consisted of a transmitter and a receiver connected by a reference cable with 100m distance apart. Generally, the transmitter generates a primary electromagnetic field above the ground, transmitting a signal to the

receiver. During this process, the alternating current passing through can generate an electromagnetic field at various frequencies (e.g. 222Hz, 444Hz, 888Hz, 1777Hz and 3555Hz) with different penetration depths. The presence of a conductive material, such as graphite, results in a detectable anomaly due to its interaction with the magnetic field.

Electromagnetic (EM) methods leverage the ground's response to the propagation of alternating electric intensity and magnetic force fields. Induced currents and their associated secondary magnetic fields exhibit a phase difference from the primary field. Consequently, detected signals can be decomposed into components that are in and out of phase with the primary field (Ernenwein and Hargrave, 2007).

When graphite concentration exceeds the critical percolation threshold, typically at 1 wt%, there is a significant increase in electrical conductivity (Wang et al., 2013), making graphite a good electrical conductor and a target for EM survey. Therefore, during the prospecting stage, ground electromagnetic surveys were also used to identify potential areas of graphite mineralisation. The ground electromagnetic surveys were conducted for Malingunde and regional exploration, including Duwi and Lifidzi deposits.

This technique was then used for the discovery of the Kasiya rutile-graphite project, which has been named the world's largest natural rutile deposit and one of the largest natural graphite deposits with a low carbon footprint on a global scale (SML, 2022). Kasiya[1] project is also owned by Sovereign Metals and is located about 50km North West of the Malingunde project, as shown in Figure 7.

This exercise used previous and new ground electromagnetic survey data compiled and analysed to guide the exploration processes. The data helped identify anomalies with low EM responses, which correlated well with aeromagnetic surveys, remote sensing observations, and other geological indicators of graphite mineralisation at Malingunde (Thatcher and Walter, 1968). This information was used to develop an exploration plan that included the establishment of east-west traverses and the planning of soil sampling and auger drillholes. As part of the exploration plan, targets and E-W traverses were established, and both soil sampling and auger drillholes were planned.

During the exploration, there was a strong correlation between the EM data and the identified graphite mineralisation. This technique was then followed for the rest of the exploration. Unfortunately, the historical data covered limited ground, prompting an intensive EM survey

[1] Please note that the Kasiya project was not included in this thesis because my involvement with Sovereign Metals ended during the initial phases of the Kasiya project, so my contribution to its development was limited.

alongside auger drilling to better understand the ore body's extent before a comprehensive drilling program. This approach yielded promising results.

It was also observed that different frequencies revealed varying intensities of the detected anomalies. For example, a low EM response on line 8436000 correlated well with medium to high-grade mineralisation, particularly in the in-phase 3555 Hz frequency and the 1777 Hz frequency, with corresponding out-of-phase responses at 444 Hz, 888 Hz, 1777 Hz, and 3555 Hz. These frequency-specific responses helped accurately delineate the graphite mineralisation and informed subsequent exploration efforts. Figure 9 is a map showing one section where ground EM was conducted.

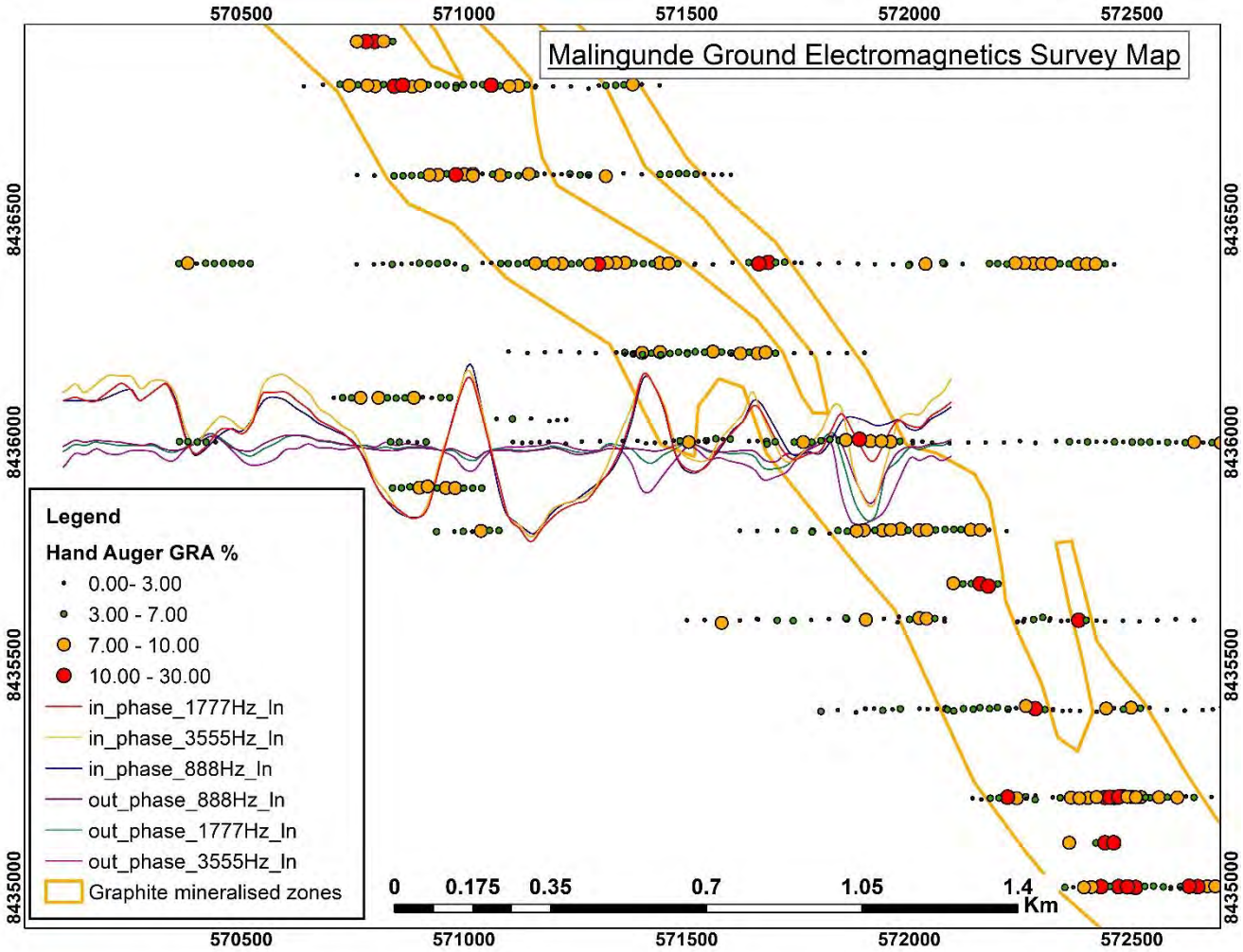


*Figure 9: Maligunde in-phase and out-phase component of frequency domain curves – (generated by Ansel Zabula)*

## 3.3 Exploration Drilling

Due to the few dispersed outcrops found in the area, mapping of the area was not done conventionally. Areas of grades (visual) were located and outlined as shown in Figure 10. The grades were grouped into low (less than 7%), medium (between 7% and 10%), and high grade (above 10%).

Auger drillhole data and soil sampling were vital in confirming the mineralisation zones.

Following remote sensing and geophysical surveys, hand auger drilling was initially used in the area to trace the extent of graphite mineralisation at shallow levels (up to 12m depth) due to its efficiency in terms of time, equipment, and human resources required. It proved to be a faster way to identify and quantify the mineralised zones.

Target lines were identified based on the aster imagery and were 200m spaced (north and/or south). After that, one auger hole was drilled at the centre of the potential target line, then both the east and west directions of the first drill hole (on that traverse) at a specified interval of 40m. If any mineralisation was encountered, infills at 20m were drilled to confirm the continuity of the mineralisation. If there was no mineralisation, the drill hole would be marked as a dead drillhole. However, before closing off that target line, we would still drill 2 to 5 drill holes in both directions to confirm there was no mineralisation. The data was collated, and using ArcGIS, maps were produced for further analysis and for locating the areas of mineralisation. This then gave a direction of the mineralised zone as indicated in Figure 10 below. Drilling continued on a line that intersected mineralised zones until we were out of the mineralised zone, which was confirmed by at least 2 to 3 drillholes drilled at 40m spacing to confirm there is no further mineralisation on that part of the line as illustrated in Figure 10.

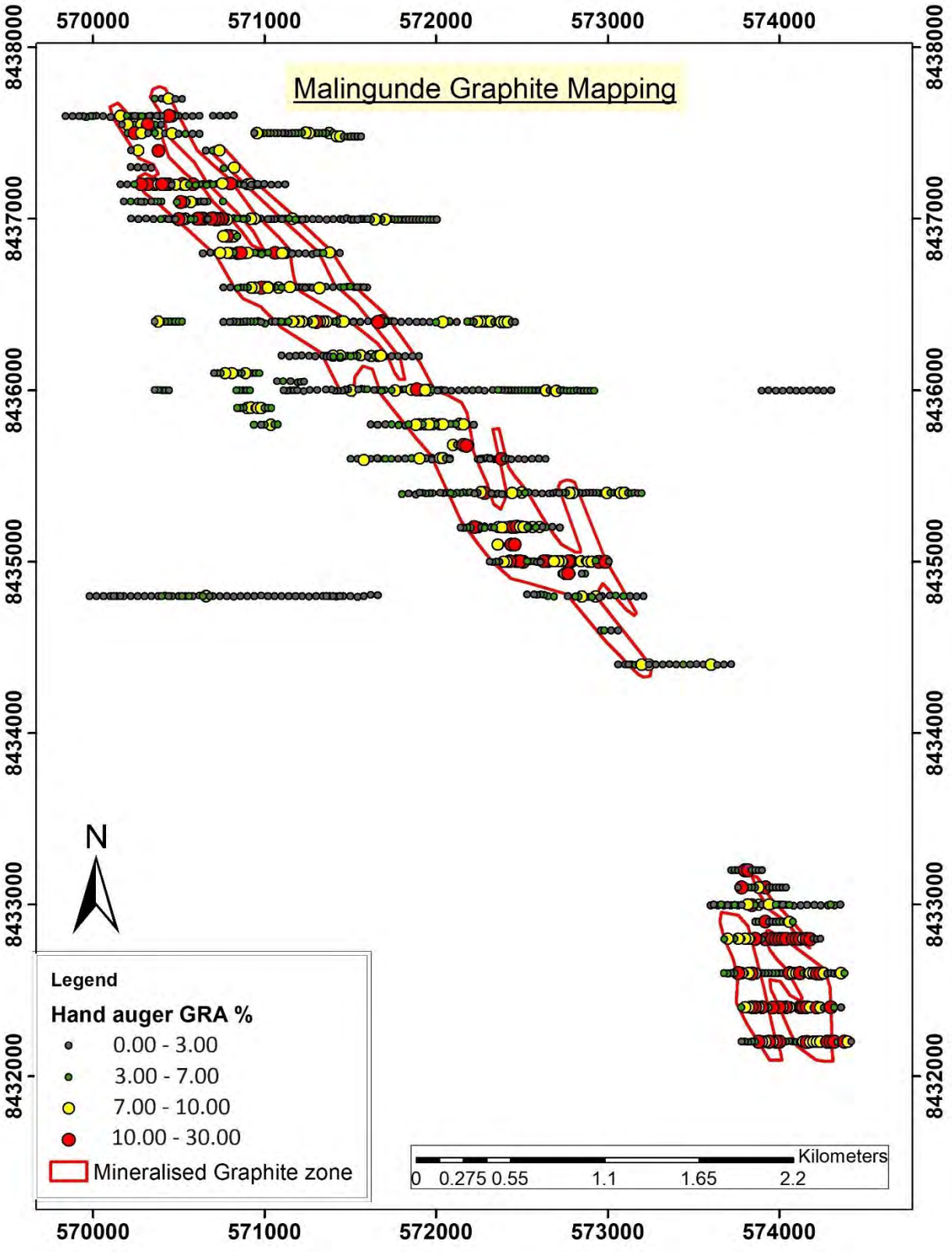


*Figure 10: Location of areas with graphite grade at Maligunde (generated by Ansel Zabula)*

Due to the limited reach of the auger technique due to striking hard rock and poor ground condition, aircore and diamond drilling programme were executed to constrain the depth extent.

Diamond drilling programmes were initiated to assess the extent of mineralisation at depth (upto 25m on average) and the structure to understand the ore body and for geotechnical services as well. Through this exercise, a number of drillholes were drilled and analysed for graphite (Total graphitic carbon) and structural studies were done on the drillcores. The diamond drilling was supplemented by air-core drilling, which was cheaper and faster.

These exploration activities helped locate areas of grade and revealed the extent and depth of mineralisation, which extended up to 33m in some drillhole locations. The depth of the mineralisation was determined by the target, which was the saprolite. However, it should be noted that there is a continuation of mineralisation below the saprolite in fresh rock: this mineralisation was not targeted because of the high cost associatedwith mining and processing methods.

Aircore and auger samples were taken and bagged at 1m intervals, or at strata change. These were split using a 50:50 or 25:75 splitter, depending on the bulk sample size. Then, the sub-sampling for analyses was based on the regolith and visual graphite grades. For instance, 1m interval samples were taken on SOIL, FERP and MOTT. For PSAP, SAPL, SAPR and fresh rock, sampling was done at 2m intervals for medium to high grade (occasionally 1m and 3m intervals where 2m did not permit) and for low grades, the intervals varied from 3m to 5m. These were initially analysed for total graphitic carbon at Intertek Genalysis laboratory services, and ALS Limited.

The remaining bulk samples from the subsamples were safely stored. These samples were subsequently subsampled and analysed for additional elements which led to the detection of potentially interesting concentrations of $TiO_2$ and $V_2O_5$. It is important to note that the initial targeting and exploration focussed primarily on graphite, which is why the exploration techniques used focusssed on electromagnetic and remote sensing. This discovery was the pillar in discovering the Kasiya rutile-graphite deposit because all projects after this also targeted rutile.

It is also important to note that SML did not target vanadium: this has been included in this study a potential mineral that would add value to the project as a byproduct.

# Chapter 4: Exploration Results and discussion

Extensive exploration in the areas revealed that there was indeed a great potential for graphite. This graphite was found in the ferruginous zone, mottled, pallid saprolite, saprolite, saprock and fresh rock. However, as previously discussed, only the regolith was investigated and not fresh rock. The exploration also revealed that the graphite generally occurred at a southeast-to-northwest strike for over 3km and 1km wide, dipping towards the east at about 45 degrees.

The results were positive as shown by the distribution of peak and average graphite concentrations plotted in Figure 11 and Figure 12, respectively.

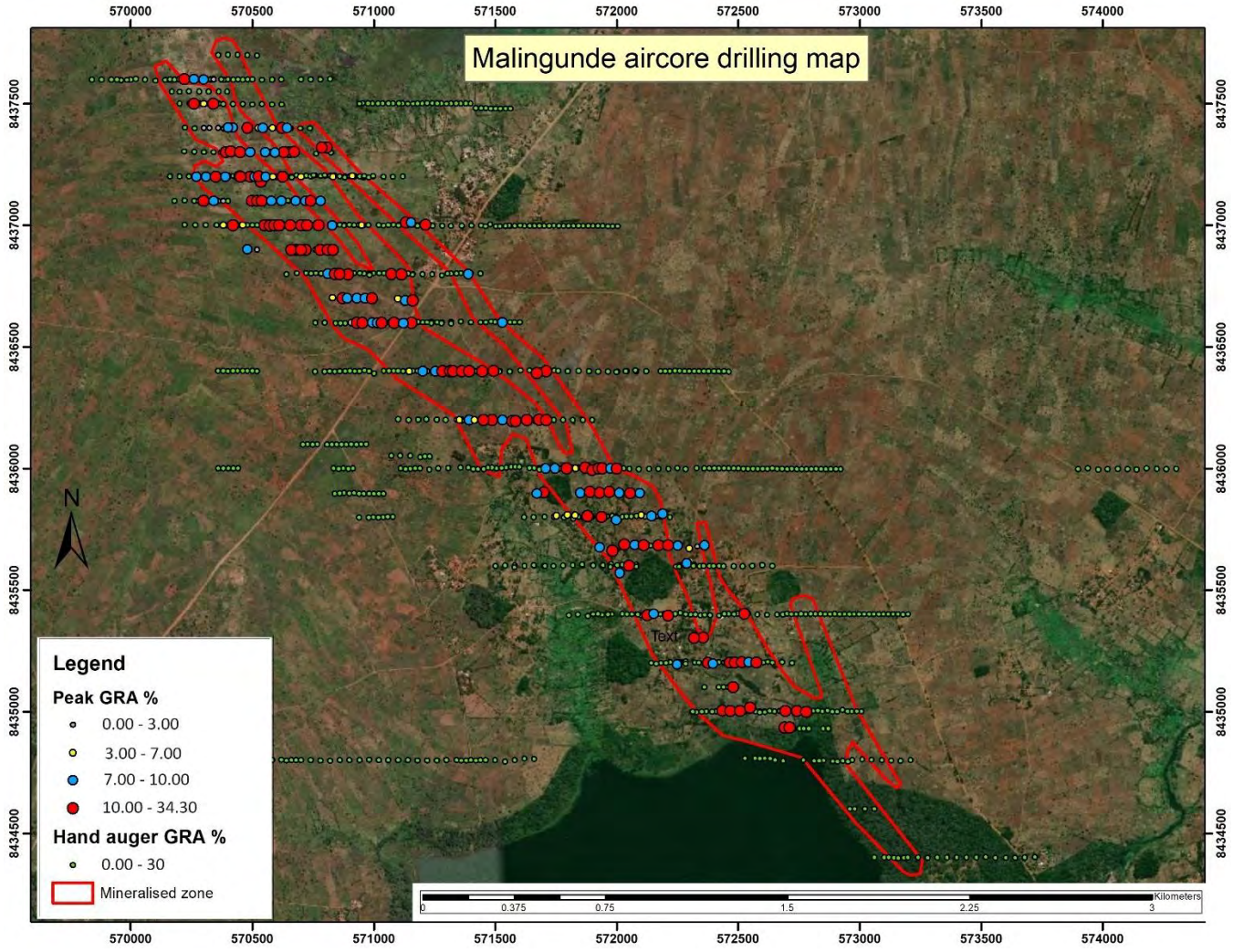


*Figure 11: Graphite mineralisation at Malingunde: Peak graphite content – (generated by Ansel Zabula)*

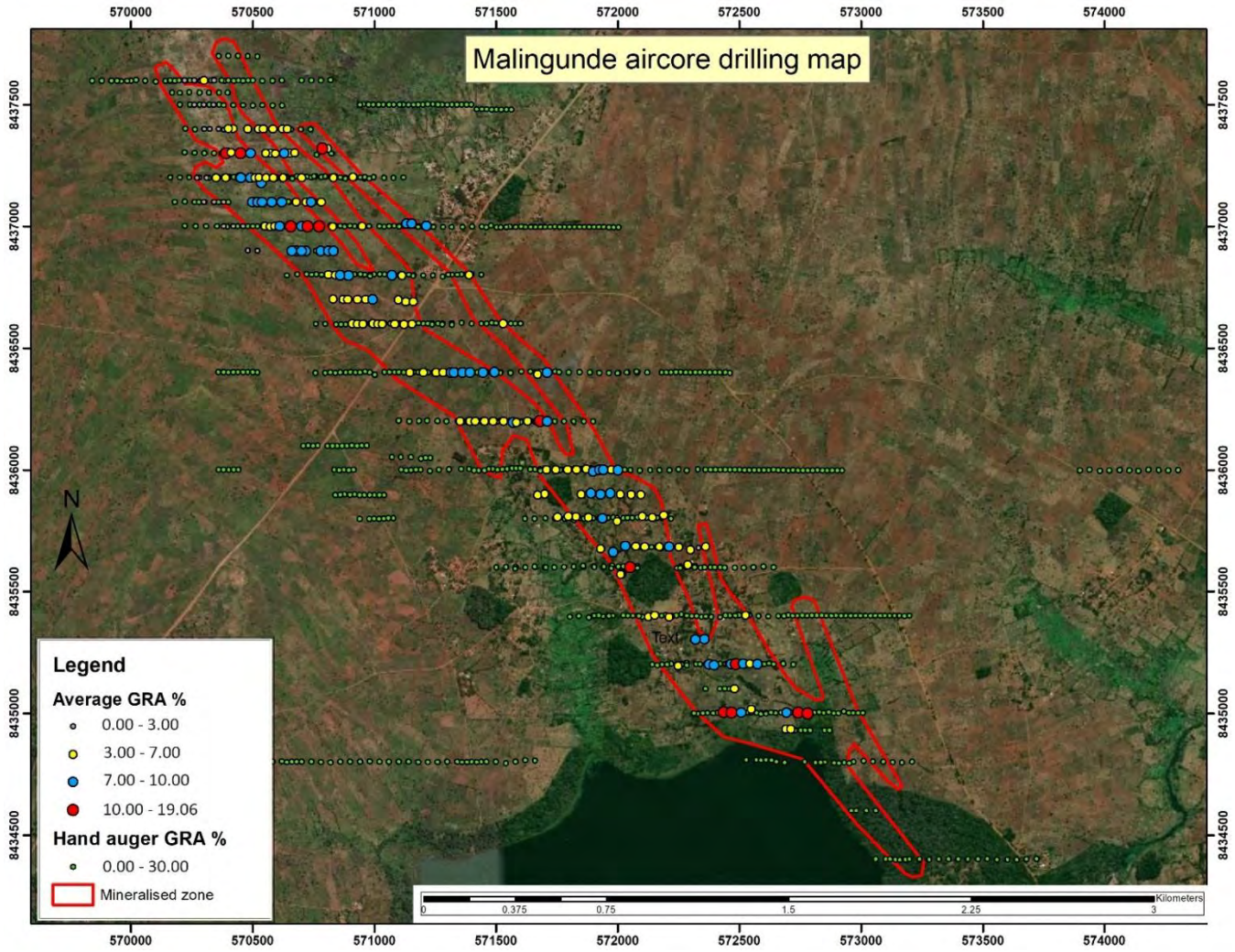


*Figure 12: Graphite mineralisation at Malingunde: average graphite content (generated by Ansel Zabula)*

Following more comprehensive assaying of some samples identified the occurrence of rutile within the graphite regions, all new samples collected were analysed for $TiO_2$ and $V_2O_5$, in addition to TGC.

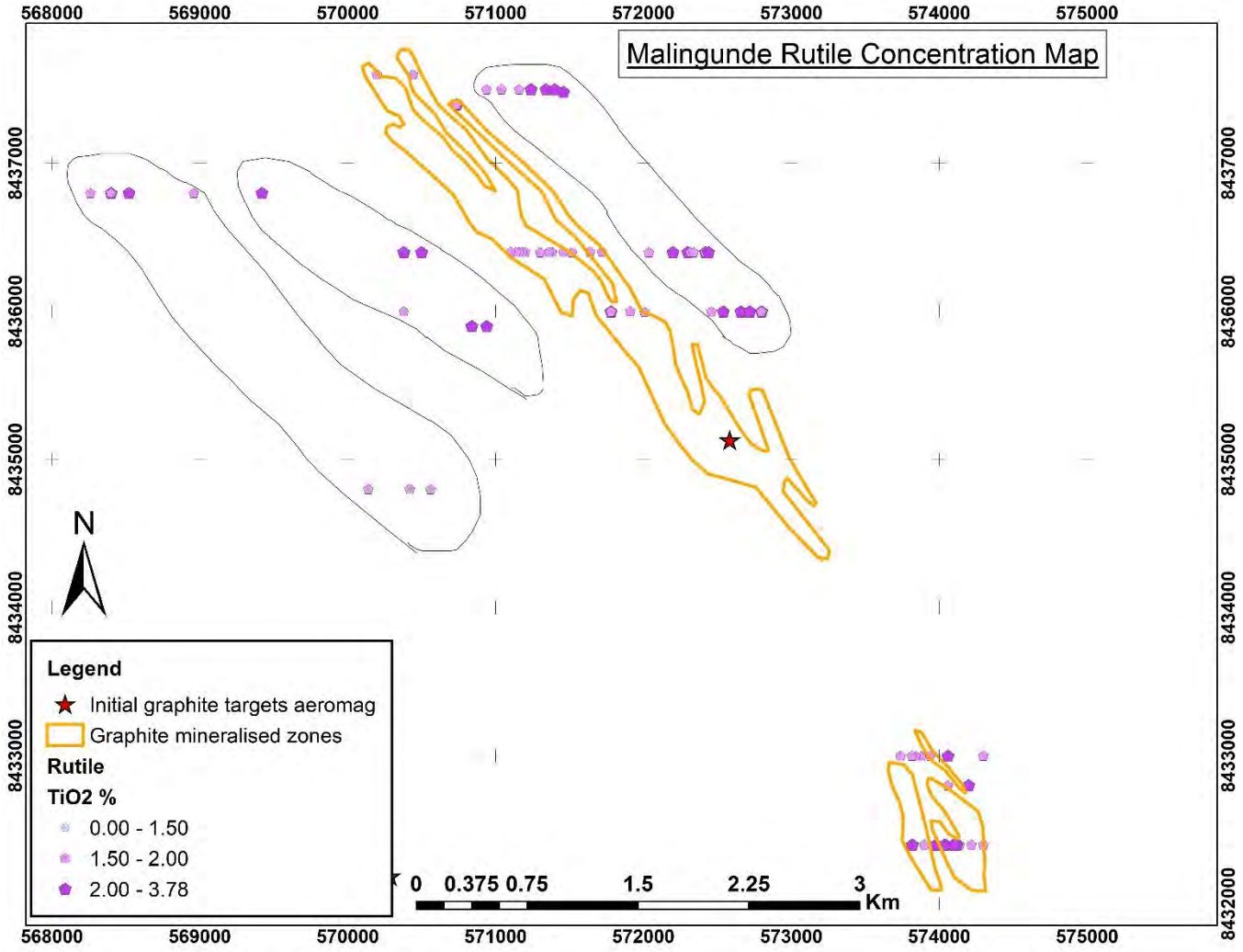


*Figure 13: Malingunde rutile concentration (generated by Ansel Zabula)*

The assay results uncovered a striking trend, showing an inverse relationship between graphite and rutile concentration: with rutile grade decreasing as the graphite grade increases in Figure 13 relative to Figure 11 and Figure 12 above.

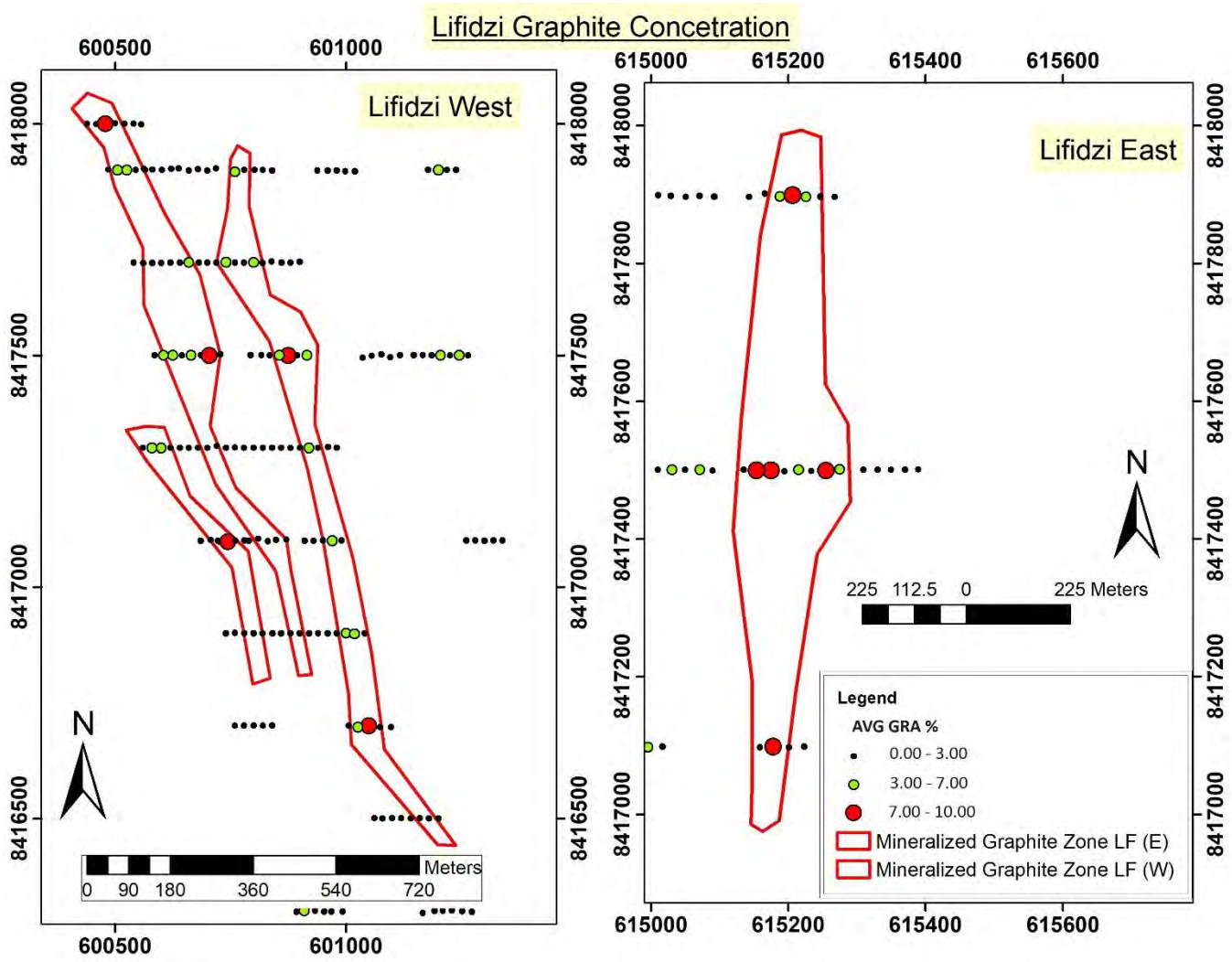


*Figure 14: Graphite concentration in Lifidzi (West and East) – (generated by Ansel Zabula)*

Figure 14 and Figure 15 show identified zones for graphite mineralisation at Lifidzi.

At Lifidzi, the dispersed mineralisation of graphite and rutile made the deposit uneconomical compared to the Maligunde deposit, which has a more concentrated localised mineralisation. As a result, the Lifidzi project was not explored extensively like the Malingunde project.

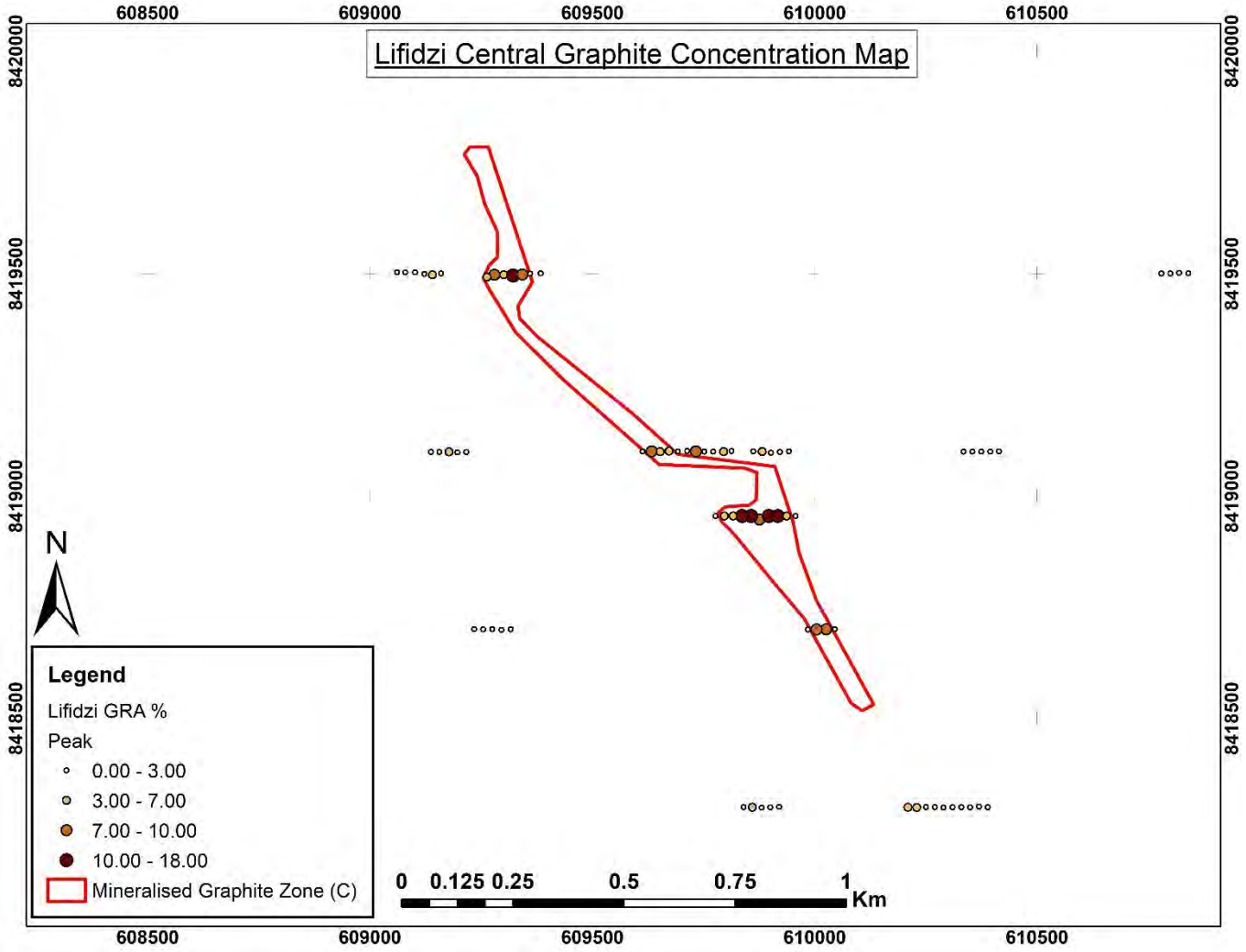


*Figure 15: Graphite concentration in Lifidzi (Central) – (generated by Ansel Zabula)*

However, this area is still important in the long term if a mine is established and production commences at the Malingunde area because these small targets would still be mined and then processed in Maligunde so long as they both fit in the flow sheet, thereby adding value to the project. Therefore, the small deposits around the area cannot be ignored entirely.

## 4.1 Geochemical analysis

In addition to various drilling programmes (auger, air core, and diamond) by SML (SML, 2018), we conducted lithological logging of all drill core and rock chip samples on site. Subsequently, the samples were stored at the company's designated core yard, where further logging was done as and when required, i.e., geotechnical logging and sampling for additional laboratory analysis. After that, subsamples were sent for assay to establish the actual graphite content.

The samples from all three locations (Duwi, Malingunde, and Lifidzi) were analysed at the Intertek-Genalysis and ALS laboratories. For each location, three samples were analysed: soil, weathered rock, and fresh rock. Part of each sample was used for petrographic analysis.

I also compiled and validated the data from Sovereign Metals Ltd and other related information. This exercise included an evaluation of assay results from previous work done by the company.

Below are some of the procedures that were carried out during the research.

### 4.1.1 Geochemical assay results

After SML carried out exploration drilling and soil sampling, the collected samples were sent to Genalysis for assay to identify the elements or compounds present in the area. The analysis aimed to highlight any significant elements or minerals, even though the company primarily focused on graphite (TGC) and rutile ($TiO_2$).

To determine the significant element's chemistry and mineralogy, X-ray fluorescence (XRF) and X-ray diffraction (XRD) were used to analyse various samples from the area. The Borate fusion XRF method was used to analyse the following oxide elements: $Al_2O_3$, $SiO_2$, $Fe_2O_3$, MgO, MnO, CaO, $K_2O$, $Na_2O$, $TiO_2$, $P_2O_5$, $V_2O_5$, $Cr_2O_3$, $ZrO_2$ and $HfO_2$. This was also supported by conducting a quantitative XRD analysis aided by the use of pressed pellets using the diffractometer method to obtain the mineralogy (SML, 2019). Therefore, both XRD and XRF were useful for identifying the minerals present and quantifying their abundance.

From the results, drill hole sections for TGC and rutile were created to demonstrate graphite mineralisation in Malingunde. Below are sections for different grids. These sections correlate very well with the high-grade mineralisation shown in Figure 11.

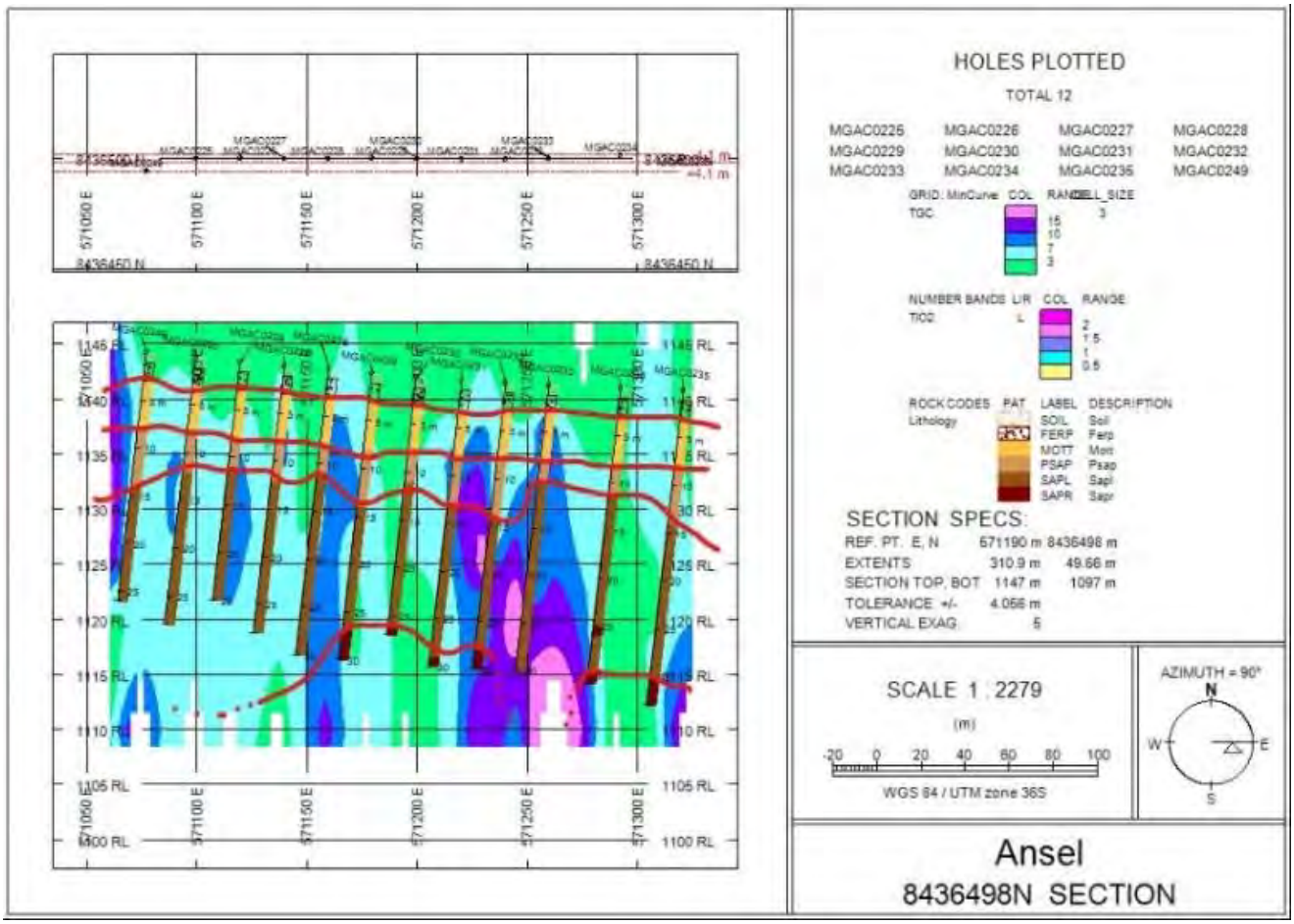


*Figure 16: Malingunde project geological drillhole section 8436498N*

Figure 16 shows section 8436498N from the Malingunde project. This section was dominated by air core drill holes that went as deep as 25m in most cases. There was a planned depth of 25m because, in most cases, the transition of saprolite to hard sap rock was around that depth, so as a guide, that set as a planned depth subject to mineralisation, and the other reason was that SML planned shallow mining. This free dig would only be between the surface and the saprolite. However, this was later changed after the metallurgy results and initial plant designs indicated that the sap rock would also be processed as the saprolite. After that, the planned depth was changed to -30m for subsequent drill programmes, and ideally, at least 2m should be drilled into sap rock once intersected.

Furthermore, Figure 16, demonstrates undulating regolith and shows that the high-grade mineralisation of graphite is beyond the sap rock. The drill holes that intersected the hard sap rock or fresh rock were considered successful as they indicated the extent of the saprock.

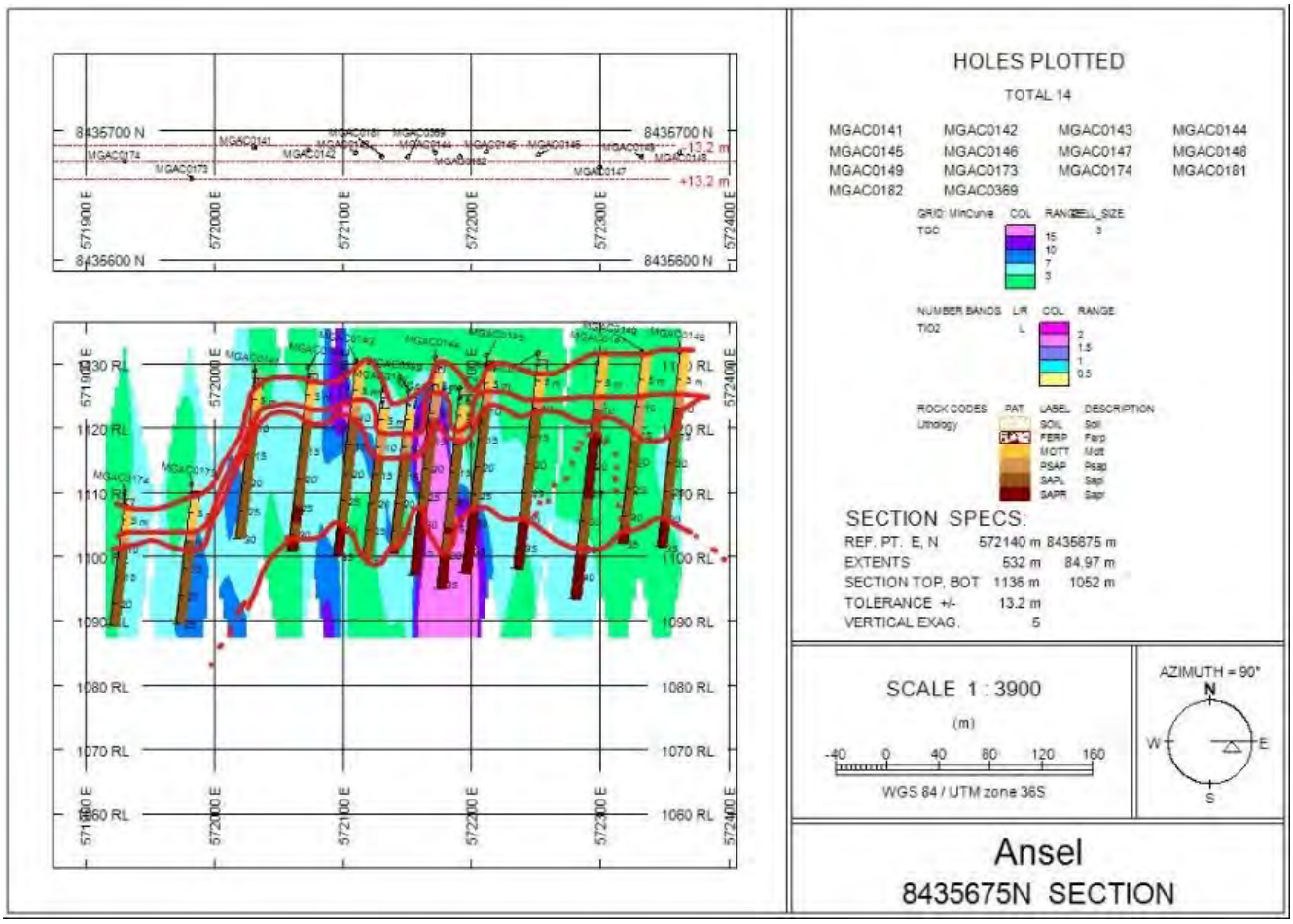


*Figure 17: Malingunde project geological drillhole section 8435675N*

Figure 17, section 8435675N also demonstrates that the high-grade mineralisation extends beyond the sap rock. The high-grade mineralisation is evident even in the fresh rock as shown in Figure 18. While these results were very encouraging, the processing cost of fresh rock defeats the economic viability of this project. Therefore, the initial phase of exploration was focussed on the shallow, free-dig saprolite ore before exploring the hard fresh rock.


*Figure 18: Malingunde diamond drilling (MGDD0003) core tray*

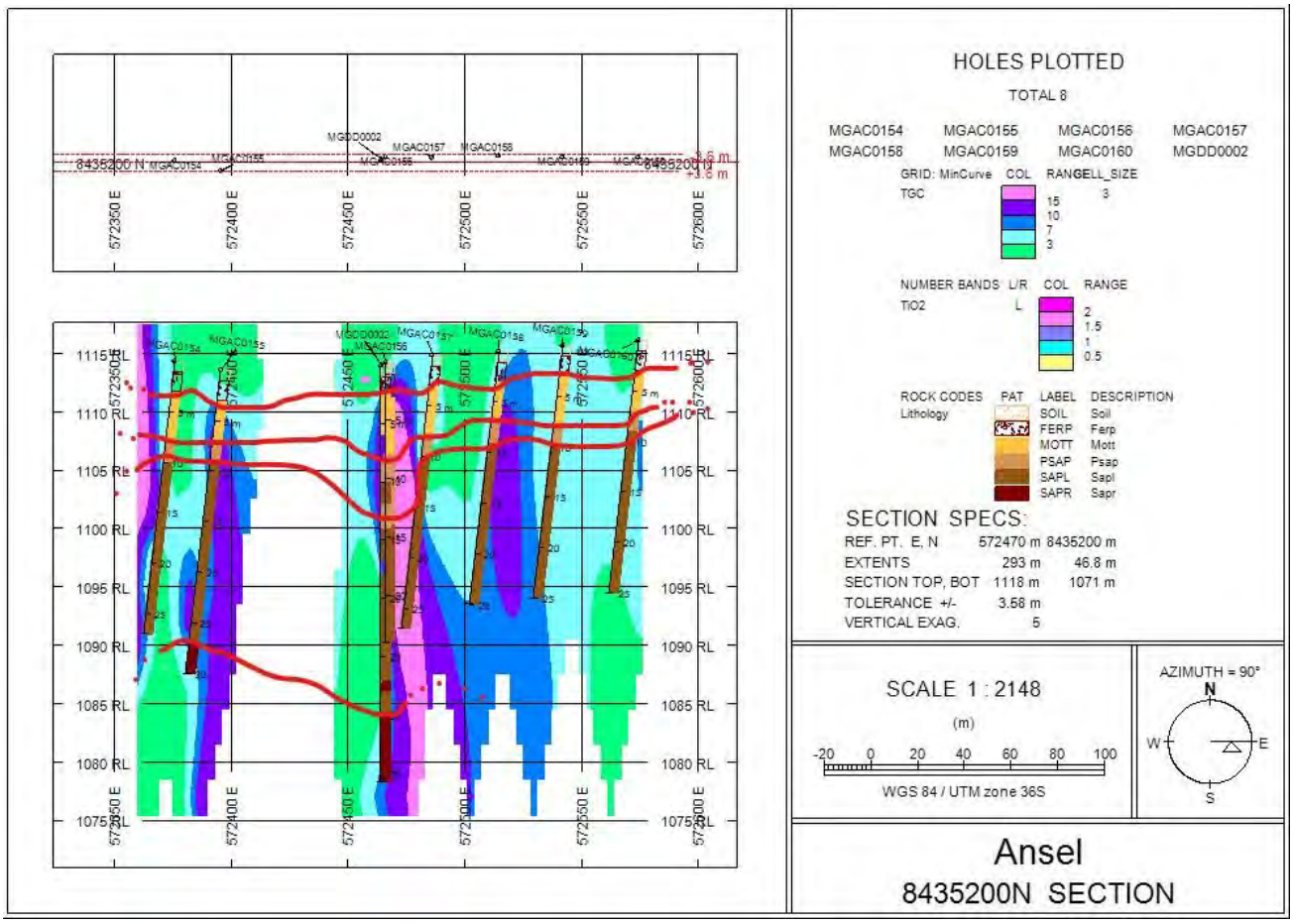


*Figure 19: Malingunde project geological drillhole section 8435200N*

Figure 19, section 8435200N, further demonstrates that the high-grade mineralisation extends beyond the 25m depth, and it also proves the undulating regolith as the diamond core MGDD0002 intersected sap rock at almost 30m on a 90° dip while high-grade mineralisation was still present.

.

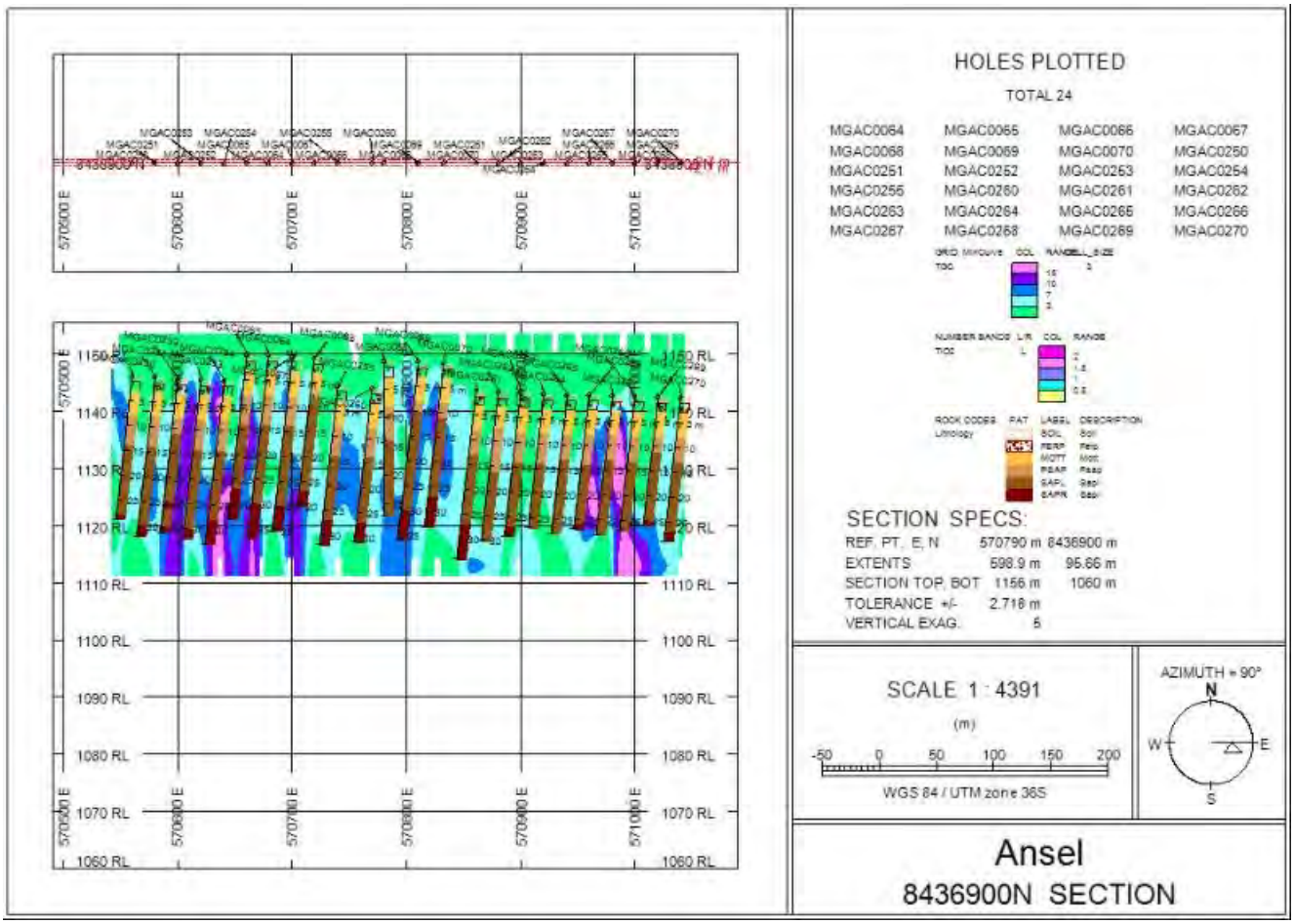


*Figure 20: Malingunde project geological drillhole section 8436900N*

Figure 20, section 8436900N correlates with the high-grade mineralisation shown in Figure 13 (a) which shows two high-grade sections. Throughout the sections, this is evident enough. The sections also give a visual representation of the mineralisation in Malingunde. More sections are found in the appendices (Appendix 8, Appendix 9, Appendix 10).

Further, a correlation matrix and a regression analysis were developed for Lifidzi, Malingunde and regional exploration.

### 4.1.2 Correlation Matrix

Correlation matrices were generated to analyse and quantify relationships between different elements. Positive correlations were used to identify key minerals (rutile and graphite).

*Table 2: Lifidzi correlation Matrix (generated by Ansel Zabula)*

| LIFIDZI | | |
|---|---|---|
| | *$TiO_2$* | *TGC* |
| $TiO_2$ | 1 | |
| TGC | -0.36924 | 1 |
| $Al_2O_3$ | 0.412779 | -0.32867 |
| BaO | -0.10399 | 0.05992 |
| CaO | -0.20142 | -0.07632 |
| $Cr_2O_3$ | 0.232506 | 0.196464 |
| $Fe_2O_3$ | 0.545472 | -0.15282 |
| $K_2O$ | -0.33829 | 0.108603 |
| MgO | -0.01742 | -0.00228 |
| MnO | 0.086217 | 0.119265 |
| $Na_2O$ | -0.42989 | -0.04768 |
| $P_2O_5$ | 0.413614 | -0.061 |
| $SO_3$ | -0.28507 | 0.487096 |
| $SiO_2$ | -0.47608 | -0.06148 |
| $V_2O_5$ | -0.18381 | 0.763246 |
| $ZrO_2$ | 0.58402 | -0.35846 |
| LOI | 0.058385 | 0.774163 |

The $TiO_2$ at Lifidzi, as shown in Table 2, has a medium to positive relationship with $Fe_2O_3$ and $ZrO_2$, with a weak relationship with $Al_2O_3$, $Cr_2O_3$, and $P_2O_5$ while the $TiO_2$ at Malingunde as shown in Table 3, has a weak relationship with $Al_2O_3$, CaO, $Cr_2O_3$, $Fe_2O_3$, MnO, $P_2O_5$, $V_2O_5$, $ZrO_2$. Lifidzi and Malingunde show that $TiO_2$ has a negative relationship with TGC, BaO, $K_2O$, MgO, $Na_2O$, and $SiO_2$ (including CaO and $SO_3$ for Lifidzi).

*Table 3: Malingunde Correlation matrix (generated by Ansel Zabula)*

| MALINGUNDE | | |
|---|---|---|
| | *$TiO_2$* | *TGC* |
| $TiO_2$ | 1 | |
| TGC | -0.06946 | 1 |
| $Al_2O_3$ | 0.281832 | -0.02134 |
| BaO | -0.12568 | 0.360662 |
| CaO | 0.206209 | -0.08625 |
| $Cr_2O_3$ | 0.345836 | 0.040815 |
| $Fe_2O_3$ | 0.379343 | -0.06385 |
| $K_2O$ | -0.41413 | 0.133981 |
| MgO | -0.11096 | 0.023435 |
| MnO | 0.365218 | -0.09899 |
| $Na_2O$ | -0.05752 | -0.01877 |
| $P_2O_5$ | 0.406558 | 0.273792 |
| $SO_3$ | 0.041673 | 0.177813 |
| $SiO_2$ | -0.2859 | -0.38771 |
| $V_2O_5$ | 0.201829 | 0.374959 |
| $ZrO_2$ | 0.497013 | -0.16866 |
| LOI | 0.177258 | 0.881297 |

The TGC at Lifidzi has a very strong positive relationship with $V_2O_5$, and this relationship would be a good guide in further exploring the occurrence of vanadium in the vicinity. The TGC as Lifidzi also shows a weak positive relationship with $SO_3$, $Cr_2O_3$, MnO, and $K_2O$ with a negative relationship with $Al_2O_3$, $P_2O_5$, $Fe_2O_5$, CaO, MgO, $Na_2O$, $SiO_2$, $ZrO_2$. At the same time, the TGC at Malingunde has a weak relationship with $Cr_2O_3$, $P_2O_5$, $V_2O_5$ and a negative relationship with $Al_2O_3$, CaO, $Fe_2O_3$, Mno, and $ZrO_2$. Both having negative relationship with $TiO_2$, $Al_2O_3$, CaO, $Fe_2O_3$, Mno, $ZrO_2$.

Generally, in both Lifidzi and Maligunde, TGC negatively correlates with $TiO_2$. This suggests that the two are not found within the same mineral, and it's also possible that the geological processes that enriched the carbon (C) and titanium (Ti) were different.

This conclusion above was a guideline in the regional exploration, in exploring for rutile on the regional scale, where graphite mineralisation was almost nonexistent in most areas where rutile was abundant, hence Table 4 does not the actual carbon.

*Table 4: Regional correlation matrix (generated by Ansel Zabula)*

| Regional exploration | | | | | | | | | | | | | | | | | |
|---|---|---|---|---|---|---|---|---|---|---|---|---|---|---|---|---|---|
| | *As* | *Ba* | *Ca* | *Co* | *Cr* | *Fe* | *Hf* | *K* | *Mn* | *Mo* | *Ni* | *S* | *Sr* | *Ti (best)* | *V* | *Zr* | *Bal* |
| As | 1 | | | | | | | | | | | | | | | | |
| Ba | 0.188534 | 1 | | | | | | | | | | | | | | | |
| Ca | 0.063909 | 0.044319 | 1 | | | | | | | | | | | | | | |
| Co | 0.005163 | -0.09305 | -0.0323 | 1 | | | | | | | | | | | | | |
| Cr | 0.043036 | -0.00922 | -0.01865 | -0.24367 | 1 | | | | | | | | | | | | |
| Fe | 0.060314 | 0.125706 | -0.03347 | 0.55398 | -0.27114 | 1 | | | | | | | | | | | |
| Hf | 0.079196 | 0.225491 | 0.042475 | 0.313426 | -0.08681 | 0.237377 | 1 | | | | | | | | | | |
| K | 0.235605 | 0.502007 | -0.0178 | -0.47495 | 0.128671 | -0.16401 | 0.001582 | 1 | | | | | | | | | |
| Mn | 0.09364 | 0.251521 | 0.088603 | 0.3664 | -0.15664 | 0.538245 | 0.226343 | 0.024403 | 1 | | | | | | | | |
| Mo | -0.0237 | 0.043758 | -0.01621 | 0.036431 | 0.096324 | -0.03984 | 0.047687 | 0.018914 | -0.02352 | 1 | | | | | | | |
| Ni | 0.021445 | 0.159727 | 0.0417 | -0.29353 | 0.038308 | 0.00632 | -0.05065 | 0.23312 | 0.119195 | -0.0425 | 1 | | | | | | |
| S | -0.00697 | 0.166427 | 0.027466 | -0.06284 | 0.011102 | -0.01605 | 0.059447 | 0.141601 | 0.039401 | 0.033404 | 0.037982 | 1 | | | | | |
| Sr | 0.086433 | 0.269614 | 0.101334 | -0.5417 | 0.212945 | -0.22731 | -0.15571 | 0.514334 | -0.01798 | 0.028625 | 0.238081 | 0.070987 | 1 | | | | |
| Ti (best) | -0.00929 | -0.09736 | 0.01332 | 0.791733 | -0.25377 | 0.264794 | 0.349095 | -0.50649 | 0.163186 | 0.03173 | -0.29411 | -0.06261 | -0.63002 | 1 | | | |
| V | 0.039445 | 0.18038 | 0.009451 | 0.145309 | -0.02669 | 0.068272 | 0.194257 | 0.091479 | 0.140505 | 0.056153 | 0.050068 | 0.030963 | 0.003722 | 0.222764 | 1 | | |
| Zr | 0.116461 | 0.040529 | 0.097321 | 0.11695 | 0.041322 | -0.07832 | 0.329288 | -0.08043 | -0.01219 | 0.035008 | -0.09478 | -0.02223 | -0.11409 | 0.288415 | 0.162452 | 1 | |
| Bal | -0.03921 | -0.02754 | 0.014474 | -0.66658 | 0.381871 | -0.67345 | -0.30089 | 0.344623 | -0.28888 | 0.028355 | 0.169835 | 0.0278 | 0.537889 | -0.67489 | -0.03068 | -0.04664 | 1 |

Furthermore, for the regional exploration, graphite was not significantly visible; therefore, it can also be concluded that at the regional scale, the processes that enriched Ti and C were different and proved that Ti and C were not found in the same mineral.

Regression analyses on $TiO_2$ and TGC Table 5 (full summaries in appendices 1-4) were done on the results for the Malingunde and Lifidzi areas. The regression also agrees that there is no positive relationship between $TiO_2$ and TGC.

Table 5 shows that in Malingunde, the concentration of graphite for each unit of vanadium ($V_2O_5$) was higher than the Lifidzi area. Specifically, the relationship between $V_2O_5$ and total graphite carbon (TGC) in Malingunde indicates that for each unit of $V_2O_5$ discovered, there are 41 units of graphite. In contrast, in Lifidzi, this relationship shows only 10.8 units of graphite for each unit of $V_2O_5$. The observed variation in graphite concentrations suggests distinct geological conditions or processes influencing the association of vanadium and graphite in these two locations.

*Table 5: Graphite and Rutile Result for Malingunde and Lifidzi Regression analysis*

| | Malingunde | | Lifidzi | |
|---|---|---|---|---|
| | $TiO_2$ | TGC | $TiO_2$ | TGC |
| $TiO_2$ | | -0.4428<br>(0.3798) | | -0.8836<br>(0.1321) |
| TGC | -0.0093<br>(0.0080) | | -0.3017<br>(0.0451) | |
| $V_2O_5$ | -0.0915<br>(1.0702) | 41.5140<br>(7.0371) | -0.7006<br>(1.7866) | 10.8846***<br>(2.8974) |
| Multiple R | 0.7977 | 0.7179 | 0.9060 | 0.9848 |
| R Square | 0.6363 | 0.5154 | 0.8209 | 0.9698 |
| Adjusted R Square | 0.6198 | 0.4933 | 0.7990 | 0.9662 |
| Standard Error | 0.3368 | 2.3281 | 0.2980 | 0.5099 |
| Observations | 346 | 346 | 139 | 139 |
| Other compounds | Yes | Yes | Yes | Yes |

Note: Standard errors in brackets. Significant levels P<0.01 ***, P<0.05 **, P<0.1 *

## 4.2 Optical microscopy and scanning electron microscope (SEM)

In the project, petrographic analyses were conducted by Intertek-Genalysis in Australia. Petrographic studies were conducted on polished thin sections to identify minerals with respective textures and relationships with a selected sample.


*Figure 21: Thin section of one of the saprolite samples for the Malingunde project (Edited from SML, 2018)*

The thin section in Figure 21 under crossed polarized lighting of graphitic saprolite ore revealed the presence of coarse rutile grains, each measuring approximately 100 µm in diameter. These rutile grains (rt) are embedded within a matrix that includes clay (cy), quartz (qz), and graphite (gp). The field of view for this section is approximately 800 µm (0.8 mm) across, providing a focused look at the mineralogical composition of the ore. This detailed view allows for the precise examination of the rutile's grain size and morphology, and its relationship with the surrounding minerals. The presence of rutile in this context is significant, as it highlights the mineral's occurrence within the saprolitic environment, providing insights into the ore's composition and potential for further processing.

The rutile concentrate, with an impressive titanium dioxide (TiO2) content of 89.93%, is analysed within a larger field of view measuring approximately 2,000 µm (2.0 mm) across. This expansive view captures a broad sample of the concentrate, showcasing the high purity of the rutile grains after processing. The high TiO2 content indicates that the rutile has been effectively separated from other minerals, resulting in a highly valuable concentrate for industrial applications, particularly in sectors that require high-purity titanium dioxide. The large field of view also allows for a detailed examination of the consistency and quality of the concentrate, providing insights into the success of the processing techniques used.

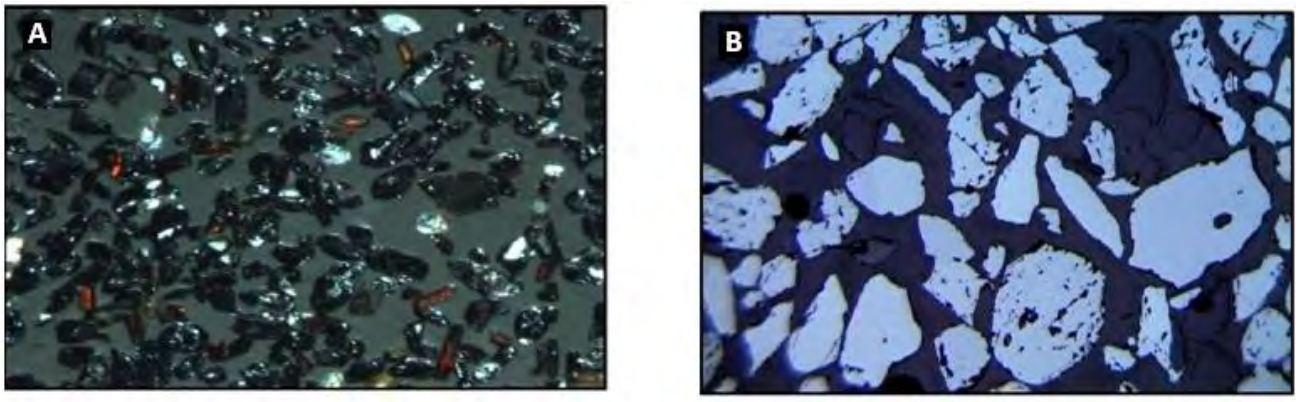


*Figure 22: Loose separated, mineral grains and polished thin section of Malingunde project rutile concentrate (A and B) (Edited from SML, 2018)*

Further analysis of Figure 22 (A, which shows an incident light view of loose separated mineral grains; and B, shows a polished section viewed under reflected light (“ore” microscope)) shows rutile concentrate, which reveals that the grains are clean, well-liberated (separated from the surrounding rock or mineral matrix), and exhibit rounded to sub-rounded shapes. The field of view for this observation is about 1,200 µm (1.2 mm) across, allowing for a detailed examination of the grain morphology and the effectiveness of the liberation process. The rounded to sub-rounded shapes of the rutile grains suggest that they have undergone significant mechanical processing, which has

liberated them from the surrounding matrix and smoothed their edges. This morphology indicates a high-quality concentrate, as the clean and well-liberated grains are likely to be free from significant impurities, enhancing the overall purity and usability of the rutile for various industrial purposes.

In addition to the rutile grains, the observations also revealed the presence of several gangue minerals, including quartz, plagioclase, and kyanite. These minerals are typically visible during field drilling or sampling and are commonly associated with the host ore. Quartz, often appearing as clear, angular crystals, is a prevalent gangue mineral in many geological settings. Plagioclase, a member of the feldspar group, is present in various textures and forms, reflecting its widespread occurrence in different rock formations. Kyanite, identified by its distinctive blue colour and elongated crystal habit, is another common mineral in metamorphic environments. Identifying these gangue minerals in the thin sections provides valuable context for the mineralogical composition of the ore. It underscores the complexity of the separation process required to produce a high-purity rutile concentrate. Understanding the presence and distribution of these gangue minerals is essential for optimising the beneficiation process and improving the overall efficiency of ore processing.

## 4.3 Metallurgical Tests

Metallurgical test work started at an earlier exploration stage to understand the methods of producing final products. It was discovered that the saprolite was the best to start with because it was less complex, and the mining process was less costly, which would help to produce the graphite with less capex and expenditure compared to the hard rock type of mineralisation. During these studies, the graphite in fresh rock was not further investigated due to its implications in processing and the anticipation of the processing costs. This stage is ongoing, at the time of this research a design for a pilot plant and bulk sampling was underway.

The metallurgy tests conducted thus far, have produced significant numbers of 78% to 90% of concentrates, highlighting the potential of leucoxene/rutile concentrate commercial production as a co-product produced from the graphite tailings at Malingunde. More work is being carried out to see if producing high-grade +95% TiO2 rutile concentrate from Malingunde tailings is possible (SML,2019).

## 4.4 Exploration Potential

The exploration strategy, which did not use conventional mapping but commenced from unexplored (covered) ground, followed by tracing and delineating the mineralisation, proved to be effective for

exploring graphite and rutile in central Malawi. This led to the discovery of a world-class rutile deposit and posed a potential for more discoveries in central Malawi and similar environments.

In addition, geochemical, geophysical, and other techniques (e.g., remote sensing) have shown great potential outside the Malingunde project. Figure 23 below shows the targets that have been established to date within the central Malawi prospects.

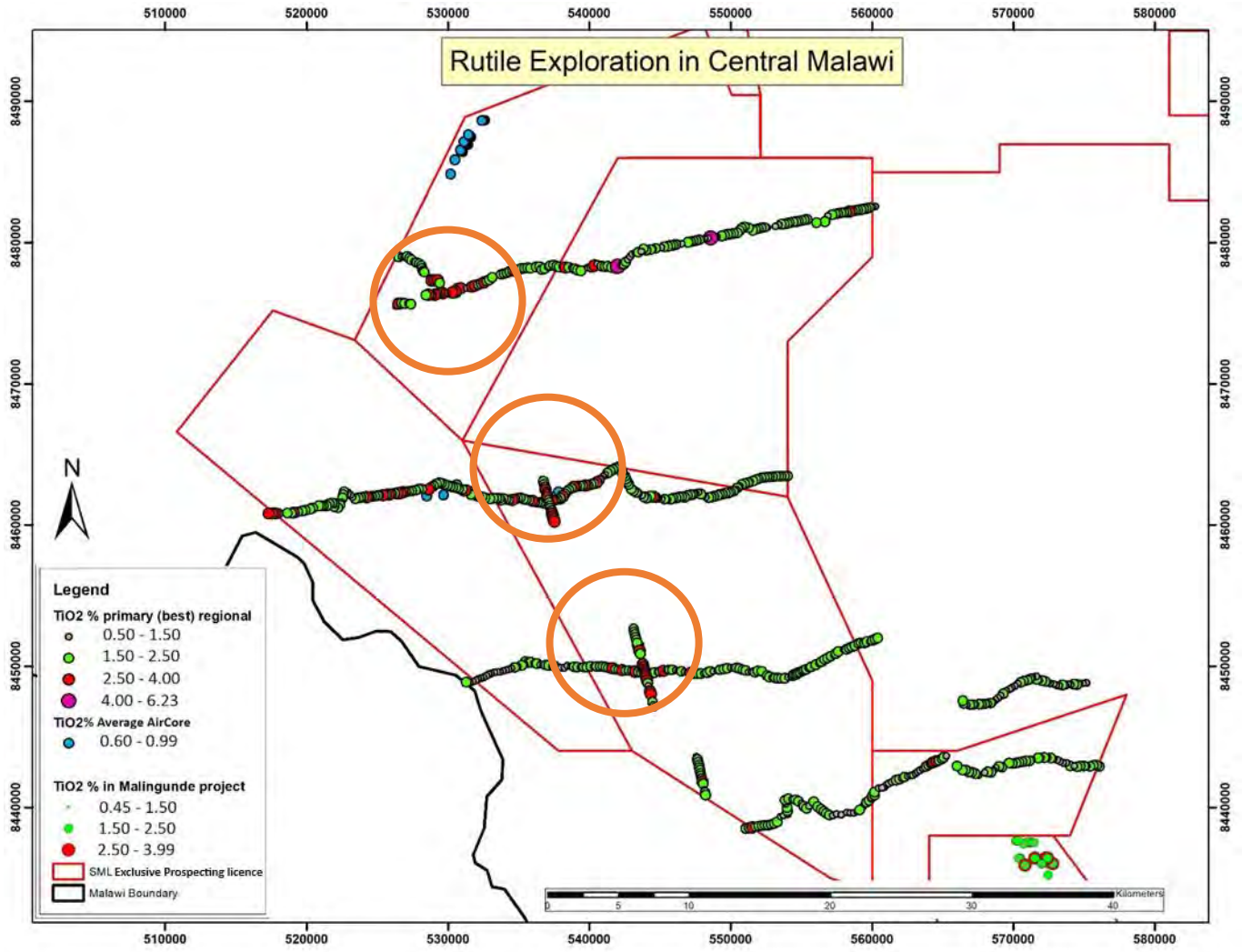


*Figure 23: Rutile regional exploration sampling for SML (generated by Ansel Zabula)*

Figure 23 shows the significant area covered by the regional sampling. The sampling led to the identification of some important high-grade rutile zones. Figure 23 highlights some of the targets that have been identified and assayed. This analysis will facilitate further stages of investigation and drilling to define the resource. Additionally, this process has identified the types of deposits present, which are placer and residual, as confirmed by distribution and subrounded grains shown in the thin sections. These subrounded grains suggest that the grains have been transported and deposited in this region.

In areas adjacent to the SML licences, Mkango Resources Ltd, is exploring for rutile as the neighbouring licence also shows potential. Initial stages of exploration revealed good grades of rutile, anatase and ilmenite mineralisation. The $TiO_2$ grades ranged from 3.17 to 4.09%. Similarly, the mineralisation was also identified to be hosted in saprolite (Mkango (2020), like the Malingunde deposit.

### 4.4.1 Vanadium pentoxide potential

While vanadium pentoxide ($V_2O_5$) was not targeted or given attention by SML, it has shown a significant correlation with the graphite at both Malingunde and Lifidzi (Table 5). In the author's opinion, more research is needed on the graphite-vanadium correlation as $V_2O_5$ would be mined as a byproduct, which could be stockpiled and sold if/when demand increases or if an offtake agreement could be secured.

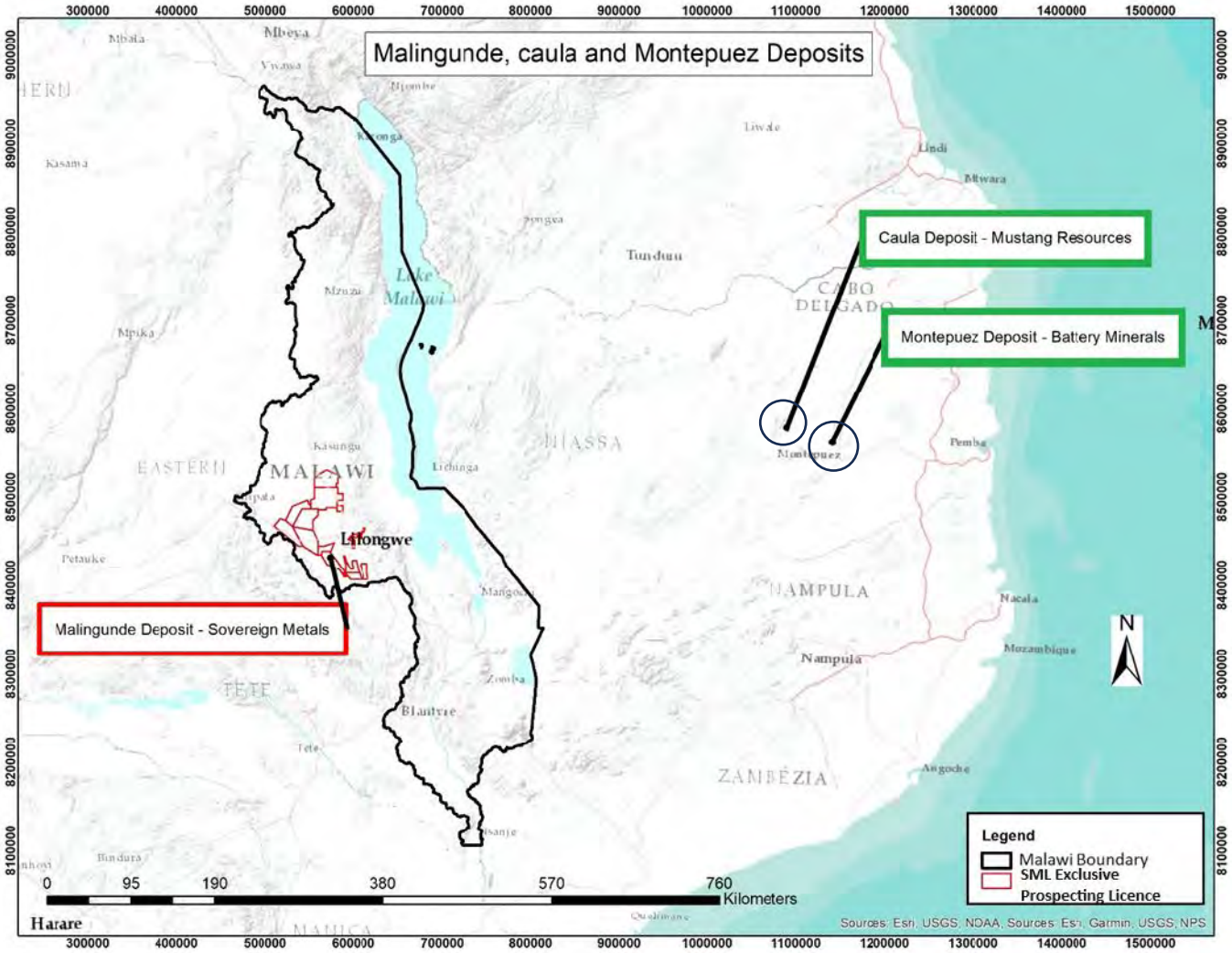


*Figure 24: Malingunde deposit proximity from Caula and Montepuez projects (Source: Ansel Zabula)*

Figure 24 shows two companies, Mustang Resources Ltd (Benton, 2020) and Battery Minerals (Battery Minerals, 2019) that have discovered $V_2O_5$ in their Caula and Montepuez graphite projects, respectively, in Mozambique. These two projects are about 600km east of the Maligunde deposit. These companies are exploring the potential of the $V_2O_5$ as a byproduct, which should also be explored for Lifidzi and other related projects.

## 4.5 Mineral resources and Reserves

The exploration carried out at the Malingunde deposit reveals that it is a large graphite deposit, covering about a 3.4km drilling strike and 120m wide, averaging visual coarse and jumbo flake graphite.

The maiden mineral resource estimate (MRE) for the Malingunde deposit reported 65.1 Mt at 7.1% TGC. This MRE defined 28.8 million tonnes of graphite in saprolite at 7.1% TGC, 17.0 million tonnes in sap rock at 7.0% TGC and 19.3Mt in fresh rock at 7.0% TGC. A total of 9.5mt at 9.5 % (% C) was reported as ore reserves for the Malingunde project (SML, 2018).

Lifidzi deposit has not been investigated sufficiently to define a resources.

No rutile resource has yet been defined for Malingunde.

# Chapter 5: Markets and economic analysis

This chapter analyses the global market for graphite, rutile and vanadium. The analysis includes their uses, demand, supply, global reserves, production, and the countries that are dominating in these commodities.

## 5.1 Graphite

### 5.1.1 Uses, demand and supply

Natural flake graphite is mainly used in refractory, foundries and crucible sectors with the refractory industry being the major consumer of flake graphite. Magnesia-carbon bricks: a mainstream, refractory brick commonly used in the steel industry, is the main refractory product consuming flake graphite. In addition to that, natural flake graphite is also used in batteries (e.g. lithium ion battery anodes) and as an industrial mineral.

Figure 25 below shows the projected demand for graphite by sector by 2026.

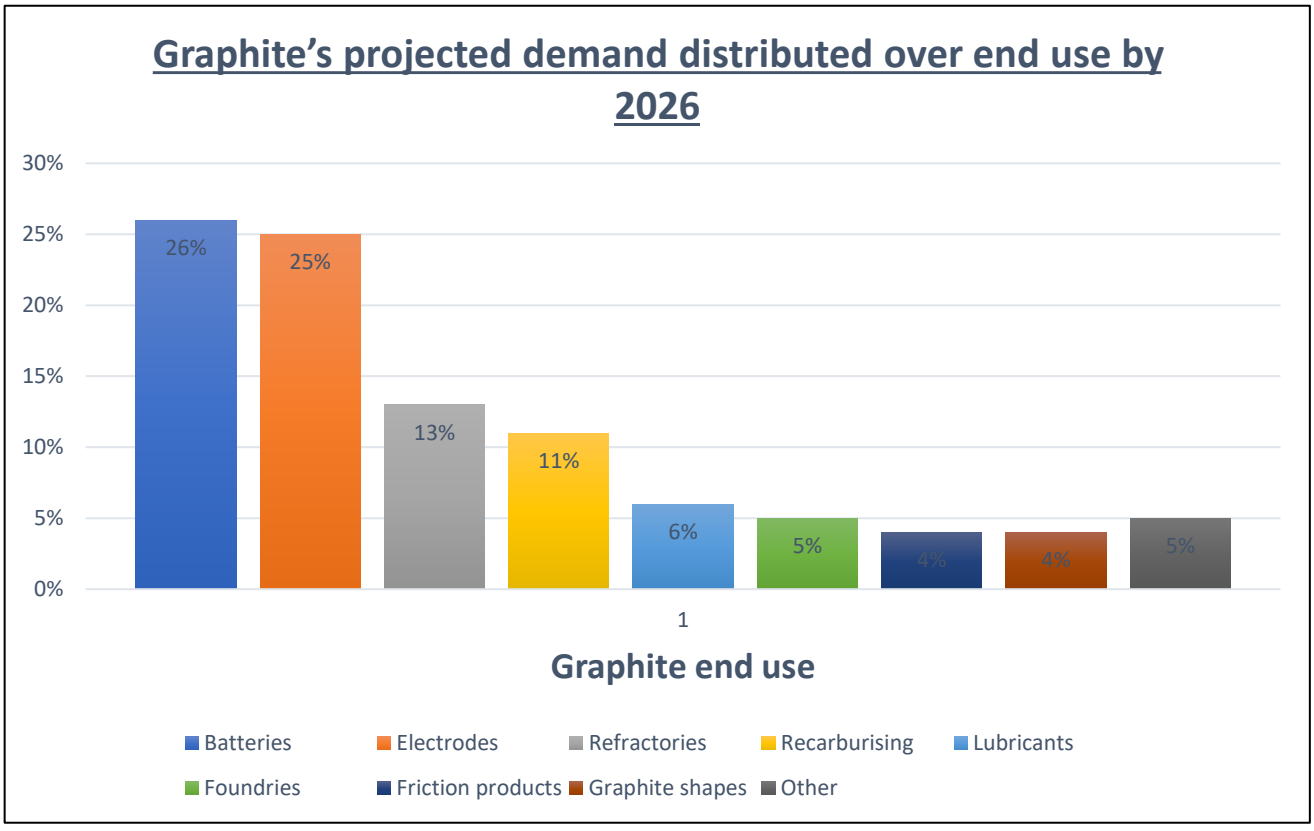


*Figure 25: Graphite's projected demand distribution by end use by 2026. (Source: Ansel Zabula, regenerated from Ritoe et al., 2022)*

The lithium-ion battery sector is the major emerging market for flake graphite. Electric vehicles are expected to increase the demand for natural flake graphite. China continued to lead worldwide

production despite announcing export restrictions in 2022. In 2023, China exported 58,000 tons of flake graphite compared to 81,000 tons in 2023 which already affects the global supply. The restriction will affect the availability of graphite in the global market, and therefore, efforts are being made to diversify graphite supply sources (U.S. Geological Survey, 2023).

### 5.1.2 Historical production

In 2023, China produced 1.23 million metric tons of graphite, accounting for 76-77% of global supply and solidifying its dominance in the market. While China's production has grown significantly, it is expected to continue increasing at a slower pace until 2027. Other major graphite producers include Madagascar, Mozambique, and Brazil. (U.S. Geological Survey, 2024).

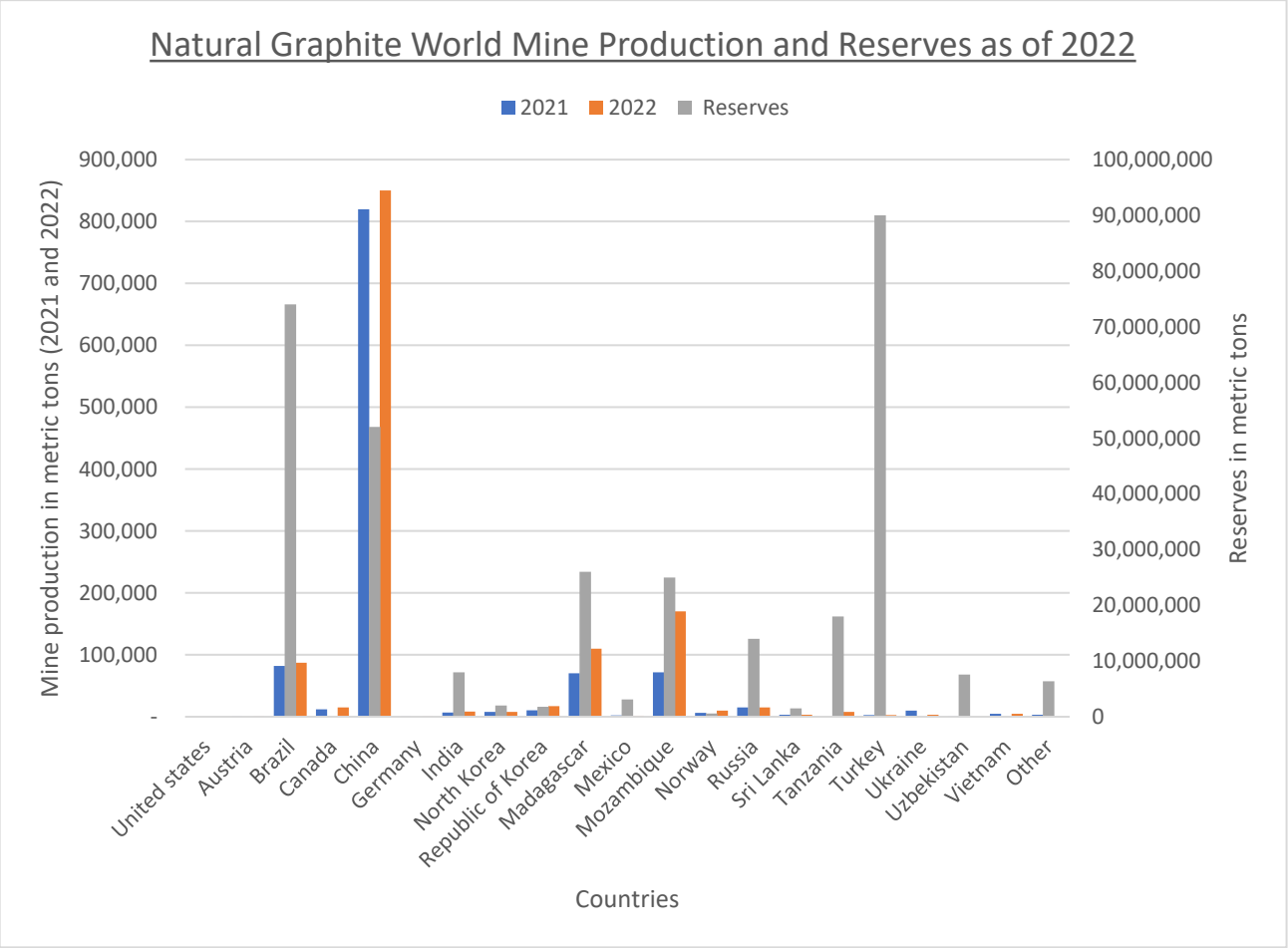


*Figure 26: Natural Graphite World Mine Production and Reserves as of 2022 (Source: U.S. Geological Survey, 2023)*

Figure 26 shows production figures and reserves for 2021 and 2022: clearly shows that China continues to lead the production of graphite. It was also noted that despite China being the biggest producer, in terms of graphite reserves, it comes second to Turkey, which has the largest reserves in terms of volume. Turkey was estimated to have 90 million metric tons of natural graphite reserves in 2023 (Appendix 11). Despite Russia and Ukraine not being the biggest producers of graphite, the war

between the two countries has seen a decrease in production in Ukraine. However, Russia's production has remain the same during the war irrespective of United States and other countries sanctioning Russia in terms of trade, with an aim of getting rid off Russia's graphite from the global market (U.S. Geological Survey, 2023).

Natural graphite reserves at the Malingunde graphite project are estimated at 9.5 million metric tons, with 32% and 68% being in proved and probable categories, respectively (Sovereign Metals Limited, 2018). Therefore, comparing the Malingunde project reserves alone by country as of 2022, as shown in Appendix 11, the project would be ranked number 8.

## 5.2 Rutile

### 5.2.1 Uses, demand and supply

There is significant economic importance in rutile because of its usage in the manufacturing of white titanium dioxide pigment which is very essential in some day-to-day life products. Heavy mineral sands have been an exploration focus worldwide because of their abundance in rutile (Meinhold, 2010)

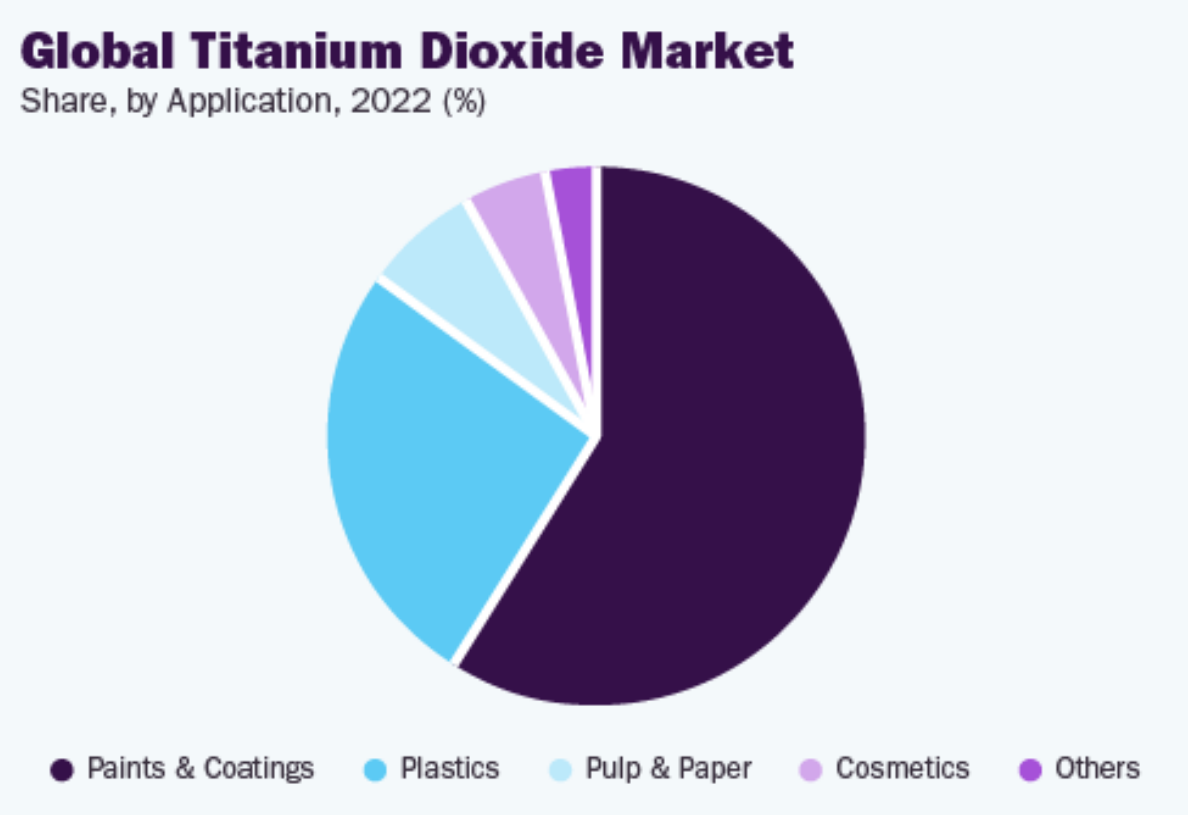


*Figure 27:Global Titanium dioxide market share ( source: www.grandviewresearch.com)*

Titanium dioxide white pigments have a significant application in paint manufacturing, which contributes 51% of total production, 19% is used in paper and 17% in the plastic industry. Additionally, titanium dioxide is utilised as a UV absorber in high sun protection factor sunscreen creams, as well as in ceramics, coated fabrics and textiles, floor coverings, printing ink, roofing granules, food colouring (E171), tablet coating, and toothpaste (Gambogi, 2008). Figure 27, summarises the general uses of titanium dioxide by market share.

Clearly, rutile has so many uses and applications and almost all the uses mentioned above play an essential role in daily life as a result the demand for rutile will continue to grow unless there are alternatives Meinhold (2010). Figure 28 shows the market size of titanium dioxide in the United States, both historically and forecasted to 2025.

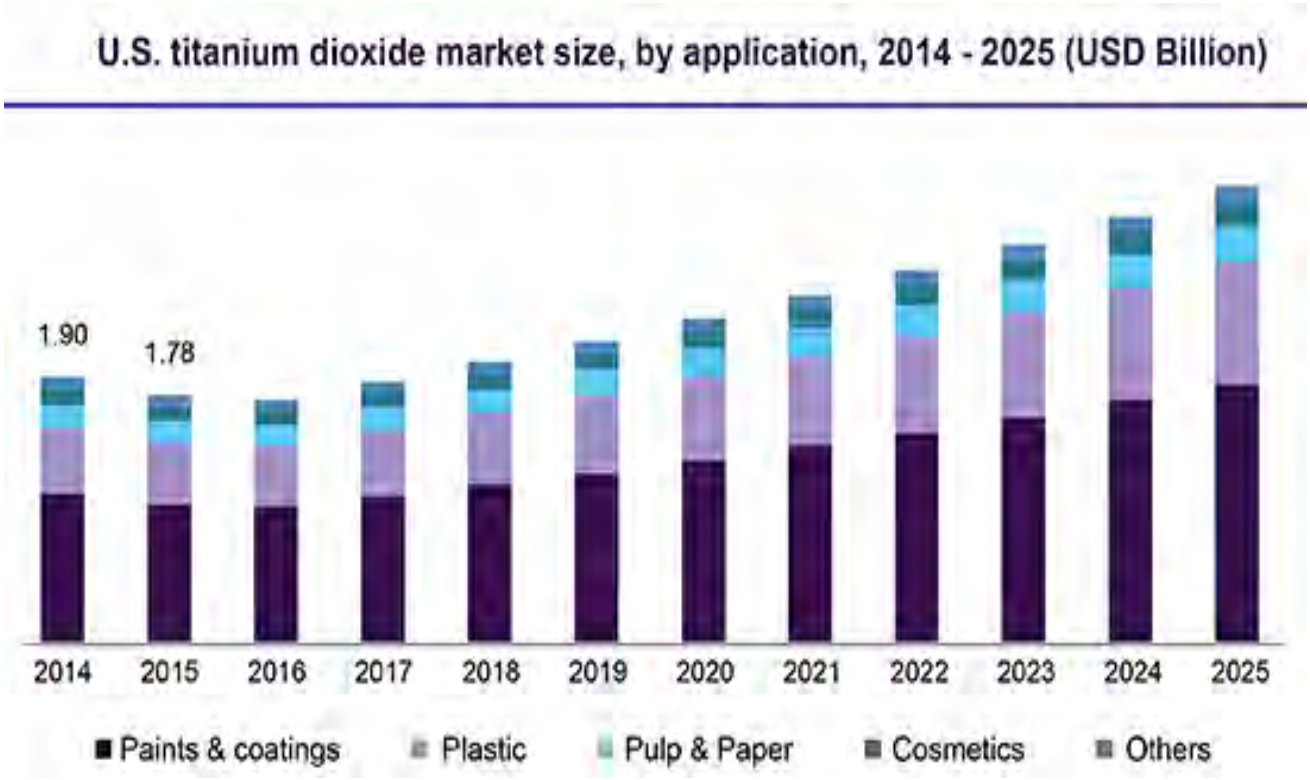


*Figure 28: U.S Titanium dioxide market size (source: www.grandviewresearch.com)*

Ilmenite and rutile-enriched heavy mineral sands (placer deposits) contribute significantly to the supply of natural rutile (Pirkle et al., 2007). Out of this, most of the world's titanium minerals demand is supplied by ilmenite (USGS, 2024). As a result of a volume limitation with rutile placer deposits which are also depleting at a fast rate, makes the rutile supply challenging in terms of fulfilling the world's demand (Korneliussen et al., 2000). Sierra Leone has one of the world's largest sedimentary deposits and largest rutile mines but clearly cannot meet the demand, thereby creating the potential for the Malingunde project to be a success and contributing to the rising demand for rutile.

In 2022, the value of global titanium dioxide was pegged at approximately USD19 billion and expected to keep growing at a rate of 6.3% annually (CAGR), the dominant application was paints and coatings which, accounted for over 59.3% of the market (Grand view research, 2023).

### 5.2.2 Historical production

According to Meinhold (2010), Sierra Leone had a rutile operation which produced more than 60% of the world's rutile production in 1994 (Mobbs, 1996), amounting to 137,000t during its time of operation before its 1995 closure. Apart from Sierra Leone, there are several other countries with Rutile placer deposits, such as Cameroon, Gambia, Guinea, Kenya, Malawi, and South Africa (Schlüter, 2008). The USA, India, Sri Lanka and Australia are among other countries mined or mining Rutile placer deposits (Pirkle et al., 2007).

As of 2009, 608,000t of natural rutile was produced worldwide, with Australia producing 309,000t, South Africa 121,000t, and Sierra Leone 95000t, making them the largest producers at the time (Gambogi, 2009).

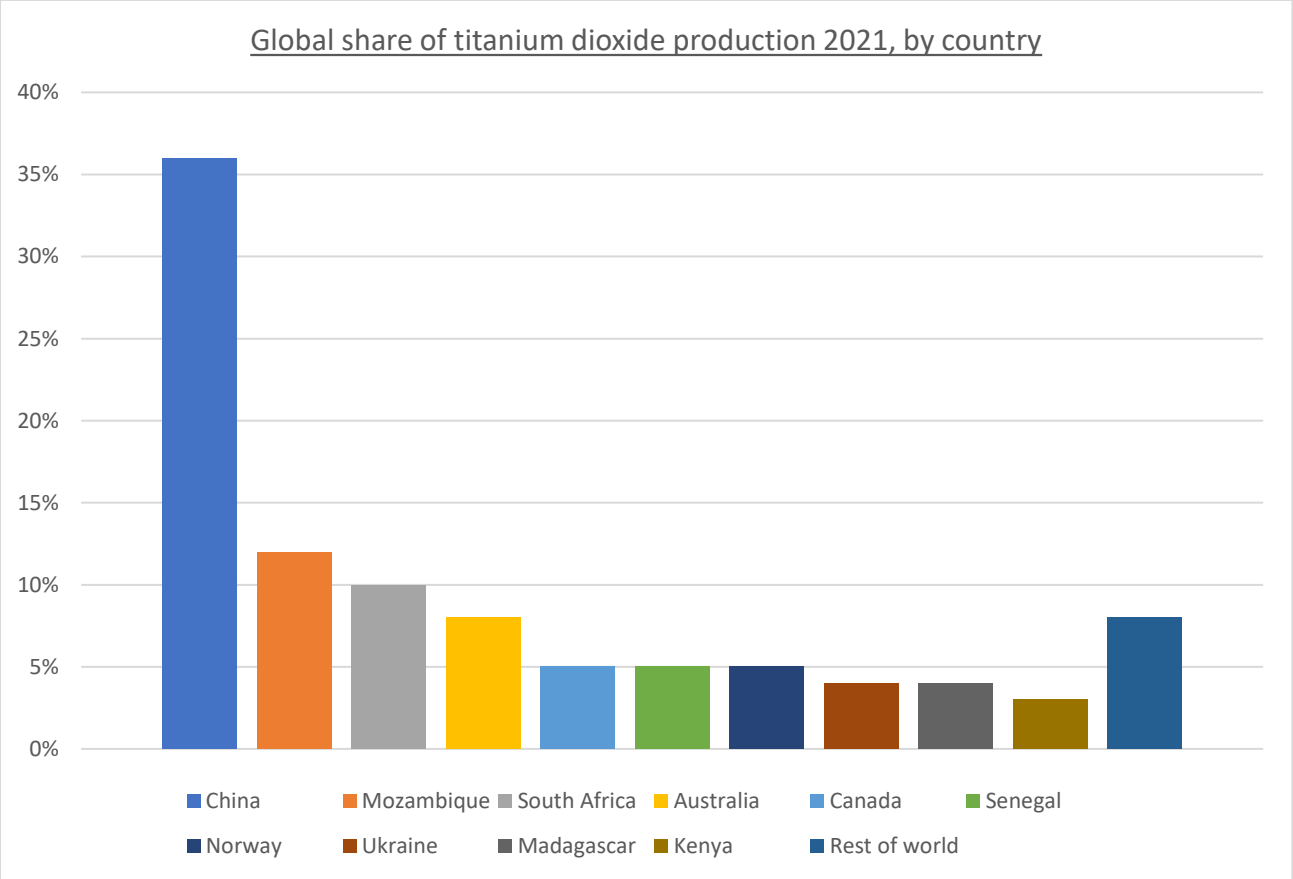


*Figure 29: Global share of titanium dioxide production 2021, by country*

As of 2021, China was the largest producer of titanium minerals by volume accounting for 36% of the global production. Mozambique followed as the second largest producer for 2021 with 12% global production of titanium minerals (U.S. Geological Survey ,2021) as shown in Figure 29 above.

As much as China is the biggest producer of titanium minerals, it mainly produces ilmenite with an average annual production of 3,400 metric tonnes (U.S.Geological Survey, 2021) as shown in Figure 30

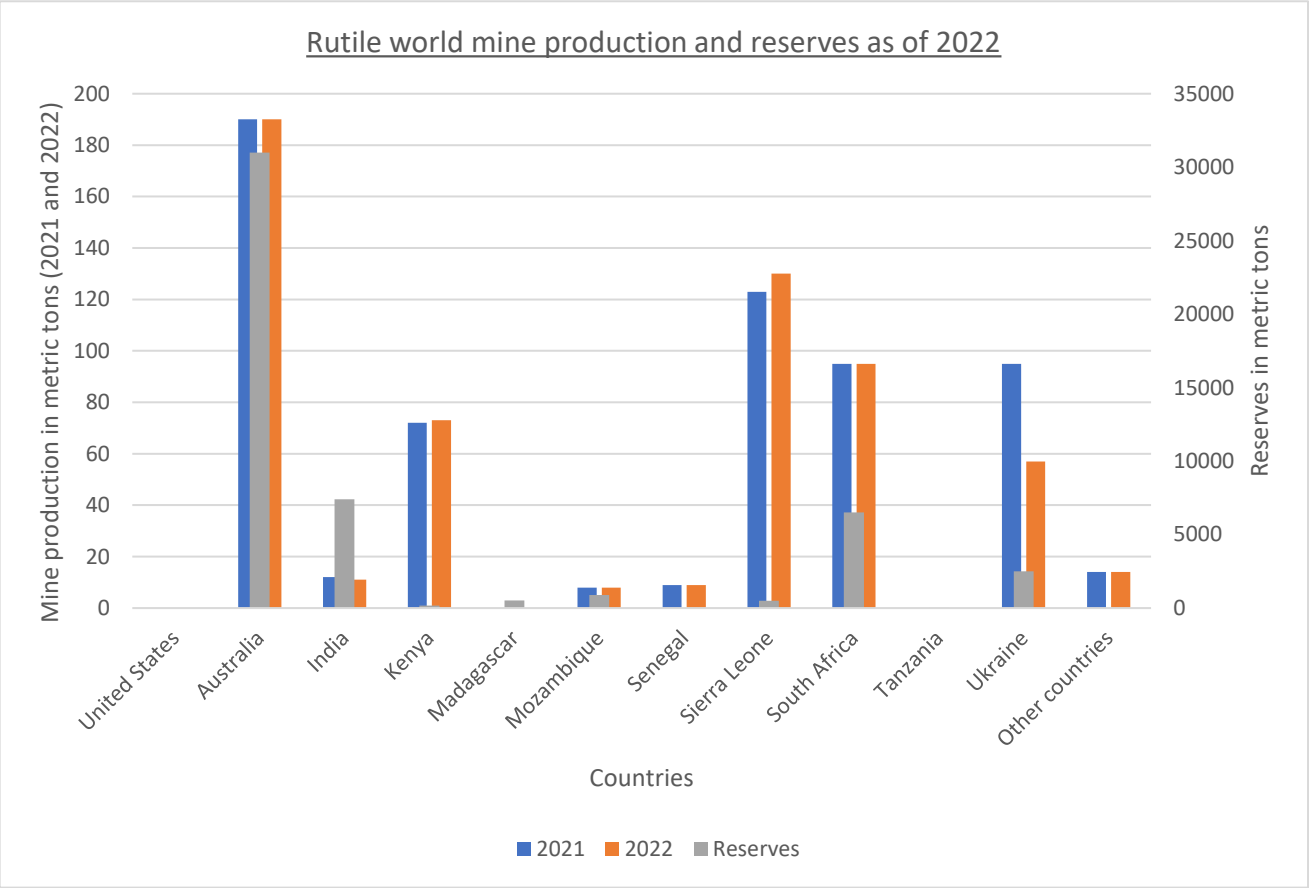


*Figure 30: Rutile world mine production and reserves as of 2022 (Source: U.S. Geological Survey, 2023)*

Figure 30 shows different readings; the left axis shows the production for 2021 and 2022, which are shown in blue and orange on the graph. The grey bars represent the reserve, and its scale is on the right axis. For example, Australia's mine production in 2021 and 2022 was around 190 metric tons for both years, and the reserves were around 34,000 metric tons. The same interpretation applies for Figure 26 and Figure 31.

## 5.3 Vanadium

### 5.3.1 Uses, Demand and Supply

With significant market segments in the automotive and construction industries, vanadium is used primarily as an alloying agent for iron and steel. It is also used as a titanium-based additive, as a catalyst for sulphuric acid production (predominantly vanadium redox flow batteries - VRFBs), and in other specialised applications such as energy storage (Polyak, 2022).

The market for vanadium alloying agents in steel will remain dominant due to emerging nations' increased vanadium demand for steel applications. In addition, rising demand is anticipated from the aerospace sector as it recovers from the COVID-19 pandemic's effects and the energy storage sector due to greater usage of VRFBs which will see high-purity vanadium oxides ($V_2O_5$ or $V_2O_3$) rise in demand (Roskill, 2021).

### 5.3.2 Historical production

China was the largest producer of Vanadium in 2020, producing about 70,000MT which was followed by Russia, which produced approximately 20,000 MT, South Africa with 8,584MT production, then Brazil with 7,582 MT production levels as shown in Figure 31. Lastly, there is more production in the rest of the world with a lot of countries with ore reserves but not in the production stage. As much as Russia comes second on the list, the difference between its production and China's is significant, therefore like other minerals china dominates the market (U.S. Geological Survey, 2023).

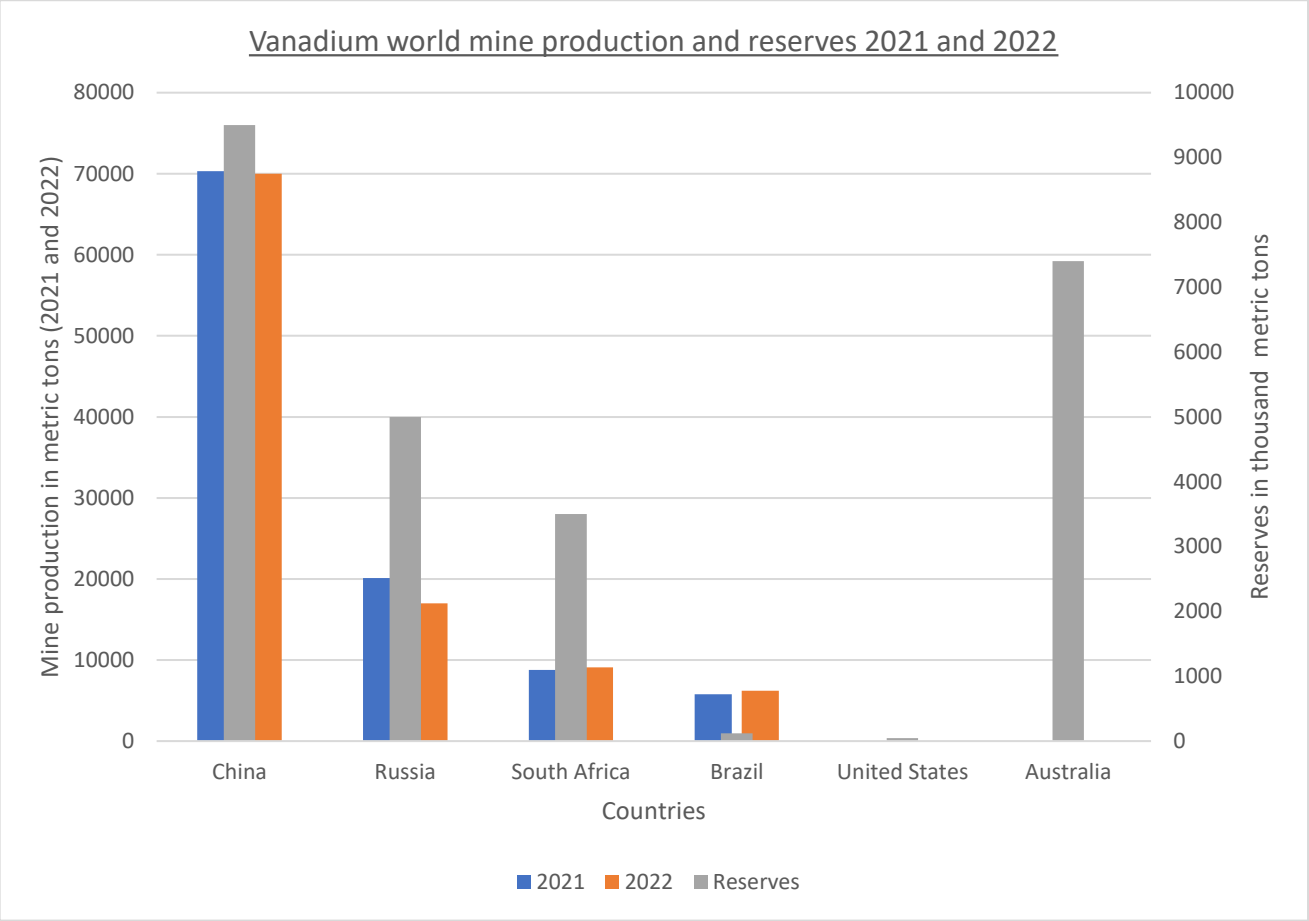


*Figure 31: Vanadium world mine production and reserves as of 2022 (Source: U.S. Geological Survey, 2023)*

Currently, post-COVID-19 recovery and the Russia-Ukraine war may interrupt Russian production as Russia is a key player in the mineral markets including vanadium production (Simandl and Paradis, 2022) as mentioned above. So far, the energy, mainly oil and gas supply from China to Europe has been impacted by the war and sanctions put in place due to the war. However, Europe can not acquire an alternative source of energy overnight. Therefore, the European countries will still have to depend on Russia for the gas. Similarly, with the global vanadium production and demand, Russia will still play a role in producing vanadium to satisfy the market until other countries like Australia start production, which would contribute to the global market.

# Chapter 6: Conclusion and recommendations

## 6.1 Conclusions

In conclusion, the comprehensive exploration of the Malingunde saprolite-hosted graphite project undertaken by Sovereign Metals Ltd (SML) has provided valuable insights into the mineralogical make-up and economic potential of the deposit. Initially conceived as a graphite-focused endeavour, the project unfolded as a multi-element exploration with the unexpected discovery of rutile, enriching the prospect's economic significance.

The unexpected discovery of rutile prompted a shift in exploration focus, leading to successfully identifying and delineating rutile-rich zones. Market analysis indicated a potential escalation in the project's value, emphasising the need for a comprehensive financial model considering graphite and rutile extraction.

The study aimed to analyse the Malingunde graphite and rutile deposit, unravelling the mineral formation processes and assessing the associated minerals. SML conducted extensive geological, geochemical, and geophysical investigations, incorporating various exploration techniques such as drilling programs, soil sampling, and remote sensing.

Exploration history, remote sensing, and geophysics, played pivotal roles in targeting potential areas. Airborne electromagnetic surveys, ground electromagnetic surveys, and GIS applications, coupled with historical data, were instrumental in identifying and quantifying mineralised zones. The correlation between remote sensing data and mineralisation further strengthened the targeting process.

Exploration, involving ground follow-up using hand auger and general soil sampling, facilitated the identification of potential targets. The collaboration of remote sensing, geophysics, and GIS contributed to identifying mineralised zones without traditional geological mapping. The hand augers proved effective in tracing graphite mineralisation at shallow levels.

Geological findings revealed that the Malingunde deposit, situated within the central region of Malawi, is hosted in saprolite, resulting from the tropical weathering of graphitic gneisses over millions of years. The mineralisation, concentrated in a 3km strike and 1km width, exhibited a complex mineral assemblage, including muscovite, kyanite, garnets, ilmenite, and rutile. The study also reviewed the classification and origin of graphite, rutile, and vanadium, shedding light on the geological processes influencing their concentration.

The exploration drilling phase, utilising air-core and diamond drilling, confirmed the extent of mineralisation at depth, reaching up to 33m. The samples collected were initially analysed for graphite, and the presence of rutile (TiO2) and vanadium (V2O5) was revealed. The unexpected $V_2O_5$ discovery highlighted the potential for additional economic by-products. Furthermore, the Malingunde saprolite hosted project is economically competitive because of the free dig element in the process and the fact that it does not require heavy crushers for crushing, which reduces the capital significantly.

Overall, the thesis successfully achieved its objectives by analysing the Malingunde graphite and rutile deposit, identifying associated minerals, exploring potential elements, and investigating its implications.

Integrating various exploration techniques, geological understanding, and market analysis positions the Malingunde project as a promising venture with economic significance beyond graphite. Further research and development is necessary to optimize extraction methods, processing techniques, and overall project valuation. More exploration and drilling programmes to cover unexplored prospective sectors within the Malingunde license area would greatly enhance the value of the project.

# 7 References


Anand, R.R. & Butt, C.R.M. (1988). A Guide to the Recognition of Laterite Profiles in Mineral Exploration. CSIRO Division of Exploration Geoscience, Perth, Australia.

Awan, R.S., Liu, C., Yang, S., Wu, Y., Zang, Q., Khan, A., & Li, G. (2021). The occurrence of vanadium in nature: its biogeochemical cycling and relationship with organic matter—a case study of the Early Cambrian black rocks of the Niutitang Formation, western Hunan, China. Science Press and Institute of Geochemistry, CAS and Springer-Verlag GmbH Germany. https://doi.org/10.1007/s11631-021-00482-2.

Battery Minerals. (2019). Substantial maiden vanadium Resource further strengthens economic outlook for Montepuez graphite project. Montepuez Project, Mozambique. https://www.investi.com.au/api/announcements/bat/01af10bf-d83.pdf

Benton, D. (2020). Mustang Resources completes 22Mt Caula Vanadium Graphite Project estimate. Mining Digital. https://miningdigital.com/supply-chain-and-operations/mustang-resources-completes-22mt-caula-vanadium-graphite-project-estimate

Bloomfield, K., Gondwe, P.C., Mason, T.P.R., Tchuwa, K.A., Habgood, F., Phiri, F.R. (1966). Geological Map of Malawi (1:1,000,000). Survey Department, Blantyre.

Boni, M., Bouabdellah, M., Boukirou, W., Putzolu, F., & Mondillo, N. (2023). Vanadium ore resources of the African continent: State of the Art. Ore Geology Reviews, 157, 105423.

Brough, C., Bowell, R., & Larkin, J. (2019). *The Geology of Vanadium Deposits. An Introduction to Vanadium* (pp. 87–117). Nova Science Publishers

Carruzzo, S., Clarke, D.B., Pelrine, K.M., MacDonald, M.A. (2006). Texture, composition, and origin of rutile in the South Mountain Batholith, Nova Scotia. *Canadian Mineralogist*, *pp. 44*, 715–729.

Carter, G. S., & Bennet, J. D. (1973). The geology and mineral resources of Malawi (Bulletin number 6, Second Edition). Ministry of Forestry and Natural Resources Geological, Government Printers Zomba, Malawi, pp. 1-62.

Cengiz, Ö. (2018). Mineralogical and geochemical characteristics of rutile-bearing quartz veins in the Central Anatolia region, Turkey: Implications for crystallization processes. Journal of Geosciences, 63(2), 175-190

Cestarolli, D.T., & Guerra, E.M. (2021). Vanadium Pentoxide (V2O5): Their Obtaining Methods and Wide Applications. Transition Metal Compounds - Synthesis, Properties, and Application. IntechOpen.

Choukroun, M., O'Reilly, S.Y., Griffin, W.L., Pearson, N.J., Dawson, J.B. (2005). Hf isotopes of MARID (mica-amphibole-rutile-ilmenite-diopside) rutile trace metasomatic processes in the lithospheric mantle. *Geology*, *pp. 33*, 45–48.

Coakley, G.J., Mobbs, P.M. (2001). The mineral industry of Malawi. In: Mineral Industries of Africa and the Middle East. U.S. Geol. Survey, Minerals Yearbook, 1998-3, pp. 29.1–29.2.

CRC Leme (2007). The Regolith Glossary: Surficial Geology, Soils, and Landscapes. Cooperative Research Centre for Landscape Environments and Mineral Exploration (CRC LEME), 2nd Edition.

Dahlkamp, F.J. (2010). Uranium deposits of the world—USA and Latin America. Springer-Verlag.

Deer, W.A., Howie, R.A., Zussman, J. (1992). An Introduction to Rock-Forming Minerals (2nd Edition). Longman Group Ltd, Harlow, UK.

Dill H.G. (2007). A review of mineral resources in Malawi: With special reference to aluminium variation in mineral deposits. *Journal of African Earth Sciences*, *pp. 47*, 153–173.

Ernenwein, E., & Hargrave, M. (2007). Archaeological Geophysics for DoD Field Use: A Guide for New and Novice Users.

Gambogi, J. (2008). Titanium Mineral Concentrates. U.S. Geological Survey, Mineral Commodity Summaries, January 2008, pp. 178-179

Gambogi, J. (2009). Titanium mineral concentrates. Mineral Commodity Summaries. U.S. Geological Survey.

Gao, J., John, T., Klemd, R., Xiong, X. (2007). Mobilization of Ti-Nb-Ta during subduction: evidence from rutile-bearing dehydration segregation and veins hosted in eclogite, Tianshan, N.W. China. Geochem. Cosmochim. Acta, 71, 4974e4996.

George J. Simandl & Suzanne Paradis (2022). Vanadium as a critical material. Economic geology with emphasis on market and the main deposit types, Applied Earth Science, DOI: 10.1080/25726838.2022.2102883.

Grand view research (2023). Titanium Dioxide Market Size, Share & Trends Analysis Report By Grade (Anatase, Rutile), By Production Process (Sulfate, Chloride), By Application, By Region, And Segment Forecasts, 2023 - 2030. Grand View Research, Inc., USA. https://www.grandviewresearch.com/industry-analysis/titanium-dioxide-industry

Habgood, F. (1962a). An account of the recent investigation of graphite occurrences in the Central Region. Records of the Geological Survey of Malawi, pp. 4, 15–24.

Habgood, F. (1962b). An examination of disseminated sulphide bodies, Nanzeka area, Ntschisi District. Records of the Geological Survey of Malawi, pp. 4, 25–28.

Hall, M. (2018). Graphite Demand and Supply in the Battery Industry. Benchmark Mineral Intelligence.

Kelley, K.D., Scott, C.T., Polyak, D.E., & Kimball, B.E. (2017). Vanadium. Critical mineral resources of the United States—Economic and environmental geology and prospects for future supply, U.S. Geological Survey Professional Paper 1802, pp. U1– U36, https://doi.org/10.3133/pp1802U.

Korneliussen, A., McLimans, R., Braathen, A., Erambert, M., Lutro, O., & Ragnhildstveit, J. (2000). Rutile in eclogites as a mineral resource in the Sunnfjord region, western Norway. Norges Geologiske Undersøkelse Bulletin, 436, pp. 39–47.

Legault, J.M., Lymburner, J., Ralph, K., Wood, P., Orta, M., Prikhodko, A., & Bournas, N. (2015). The Albany graphite discovery - an airborne and ground time-domain E.M. SEG Technical Program Expanded Abstracts, 2056-2060. https://doi.org/10.1190/segam2015-5908480.1

Market Screener (2018). Mustang Resources Limited Provides Update on Caula Vanadium-Graphite Project in Mozambique. S&P Capital I.Q. 2018. https://www.marketscreener.com/quote/stock/GOLDOZ-46661548/news/Mustang-Resources-Limited-Provides-Update-on-Caula-Vanadium-Graphite-Project-in-Mozambique-34645257/ [Accessed: 07/12/2022]

Meinhold G. (2010). Rutile and its applications in earth sciences. *Earth-Science Reviews*, *pp. 102*, 1–28, Elsevier ScienceDirect, 181a Huntingdon Road, Cambridge.

Meinhold, G., Birte Anders, B., Kostopoulos, D., & Reischmann, T.(2008)''Rutile chemistry and thermometry as provenance indicator: An example from Chios Island, Greece''Sedimentary Geology, Volume 203, Issues 1–2, https://doi.org/10.1016/j.sedgeo.2007.11.004.

Ministry of Energy and Mining. (1997). Mineral potential of Malawi Opportunities for investment. Lilongwe, Malawi, Ministry of Energy and Mines, pp. 14.

Ministry of Mines and Natural Resources and Environment. (2004). Mineral potential of Malawi-opportunities for mineral investment. Ministry of Mines and Natural Resources and Environment, Lilongwe, pp. 24.

Mkango (2020). Mkango announces rutile and ilmenite discovery in Malawi. Vancouver, Canada. https://www.mkango.ca/site/assets/files/4776/2020-09-15-mka-nr.pdf [Accessed: 29th September 2020]

Mobbs, P.M. (1996). The mineral industry of Sierra Leone. Minerals Information. U.S. Geological Survey.

Morton, A.C. & Hallsworth, C.R. (1999) Processes controlling the composition of heavy mineral assemblages in sandstones. Sedimentary Geology 124, 3–29.DOI 10.1016/S0037-0738(98)00118-3

OEC(2020). Product complexity in niobium, tantalum, vanadium and zirconium ore In Malawi. https://oec.world/en/profile/bilateral-product/niobium-tantalum-vanadium-and-zirconium-ore/reporter/mwi [Accessed on 12/09/2022]

Olson, D.W. (2011). Graphite (natural): U.S. Geological Survey Mineral Commodity Summaries 2011, pp. 68–69.

Pereira, I., Storey, C., Darling, J., Lana, C., Alkmim, A.R., (2019). *Two billion years of evolution enclosed in hydrothermal rutile: Recycling of the São Francisco Craton Crust and constraints on gold remobilisation processes*. Gondwana Res. 68, 69–92.https://doi.org/10.1016/j.gr.2018.11.008.

Pirkle, F.L., Pirkle, W.A., Pirkle, E.C. (2007). Heavy-mineral sands of the Atlantic and Gulf coastal plains, USA. In: Mange, M., Wright, D.T. (Eds.), Heavy Minerals In Use: Developments in Sedimentology, vol. 58, pp. 1145–1232.

Polyak D.E. (2022). Vanadium. Mineral Commodity Summaries: United States Geological Survey, [Accessed 2024 January 10]. https://pubs.usgs.gov/periodicals/mcs2022/mcs2022-vanadium.pdf.

Ritoe, A., Patrahau,I., Rademaker, M. (2022).Graphite Supply chain challenges & recommendations for a critical mineral. The Hague Centre for Strategic Studies. https://hcss.nl/wp-content/uploads/2022/03/Graphite-HCSS-2022.pdf

Robinson G. R., Hammarstrom J. M., & Olson D. W. (2017). Graphite. Critical mineral resources of the United States—Economic and environmental geology and prospects for future supply: U.S. Geological Survey Professional Paper 1802, pp. J1–J24.

Roskill Information Services Ltd (2020). *Natural and synthetic Graphite – Global industry markets and outlook* (13th Ed.). London, Roskill Information Services Ltd.

Roskill Information Services Ltd (2021). *Vanadium, Outlook to 2030* (19th Edition). Roskill. https://roskill.com/market-report/vanadium/ [accessed 2021 July 20].

Roskill Information Services Ltd (2023). "Natural and Synthetic Graphite: A Strategic Market Analysis." Roskill.

Sakoma, E.M., Martin, R.F. (2002). Oxidation-induced postmagmatic modifications of primary ilmenite, NYG-related aplite dyke, Tibchi Complex, Kalato, Nigeria. Mineralogical Magazine, 66, pp. 591–604.

Schlüter, T. (2008). *Geological Atlas of Africa, With Notes on Stratigraphy, Tectonics, Economic Geology, Geohazards, Geosites and Geoscientific Education of Each Country* (2nd Edition). Springer-Verlag, Berlin. pp. 307

Scogings, A. (2000). Graphite exploration methods - Graphite exploration, the importance of planning. Industrial minerals.

Scogings, A. J. (2015). Graphite exploration - the importance of planning – Graphite exploration methods. Industrial Minerals Magazine, pp. 42-46.

Silva, A.C., Souza, C.R.G., Castro, D.L., Santos, L.C.M.L. and Silva, F.C.A., (2016). Provenance and weathering of the Pliocene and Quaternary fluvial sediments in the Barreiras Formation, eastern Amazonia. Journal of South American Earth Sciences, 70, pp.25-38.

Simandl, G.J., Paradis, S., and Akam, C. (2015). Graphite deposit types, their origin, and economic significance. In: Simandl, G.J. and Neetz, M., (Eds.), Symposium on Strategic and Critical Materials Proceedings, November 13-14, 2015, Victoria, British Columbia, British Columbia Ministry of Energy and Mines, British Columbia Geological Survey Paper 2015-3, pp. 163-171.

Sovereign Metals Limited (2016). June 2016 quarterly report. Sovereign Metals Limited. Retrieved from http://www.investi.com.au/api/announcements/svm/59ad210d-22f.pdf/ [Accessed: 08th February 2019]

Sovereign Metals Limited (2017). High Grade Saprolite-Hosted Graphite Results Continue At Malingunde. Sovereign Metals Limited. Retrieved from https://www.investi.com.au/api/announcements/svm/3d7a4040-e1f.pdf [Accessed: 14th January 2024]

Sovereign Metals Limited (2018). Malingunde PFS - Lowest operating cost coarse flake graphite project globally. Sovereign Metals Limited. Retrieved from https://www.investi.com.au/api/announcements/svm/ee6e1590-633.pdf [Accessed: 29th November 2023]

Sovereign Metals Limited (2019). December 2018 quarterly report. Retrieved from http://www.investi.com.au/api/announcements/svm/ee2db168-9c8.pdf/ [Accessed: 08th February 2019]

Sovereign Metals Limited (2022). 1.8 Billion Tonne Jorc Resource Confirms Kasiya As The Largest Rutile Deposit Ever Discovered. Sovereign Metals Limited. Retrieved from https://www.investi.com.au/api/announcements/svm/23386445-167.pdf [Accessed: 20th December, 2023]

Sutradhar, M., Da Silva, J.A.L., & Pombeiro, A.J.L. (2020). Vanadium, Its Compounds and Applications, in Vanadium Catalysis, Chapter 1, pp. 1-11. *DOI: 10.1039

Tamashausky, A.V. (2006). An Introduction to Synthetic Graphite. Technical Services Department of the Asbury Graphite Mills, Inc.

Thatcher, E.C. (1974). The geology of the Nyika area. Bulletin of the Geological Survey of Malawi, 40, 1–90.

Thatcher, E.C., & Walter, M. J. (1968). The geology of the South Lilongwe plain and Dzalanyama range, Bulletin number 23, Ministry of Forestry and Natural Resources Geological Survey, Government Printers, Zomba, Malawi.

Tian, M., Liu, C., Ge, J., Geohegan, D., Duscher, G., & Eres, G. (2019). Recent progress in characterization of the core–shell structure of black titania. Journal of Materials Research, 34(7), 1-16. DOI: 10.1557/jmr.2019.46.

Tonje, J.C., Ndjigui, P.D., Nyeck, B., Paul, B. (2014). Geochemical features of the Matomb alluvial rutile from the Neoproterozoic Pan-African belt, Southern Cameroon. Chem. Erde, 74, 557e570.

U.S. Geological Survey. (2021). Mineral commodity summaries 2021. U.S. Geological Survey. https://doi.org/10.3133/mcs2021

U.S. Geological Survey. (2023). Mineral commodity summaries 2023. U.S. Geological Survey. https://doi.org/10.3133/mcs2023.

U.S. Geological Survey (2024), Mineral commodity summaries 2024: U.S. Geological Survey. https://doi.org/10.3133/mcs2024.

Valentine, P.C., & Commeau, J.A. (1990). Fine-grained rutile in the Gulf of Maine—diagenetic origin, source rocks, and sedimentary environment of deposition. Economic Geology, 85(4), 862–876.

Wang, D., Karato, S.-I., & Jiang, Z. (2013). An experimental study of the influence of graphite on the electrical conductivity of olivine aggregates. Geophysical Research Letters, 40, 2028-2032. DOI: 10.1002/grl.50471.

Walter, M. J. (1972). The geology of the Lilongwe-Dowa area. Bulletin number 26, Ministry of Forestry and Natural Resources Geological Survey, Government Printers, Zomba, Malawi.

Wilde, S.A., Dorsett-Bain, H.L., & Lennon, R.G. (1999). Geological setting and controls on the development of graphite, sillimanite, and phosphate mineralisation within the Jiasmusi

Massif – An exotic fragment of Gondwanaland located in northeastern China. *Gondwana Research*, 2(1), pp. 21-46.

Zhang, R.Y., Zhai, S.M., Fei, Y.W., Liou, J.G. (2003). Titanium solubility in coexisting garnet and clinopyroxene at very high pressure: the significance of exsolved rutile in garnet. *Earth and Planetary Science Letters*, *pp. 216*, 591–601.

# 8 Appendices

| SUMMARY OUTPUT | | | | Malingunde $TiO_2$ | | | | |
|---|---|---|---|---|---|---|---|---|
| *Regression Statistics* | | | | | | | | |
| Multiple R | 0.797673113 | | | | | | | |
| R Square | 0.636282394 | | | | | | | |
| Adjusted R Square | 0.619749776 | | | | | | | |
| Standard Error | 0.336760325 | | | | | | | |
| Observations | 346 | | | | | | | |
| ANOVA | | | | | | | | |
| | *df* | *SS* | *MS* | *F* | *Significance F* | | | |
| Regression | 15 | 65.4698525 | 4.364656833 | 38.48648639 | 2.9135E-63 | | | |
| Residual | 330 | 37.42448038 | 0.113407516 | | | | | |
| Total | 345 | 102.8943329 | | | | | | |
| | *Coefficients* | *Standard Error* | *t Stat* | *P-value* | *Lower 95%* | *Upper 95%* | *Lower 95.0%* | *Upper 95.0%* |
| Intercept | 0.700509116 | 0.350925578 | 1.996175714 | 0.046736174 | 0.010175803 | 1.390842428 | 0.010175803 | 1.390842428 |
| TGC | -0.009264952 | 0.007946468 | -1.165920814 | 0.244488428 | -0.024897074 | 0.00636717 | -0.024897074 | 0.00636717 |
| $Al_2O_3$ | 0.011286883 | 0.007671921 | 1.471193882 | 0.142191601 | -0.003805156 | 0.026378923 | -0.003805156 | 0.026378923 |
| BaO | -0.1701369 | 0.341027201 | -0.498895395 | 0.618185471 | -0.840998337 | 0.500724537 | -0.840998337 | 0.500724537 |
| CaO | 0.288529043 | 0.066275416 | 4.353485188 | 1.78984E-05 | 0.158153457 | 0.418904628 | 0.158153457 | 0.418904628 |
| $Cr_2O_3$ | 2.67380562 | 2.357806922 | 1.134022296 | 0.257608312 | -1.964421876 | 7.312033115 | -1.964421876 | 7.312033115 |
| $Fe_2O_3$ | -0.017882302 | 0.007615263 | -2.348218683 | 0.019453299 | -0.032862885 | -0.00290172 | -0.032862885 | -0.00290172 |
| $K_2O$ | -0.171689414 | 0.040196081 | -4.271297382 | 2.54478E-05 | -0.250762287 | -0.092616542 | -0.250762287 | -0.092616542 |
| MgO | 0.050369879 | 0.034531181 | 1.458678116 | 0.14560484 | -0.017559125 | 0.118298882 | -0.017559125 | 0.118298882 |
| MnO | 1.76936076 | 0.390233099 | 4.534112465 | 8.10395E-06 | 1.001702529 | 2.537018991 | 1.001702529 | 2.537018991 |
| $Na_2O$ | -0.283251188 | 0.119684328 | -2.366652276 | 0.018526736 | -0.518691646 | -0.04781073 | -0.518691646 | -0.04781073 |
| $P_2O_5$ | 2.982144137 | 0.430797577 | 6.922379089 | 2.32359E-11 | 2.134688331 | 3.829599943 | 2.134688331 | 3.829599943 |
| $SO_3$ | -0.07919701 | 0.082262373 | -0.962736757 | 0.336384563 | -0.241021796 | 0.082627776 | -0.241021796 | 0.082627776 |
| $SiO_2$ | -0.005734485 | 0.003865258 | -1.483597046 | 0.138870293 | -0.013338138 | 0.001869168 | -0.013338138 | 0.001869168 |
| $V_2O_5$ | -0.091503172 | 1.070240238 | -0.085497787 | 0.931917503 | -2.196856945 | 2.013850602 | -2.196856945 | 2.013850602 |
| $ZrO_2$ | 19.54266435 | 1.943450933 | 10.05565102 | 6.30694E-21 | 15.71954912 | 23.36577959 | 15.71954912 | 23.36577959 |

*Appendix 1: Maligunde $TiO_2$ regression analysis*

**SUMMARY OUTPUT**

**LIFIDZI $TiO_2$**

| *Regression Statistics* | |
|---|---|
| Multiple R | 0.906007242 |
| R Square | 0.820849122 |
| Adjusted R Square | 0.799001454 |
| Standard Error | 0.297960463 |
| Observations | 139 |

ANOVA

| | *df* | *SS* | *MS* | *F* | *Significance F* |
|---|---|---|---|---|---|
| Regression | 15 | 50.0341803 | 3.33561202 | 37.57147542 | 1.11457E-38 |
| Residual | 123 | 10.9199938 | 0.088780437 | | |
| Total | 138 | 60.9541741 | | | |

| | *Coefficients* | *Standard Error* | *t Stat* | *P-value* | *Lower 95%* | *Upper 95%* | *Lower 95.0%* | *Upper 95.0%* |
|---|---|---|---|---|---|---|---|---|
| Intercept | 28.18362219 | 3.765067304 | 7.485556012 | 1.18774E-11 | 20.73090232 | 35.63634207 | 20.73090232 | 35.63634207 |
| $Al_2O_3$ | -0.349437351 | 0.05257113 | -6.646943883 | 8.68791E-10 | -0.45349868 | -0.245376023 | -0.45349868 | -0.245376023 |
| BaO | 0.962234958 | 1.109008512 | 0.867653357 | 0.387273751 | -1.232979393 | 3.15744931 | -1.232979393 | 3.15744931 |
| CaO | -0.390904258 | 0.075040851 | -5.209219392 | 7.73363E-07 | -0.539443022 | -0.242365494 | -0.539443022 | -0.242365494 |
| $Cr_2O_3$ | 5.935004702 | 2.097208959 | 2.829953915 | 0.00543891 | 1.783708159 | 10.08630125 | 1.783708159 | 10.08630125 |
| $Fe_2O_3$ | -0.302897233 | 0.044532091 | -6.801774251 | 3.99381E-10 | -0.391045778 | -0.214748689 | -0.391045778 | -0.214748689 |
| $K_2O$ | -0.336806477 | 0.082934387 | -4.061119747 | 8.63141E-05 | -0.50097001 | -0.172642943 | -0.50097001 | -0.172642943 |
| MgO | -0.269188352 | 0.067156238 | -4.00838939 | 0.000105233 | -0.402120007 | -0.136256696 | -0.402120007 | -0.136256696 |
| MnO | -1.207925537 | 0.514326605 | -2.348557368 | 0.020441177 | -2.226003516 | -0.189847559 | -2.226003516 | -0.189847559 |
| $Na_2O$ | 0.070735299 | 0.102711283 | 0.688680899 | 0.492321039 | -0.132575389 | 0.274045987 | -0.132575389 | 0.274045987 |
| $P_2O_5$ | 0.590109064 | 0.180186084 | 3.274998005 | 0.001372733 | 0.23344176 | 0.946776369 | 0.23344176 | 0.946776369 |
| $SO_3$ | -0.718303628 | 0.146220002 | -4.912485415 | 2.8024E-06 | -1.007737157 | -0.428870099 | -1.007737157 | -0.428870099 |
| $SiO_2$ | -0.278536057 | 0.037773967 | -7.373757032 | 2.12819E-11 | -0.353307309 | -0.203764805 | -0.353307309 | -0.203764805 |
| $V_2O_5$ | -0.700592519 | 1.786551418 | -0.392147974 | 0.69562754 | -4.236961508 | 2.83577647 | -4.236961508 | 2.83577647 |
| $ZrO_2$ | 4.17490892 | 1.406235557 | 2.968854613 | 0.003594122 | 1.391351859 | 6.958465981 | 1.391351859 | 6.958465981 |
| TGC | -0.301742296 | 0.045122988 | -6.687107983 | 7.10682E-10 | -0.391060485 | -0.212424107 | -0.391060485 | -0.212424107 |

*Appendix 2: Lifidzi $TiO_2$ regression analysis*

**SUMMARY OUTPUT** — **Malingunde TGC**

| *Regression Statistics* | |
|---|---|
| Multiple R | 0.717886794 |
| R Square | 0.515361449 |
| Adjusted R Square | 0.493332424 |
| Standard Error | 2.328076083 |
| Observations | 346 |

ANOVA

| | *df* | *SS* | *MS* | *F* | *Significance F* |
|---|---|---|---|---|---|
| Regression | 15 | 1901.963808 | 126.7975872 | 23.39465533 | 2.77758E-43 |
| Residual | 330 | 1788.579621 | 5.419938246 | | |
| Total | 345 | 3690.543429 | | | |

| | *Coefficients* | *Standard Error* | *t Stat* | *P-value* | *Lower 95%* | *Upper 95%* | *Lower 95.0%* | *Upper 95.0%* |
|---|---|---|---|---|---|---|---|---|
| Intercept | 24.18010233 | 2.045679855 | 11.82008137 | 4.02565E-27 | 20.15588455 | 28.20432012 | 20.15588455 | 28.20432012 |
| $TiO_2$ | -0.44278783 | 0.379775217 | -1.165920814 | 0.244488428 | -1.189873539 | 0.304297878 | -1.189873539 | 0.304297878 |
| $Al_2O_3$ | -0.270932074 | 0.051077925 | -5.304288964 | 2.07756E-07 | -0.371411479 | -0.170452669 | -0.371411479 | -0.170452669 |
| BaO | 7.015280424 | 2.32663101 | 3.015209715 | 0.002767172 | 2.438381517 | 11.59217933 | 2.438381517 | 11.59217933 |
| CaO | 0.287046929 | 0.470880514 | 0.609596108 | 0.542548877 | -0.639259177 | 1.213353035 | -0.639259177 | 1.213353035 |
| $Cr_2O_3$ | -3.86772539 | 16.33022449 | -0.236844594 | 0.812924308 | -35.99219476 | 28.25674398 | -35.99219476 | 28.25674398 |
| $Fe_2O_3$ | -0.401883349 | 0.048253844 | -8.328525083 | 2.21475E-15 | -0.496807281 | -0.306959416 | -0.496807281 | -0.306959416 |
| $K_2O$ | -0.174244946 | 0.2852985 | -0.6107461 | 0.541788094 | -0.735478071 | 0.386988179 | -0.735478071 | 0.386988179 |
| MgO | -0.008904363 | 0.239487242 | -0.037180949 | 0.97036321 | -0.480018559 | 0.462209833 | -0.480018559 | 0.462209833 |
| MnO | -9.961764848 | 2.72589101 | -3.654498589 | 0.000299674 | -15.32407951 | -4.599450184 | -15.32407951 | -4.599450184 |
| $Na_2O$ | -0.21095198 | 0.83430751 | -0.252846795 | 0.800544033 | -1.852183921 | 1.430279962 | -1.852183921 | 1.430279962 |
| $P_2O_5$ | 8.201961421 | 3.154929909 | 2.59972857 | 0.009748983 | 1.995650584 | 14.40827226 | 1.995650584 | 14.40827226 |
| $SO_3$ | -1.927840005 | 0.559515115 | -3.445554827 | 0.000643517 | -3.028506207 | -0.827173802 | -3.028506207 | -0.827173802 |
| $SiO_2$ | -0.260432192 | 0.022655039 | -11.4955526 | 5.98372E-26 | -0.304998702 | -0.215865683 | -0.304998702 | -0.215865683 |
| $V_2O_5$ | 41.51403496 | 7.037047347 | 5.89935422 | 9.04143E-09 | 27.67090549 | 55.35716444 | 27.67090549 | 55.35716444 |
| $ZrO_2$ | 6.748098203 | 15.3519267 | 0.439560345 | 0.660543275 | -23.45188462 | 36.94808103 | -23.45188462 | 36.94808103 |

*Appendix 3: Maligunde TGC regression analysis*

**SUMMARY OUTPUT** **Lifidzi TGC**

| *Regression Statistics* | |
|---|---|
| Multiple R | 0.984802023 |
| R Square | 0.969835024 |
| Adjusted R Square | 0.966156368 |
| Standard Error | 0.50988438 |
| Observations | 139 |

ANOVA

| | *df* | *SS* | *MS* | *F* | *Significance F* |
|---|---|---|---|---|---|
| Regression | 15 | 1028.119039 | 68.54126924 | 263.6384361 | 8.43095E-86 |
| Residual | 123 | 31.97779595 | 0.259982081 | | |
| Total | 138 | 1060.096835 | | | |

| | *Coefficients* | *Standard Error* | *t Stat* | *P-value* | *Lower 95%* | *Upper 95%* | *Lower 95.0%* | *Upper 95.0%* |
|---|---|---|---|---|---|---|---|---|
| Intercept | 80.89872442 | 2.686010509 | 30.11854353 | 1.31716E-58 | 75.58193131 | 86.21551753 | 75.58193131 | 86.21551753 |
| $TiO_2$ | -0.883613467 | 0.132136862 | -6.687107983 | 7.10682E-10 | -1.145170284 | -0.62205665 | -1.145170284 | -0.62205665 |
| $Al_2O_3$ | -1.079796412 | 0.038999425 | -27.68749579 | 1.10059E-54 | -1.156993382 | -1.002599442 | -1.156993382 | -1.002599442 |
| BaO | 0.510238027 | 1.90303192 | 0.26811848 | 0.789057249 | -3.256696974 | 4.277173027 | -3.256696974 | 4.277173027 |
| CaO | -1.062879901 | 0.104610545 | -10.16035149 | 5.57738E-18 | -1.26995006 | -0.855809743 | -1.26995006 | -0.855809743 |
| $Cr_2O_3$ | 1.216791291 | 3.702214388 | 0.32866581 | 0.742967202 | -6.111515088 | 8.545097671 | -6.111515088 | 8.545097671 |
| $Fe_2O_3$ | -0.927944242 | 0.031478821 | -29.47836704 | 1.3451E-57 | -0.990254638 | -0.865633846 | -0.990254638 | -0.865633846 |
| $K_2O$ | -0.628431005 | 0.140112901 | -4.485175899 | 1.64898E-05 | -0.9057759 | -0.351086109 | -0.9057759 | -0.351086109 |
| MgO | -0.853424036 | 0.094924241 | -8.99058056 | 3.63848E-15 | -1.04132075 | -0.665527321 | -1.04132075 | -0.665527321 |
| MnO | -2.855436173 | 0.86203043 | -3.312454032 | 0.001214664 | -4.561772554 | -1.149099793 | -4.561772554 | -1.149099793 |
| $Na_2O$ | 0.486129102 | 0.170560773 | 2.850181155 | 0.005125019 | 0.148514509 | 0.823743695 | 0.148514509 | 0.823743695 |
| $P_2O_5$ | -0.474646701 | 0.318644744 | -1.489579569 | 0.138894556 | -1.105384435 | 0.156091033 | -1.105384435 | 0.156091033 |
| $SO_3$ | -0.914830352 | 0.260939006 | -3.505916439 | 0.000635764 | -1.431343116 | -0.398317588 | -1.431343116 | -0.398317588 |
| $SiO_2$ | -0.808705668 | 0.026615264 | -30.38503324 | 5.06265E-59 | -0.861388951 | -0.756022386 | -0.861388951 | -0.756022386 |
| $V_2O_5$ | 10.88462767 | 2.89743835 | 3.756638229 | 0.000264546 | 5.149326114 | 16.61992923 | 5.149326114 | 16.61992923 |
| $ZrO_2$ | -8.215587181 | 2.37845981 | -3.454162709 | 0.000757892 | -12.92360254 | -3.507571822 | -12.92360254 | -3.507571822 |

*Appendix 4: Lifidzi regression statistics TGC*

| SUMMARY OUTPUT | | | | | | | | |
|---|---|---|---|---|---|---|---|---|
| | | | | | | | | |
| *Regression Statistics* | | | | | | | | |
| Multiple R | 0.369243744 | | | | | | | |
| R Square | 0.136340942 | | | | | | | |
| Adjusted R Square | 0.130036862 | | | | | | | |
| Standard Error | 0.619887113 | | | | | | | |
| Observations | 139 | | | | | | | |
| | | | | | | | | |
| ANOVA | | | | | | | | |
| | *df* | *SS* | *MS* | *F* | *Significance F* | | | |
| Regression | 1 | 8.310549539 | 8.310549539 | 21.62741066 | 7.70859E-06 | | | |
| Residual | 137 | 52.64362456 | 0.384260033 | | | | | |
| Total | 138 | 60.9541741 | | | | | | |
| | | | | | | | | |
| | *Coefficients* | *Standard Error* | *t Stat* | *P-value* | *Lower 95%* | *Upper 95%* | *Lower 95.0%* | *Upper 95.0%* |
| Intercept | 2.031107033 | 0.063016027 | 32.23159437 | 8.033E-66 | 1.906497174 | 2.155716893 | 1.906497174 | 2.155716893 |
| TGC | -0.088540527 | 0.019038812 | -4.650527998 | 7.70859E-06 | -0.126188468 | -0.050892586 | -0.126188468 | -0.050892586 |

*Appendix 5: Lifidzi regression statistics TGC*

SUMMARY OUTPUT

| *Regression Statistics* | |
|---|---|
| Multiple R | 0.069456762 |
| R Square | 0.004824242 |
| Adjusted R Square | 0.001931289 |
| Standard Error | 0.545589999 |
| Observations | 346 |

ANOVA

| | *df* | *SS* | *MS* | *F* | *Significance F* |
|---|---|---|---|---|---|
| Regression | 1 | 0.496387135 | 0.496387135 | 1.667583984 | 0.197449492 |
| Residual | 344 | 102.3979457 | 0.297668447 | | |
| Total | 345 | 102.8943329 | | | |

| | *Coefficients* | *Standard Error* | *t Stat* | *P-value* | *Lower 95%* | *Upper 95%* | *Lower 95.0%* | *Upper 95.0%* |
|---|---|---|---|---|---|---|---|---|
| Intercept | 1.787889537 | 0.036357712 | 49.17497341 | 1.1345E-157 | 1.716378133 | 1.859400941 | 1.716378133 | 1.859400941 |
| TGC | -0.011597519 | 0.008980929 | -1.291349675 | 0.197449492 | -0.029261964 | 0.006066926 | -0.029261964 | 0.006066926 |

*Appendix 6: Malingunde regression statistics TGC*

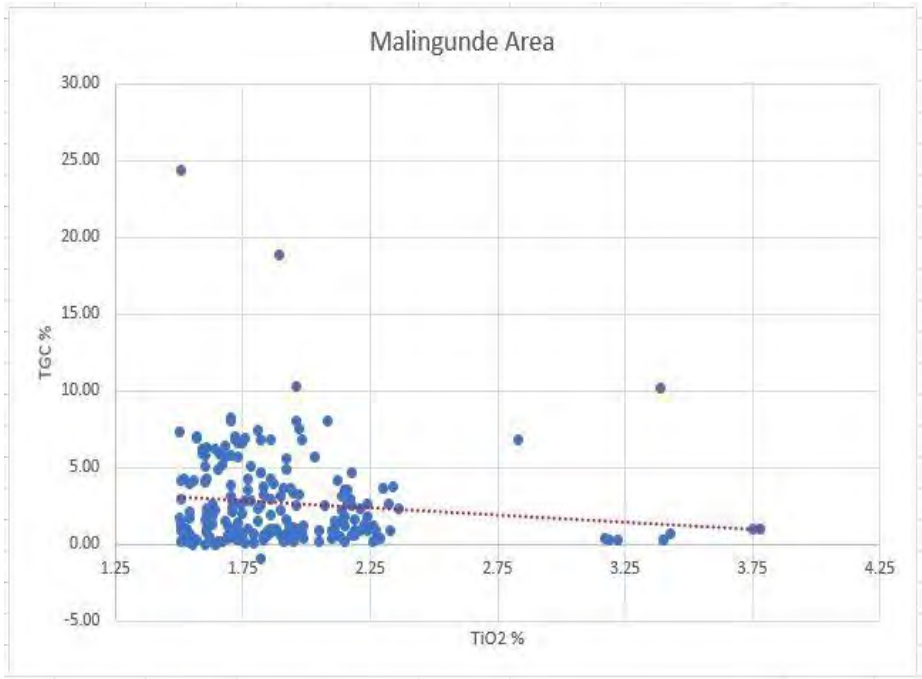


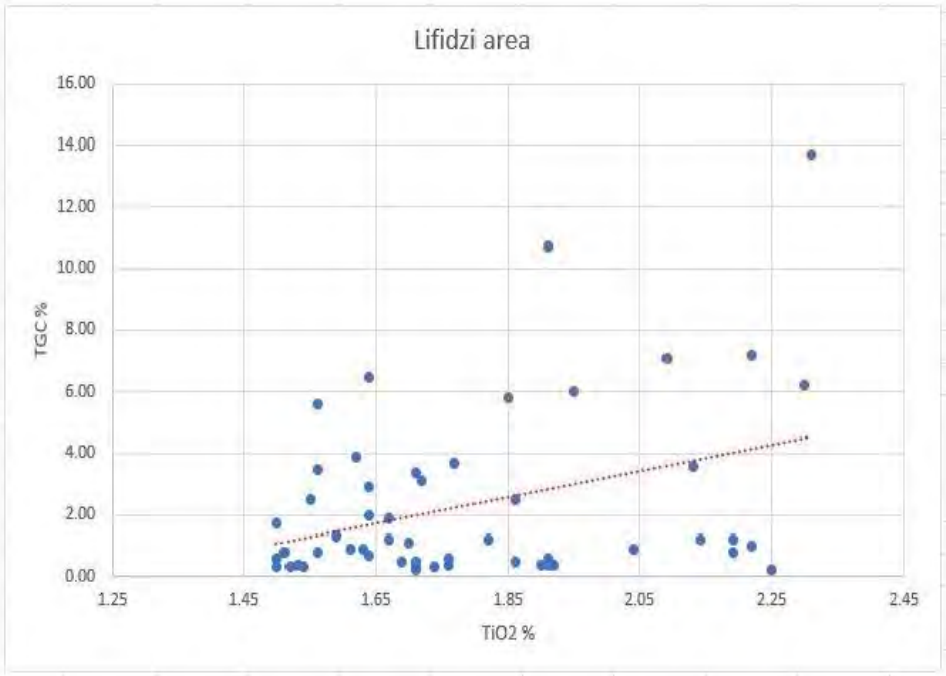


*Appendix 7: TGC vs TiO2 correlation for Malingunde vs Lifidzi*

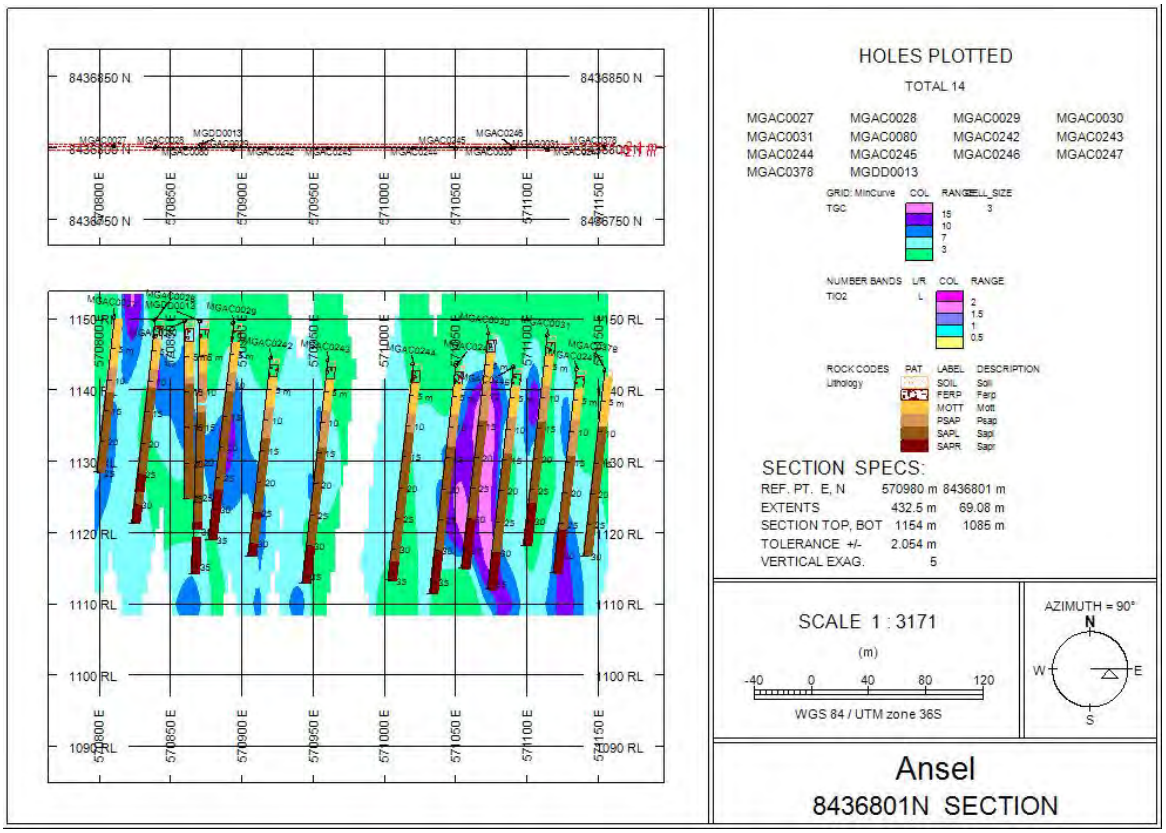


*Appendix 8: Malingunde project geological drillhole section 8436801N*

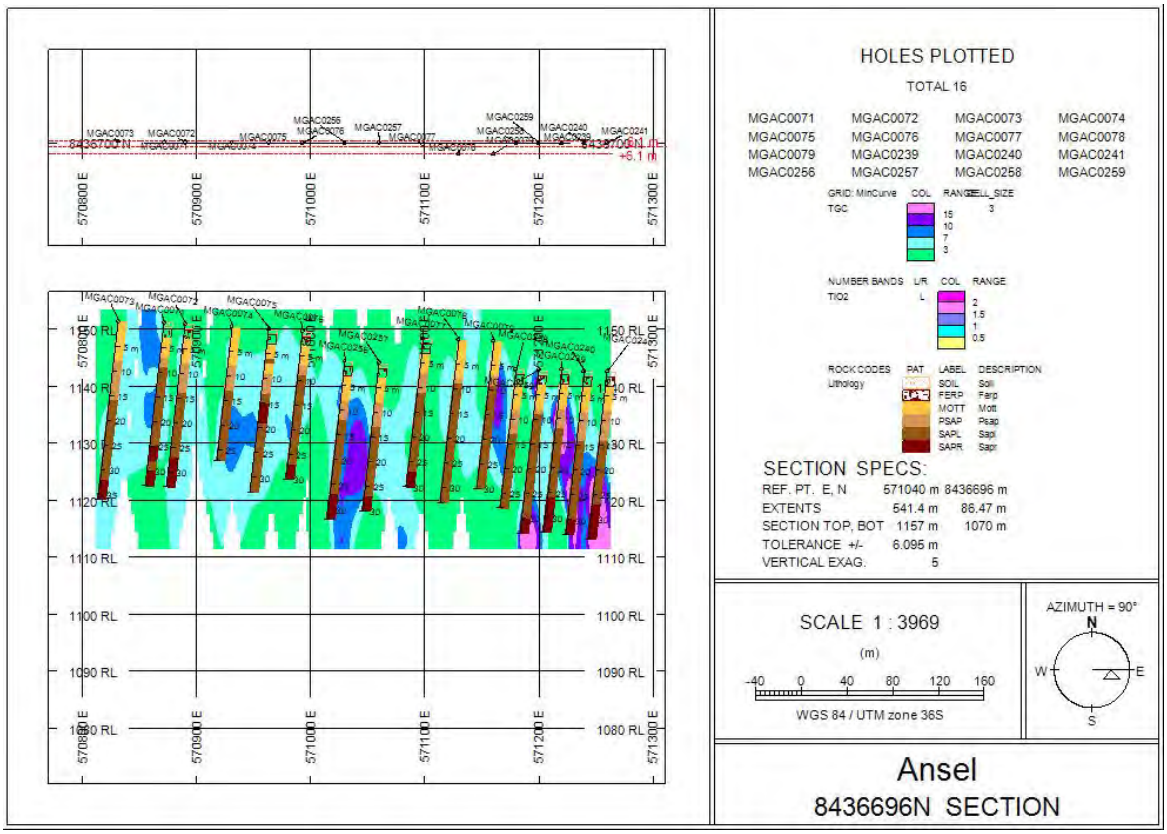


*Appendix 9: Malingunde project geological drillhole section 8436696N*

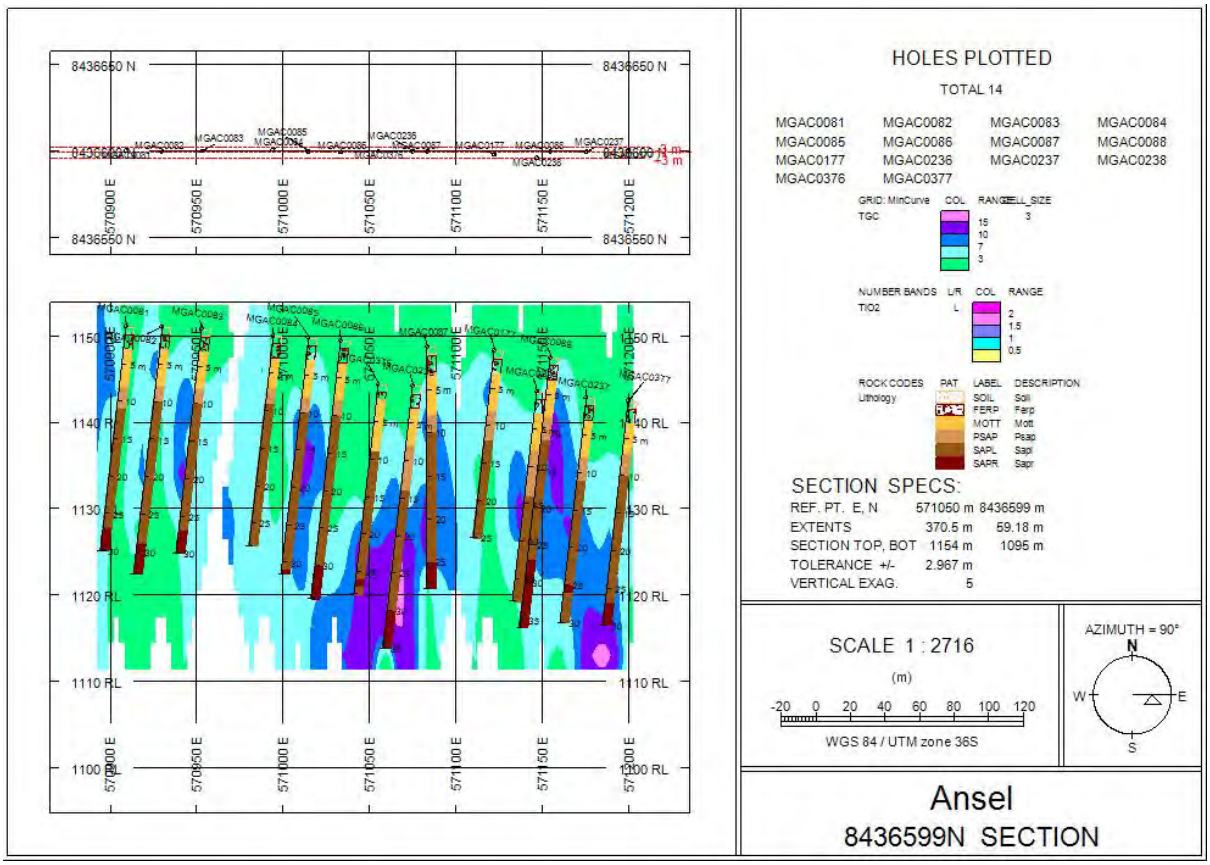


*Appendix 10: Malingunde project geological drillhole section 8436599N*

| Graphite (natural) world mine production and reserves 2021 and 2022 in metric tons | | | |
|---|---|---|---|
| Country | 2021 | 2022 | Reserves |
| United States | NA | NA | Included in the World's total |
| Austria | 500 | 500 | Included in the World's total |
| Brazil | 82000 | 87000 | 74,000,000 |
| Canada | 12000 | 15000 | |
| China | 820000 | 850000 | 52,000,000 |
| Germany | 250 | 250 | Included in the World's total |
| India | 7000 | 8300 | 8,000,000 |
| North Korea | 8100 | 8100 | 2,000,000 |
| Republic of Korea | 10500 | 17000 | 1,800,000 |
| Madagascar | 70000 | 110000 | 26,000,000 |
| Mexico | 2100 | 1900 | 3,100,000 |
| Mozambique | 72000 | 170000 | 25,000,000 |
| Norway | 6290 | 10000 | 600,000 |
| Russia | 15000 | 15000 | 14,000,000 |
| Sri Lanka | 3000 | 3000 | 1,500,000 |
| Tanzania | NA | 8000 | 18,000,000 |
| Turkey | 2700 | 2900 | 90,000,000 |
| Ukraine | 10000 | 3000 | Included in the world's total |
| Uzbekistan | 110 | NA | 7,600,000 |
| Vietnam | 5000 | 5000 | Included in the World's total |
| Other | 3450 | | 6,400,000 |
| World total rounded | 1130000 | 1300000 | 330,000,000 |

*Appendix 11: Graphite (natural) world mine production and reserves 2021 and 2022 data (Source: U.S Geological survey, 2023)*

| Rutile world mine production and reserves | | | |
|---|---|---|---|
| | **2021** | **2022** | **Reserves** |
| United States | | | |
| Australia | 190 | 190 | 31000 |
| India | 12 | 11 | 7400 |
| Kenya | 72 | 73 | 170 |
| Madagascar | | | 520 |
| Mozambique | 8 | 8 | 890 |
| Senegal | 9 | 9 | |
| Sierra Leone | 123 | 130 | 490 |
| South Africa | 95 | 95 | 6500 |
| Tanzania | | | 20 |
| Ukraine | 95 | 57 | 2500 |
| Other countries | 14 | 14 | |

*Appendix 12: Rutile world mine production and reserves (Source: U.S Geological survey, 2023)*